CERN 65-24
Volume I.
16 June 1965

ORGANISATION EUROPÉENNE POUR LA RECHERCHE NUCLÉAIRE
CERN EUROPEAN ORGANIZATION FOR NUCLEAR RESEARCH

PROCEEDINGS OF THE 1965 EASTER SCHOOL FOR PHYSICISTS

Using the CERN Proton Synchrotron
and Synchro-Cyclotron

Bad Kreuznach, April 1 - 15, 1965

Volume I.
Lectures by:

N. Schmitz
H. Pilkuhn
A. M. Wetherell

GENEVA
1965

Genève - Service d'Information scientifique - SIS/H/063 - 3000 - 30.6.65

SCIENTIFIC ORGANIZING COMMITTEE

Dr. R. Armenteros	(CERN)
Prof. H. Ehrenberg	(University of Mainz)
Dr. K. Gottstein	(Max-Planck Institut für Physik, Munich)
Dr. W.O. Lock	(CERN)
Dr. U. Meyer-Berkhout	(DESY, Hamburg)
Miss E.W.D. Steel	(CERN)
Prof. M. Teucher, Chairman	(DESY, Hamburg)
Prof. L. Van Hove	(CERN)

EDITORIAL BOARD FOR THE PROCEEDINGS

Dr. K. Gottstein	(Max-Planck Institute für Physik, Munich)
Dr. W.O. Lock	(CERN)

PREFACE

The 1965 Easter School at Bad Kreuznach, Germany, was the fourth in a series that began in 1962. Wheareas the first two Schools, held at St. Cergue (Switzerland) in 1962 and 1963, were devoted to introducing young emulsion physicists to the experimental possibilities offered at CERN, and to the modern developments of high-energy nuclear physics, the scope of the 1964 School which took place at Herceg Novi (Yugoslavia) was widened to include also the bubble chamber technique. For the 1965 School no restriction as to the experimental technique was applied: young research students working in elementary particle physics with any technique were eligible for admission, the only restrictions being due to the limited space available in the Kurhaus hotel and its lecture rooms.

The lectures of the 1965 Easter School at Bad Kreuznach started in the morning of 2 April. The School closed on 14 April with an after-dinner speech by Professor W. Jentschke. It was attended by about 90 students from 22 countries in Western Europe, Eastern Europe, Asia, and the United States.

The purpose of the School was to familiarize the students with the current theoretical and experimental situation in Elementary Particle Physics. Eighteen lecturers contributed to this end. Their respective lecture courses varied in length, some lasting two hours, and two (by Van Hove and by Veltman) consisting of six lessons of 90 minutes duration each.

In the interest of speedy publication of the Proceedings of the School we are reducing to a minimum any editorial changes in the manuscripts as they are kindly supplied by the lecturers. As a consequence, some topics will be treated several times by different authors. In some cases the notations used will not be consistent. It was felt, however, that any inconvenience derived from these facts is not serious, and is in any case amply outweighed by the advantage that the Proceedings will be available sooner.

Volume I contains the lectures by N. Schmitz, H. Pilkuhn, and A.M. Wetherell. Further volumes will follow in due course.

We are grateful to the authors for their co-operation in preparing the manuscripts and checking the typed texts. Our thanks are also due to Miss S. Bloch and Miss M. Hutin for their careful typing; Mr. P. Theurillat and his colleagues of the Scientific Information Service, and Miss A. Lutke and Mrs. D. Bader of the MSC Drawing Office for their preparation of certain figures; and to Mrs. K. Wakley for her careful checking of the final text.

Editorial Board

CONTENTS

N. Schmitz

PERIPHERAL COLLISIONS

H. Pilkuhn

THE PERIPHERAL MODEL

A.M. Wetherell

HIGH-ENERGY ELASTIC SCATTERING

* * *

PERIPHERAL COLLISIONS

N. Schmitz,
Max-Planck Institut für Physik and Astrophysik,
München.

I. INTRODUCTION TO THE PERIPHERAL MODEL

During the last years many elementary particle reactions in which particles are produced (inelastic collisions) have been studied at various primary momenta above ~ 1 GeV/c. The majority of the experiments has been carried out by bombarding the protons in hydrogen bubble chambers by nucleons, antinucleons, kaons, and pions. The inelastic production processes were found to be characterized by two major features:

a) In many cases inelastic reactions do not proceed directly to the final state which is observed in the bubble chamber, but go via the production of strongly decaying particles (mesonic and baryonic resonances such as ρ, ω, f, K*, N*, Y*, etc.) as intermediate states. The resonant states then decay strongly, i.e. with an extremely short lifetime into the final state. An important role in this category of reactions play the quasi-two-body processes of the type

$$a + b \rightarrow c + d \quad (\text{e.g. } \pi N \rightarrow \rho N) \qquad (1)$$

where c or/and d are resonances.

b) Many inelastic reactions are characterized by the tendency of the secondary particles to go in the forward-backward direction in the centre-of-mass system (dominance of small momentum transfers, see below). Generally speaking, one can often group the secondary particles together into two particle systems c and d, such that c maintains preferentially nearly the direction of the incident particle a, and d the direction of the incident particle b, in the c.m.s. of the reaction. (For the two systems we use the same symbols c and d as for the particles in reaction (1) since, for example, the system c may consist of the decay products of a resonance and is therefore identical with the resonance itself as far as kinematics are concerned.) The forward-backward preference generally increases with increasing primary momentum and decreases with increasing number of secondary particles.

The observed forward-backward preference has led to the development of the peripheral model for strong interactions. This model has turned out to describe rather successfully the main features of many inelastic reactions with relatively small numbers of secondaries, and in particular of quasi-two-body processes of type (1) in the energy range between ~ 1 GeV and ~ 10 GeV. Descriptively speaking, this model is based on the following idea: in most of the cases the two incident particles a and b do not collide in a head-on collision but rather in a peripheral collision in which the particles only "glance at each other" (glancing collision); the two particles interact with each other preferentially by their peripheries. As a consequence of this peripheral interaction, the original directions are not changed very much; the particles in the final state keep predominantly the directions of the incident particles. In the case of inelastic nucleon-nucleon collision for instance,

one would say that the interaction takes place in the pion clouds of the nucleons; in pion-nucleon collision the incident pion interacts with the pion cloud of the nucleon and not with the "nucleon itself", which merely plays the role of a "spectator".

More physically speaking this picture means: the interaction between two particles is dominated by the long range forces. These forces are due to the exchange of a virtual particle (in this lecture we discuss only one-particle exchanges). The lighter the exchanged particle is, the longer the range of the force. This can be seen, for instance, from the form e^{-mr}/r of the Yukawa potential, where m is the mass of the exchanged particle. Since the pion is the lightest amongst the strongly interacting particles, and thereby responsible for the forces of longest range, the one-pion exchange (OPE) mechanism has been treated and applied most extensively in the framework of the peripheral model during the past years. There are, however, several reactions for which OPE is forbidden, as will be discussed later.

The theoretical formulation of the peripheral one-particle-exchange model starts from the Feynman diagram shown in Fig. 1. The incident particles a and b interact with each other by the exchange of particle e; this interaction leads to the particle systems c and d. The most important quantity for the diagram of Fig. 1 is the relativistically invariant square

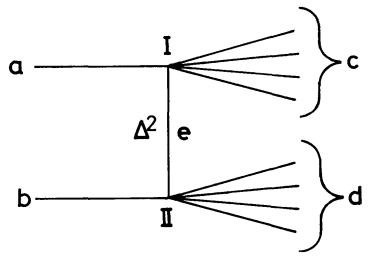

Fig. 1

Δ^2 of the four-momentum transfer (from now on called briefly "momentum transfer") between c and a (or d and b); it is defined by

$$\begin{aligned}\Delta^2 &= -(\underline{p}_c - \underline{p}_a)^2 = -(\underline{p}_d - \underline{p}_b)^2 \\ &= (\vec{p}_c - \vec{p}_a)^2 - (E_c - E_a)^2 \\ &= -(m_c^2 + m_a^2) + 2E_cE_a - 2p_cp_a \cos\Theta^* \quad .\end{aligned} \tag{2}$$

$\underline{p}$, $\vec{p}$, E, and m are, respectively, the four-momentum, three-momentum, total energy, and mass of the particle or particle system indicated by the index. $\underline{p}_c = (\vec{p}_c, E_c)$, for instance, is the sum of the four-momenta of all particles of which the system c consists; $m_c = \sqrt{E_c^2 - \vec{p}_c^2}$ is the

relativistically invariant effective mass of the system c. It is equal to the total energy of all particles of the system c in their c.m.s. (rest frame of c) since in that system $\vec{p}_c = 0$. Θ^* is the scattering or production angle.

For fixed values of m_c and m_d one obtains the lower and upper limit of the physical Δ^2 range by evaluating the right-hand side of (2) in the c.m.s. and putting $\cos\Theta^* = \pm 1$. Since the process $a + b \to c + d$ of Fig. 1 is a two-body process, the momenta p_a and p_c and the energies E_a and E_c can be expressed by the total c.m.s. energy E and the four masses, using energy and momentum conservation. One then obtains the following formula for the lower and upper limit of Δ^2:

$$\Delta^2_{\substack{\min\\ \max}} = \left\{ \sqrt{\left(\frac{E^2 + m_c^2 - m_d^2}{2E} \right)^2 - m_c^2} \mp \sqrt{\left(\frac{E^2 + m_a^2 - m_b^2}{2E} \right)^2 - m_a^2} \right\}^2 - \left\{ \frac{(m_c^2 - m_a^2) - (m_d^2 - m_b^2)}{2E} \right\}^2 \quad *) \qquad (3)$$

Since, due to four-momentum conservation at the vertex I of Fig. 1, the quantity $(\underline{p}_c - \underline{p}_a)$ is equal to the four-momentum of the virtual particle e, the momentum transfer Δ^2 can, according to (2), be interpreted as the negative square of the virtual mass of e. At the point $\Delta^2 = -m_e^2$ (m_e being the physical mass of e) the exchanged particle becomes real ("on the mass shell"). This point, however, lies in the unphysical Δ^2 region, since Δ^2 is usually positive for reactions of the type $a + b \to c + d$, i.e. the particle e is virtual ["off the mass shell", see (3)].

According to the Feynman rules the matrix element M_{fi} for the diagram of Fig. 1 has the following general structure:

$$M_{fi} = M_I(\Delta^2, m_c) \frac{1}{\Delta^2 + m_e^2} M_{II}(\Delta^2, m_d) \; . \qquad (4)$$

In this formula $1/(\Delta^2 + m_e^2)$ is the propagator of the exchanged particle. The quantities M_I and M_{II} are the vertex functions of the vertices I and II in Fig. 1. At the point $\Delta^2 = -m_e^2$ they are equal to the matrix elements for the physical processes

$$\begin{aligned} a + e &\to c \\ b + e &\to d \end{aligned} \qquad (5)$$

if c and d are systems of particles. If, on the other hand, for instance, c is a single particle (e.g. a resonance) M_I at $\Delta^2 = -m_e^2$ is apart from a known constant factor equal to the aec coupling constant.

The differential cross-section in Δ^2 (Δ^2 distribution) for the process of Fig. 1 is given by the Δ^2 dependence of the propagator and of the vertex functions. From the propagator the cross-section has a pole at the unphysical point $\Delta^2 = -m_e^2$ where the particle e is real. Moreover, one sees from (4) that the propagator tends to make the cross-section large for small

---

*) **Exercise:** derive formula (3).

physical Δ^2 values which are closest to the pole. Small Δ^2 values, however, correspond according to (2) to small c.m.s. scattering angles Θ^* [if one evaluates the right-hand side of (2) in the c.m.s.]. The propagator thus favours small scattering angles; therefore, the peripheral model should be able to explain at least qualitatively the observed preference for the forward-backward direction mentioned above, if the Δ^2 dependence of the vertex functions does not have a strong opposite effect on the angular distribution. A further discussion of this point will be given in a later section on Δ^2 distributions (Section VIII).

One of the main applications of the peripheral model during the last years has been the determination and study of the cross-section for the reaction $\pi\pi \to \pi\pi$ which cannot yet be investigated in a direct scattering experiment since there are no free pion targets[1,2]. We do not discuss this subject in detail here but nevertheless mention it because of its importance. If one applies the idea of the peripheral model to the reaction

$$\pi N \to N\pi\pi \qquad (6)$$

one would say that the incident pion interacts with a virtual pion in the nucleon cloud and makes it free. The corresponding one-pion exchange diagram, a special case of Fig. 1, is shown in Fig. 2. At the unphysical point $\Delta^2 = -\mu^2$ (μ = pion mass) the vertex function of the lower vertex of Fig. 2 is equal to the $\pi\pi$ scattering amplitude. So from a study of reaction (6) it was possible to obtain information about the elastic $\pi\pi$ scattering $\pi\pi \to \pi\pi$, a special case of reaction (5).

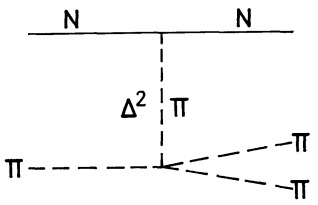

Fig. 2

More recently the peripheral model has been applied to quasi-two-body reactions of the general type

$$a + b \to c + d \qquad (1)$$

where c or/and d are strongly decaying resonances[3-7]. A one-meson exchange model (OME) has been developed which describes the production and the decay of resonances. From now on we want to concentrate on reactions of type (1) only and discuss the experimental and some theoretical aspects of the OME model in greater detail. First we list a few examples for reaction (1):

$$
\left.\begin{array}{l}
\pi^{\pm}p \to \rho^{\pm}p \\
\pi^{+}p \to \pi^{o}N^{*++} \\
\pi^{+}p \to \rho^{o}N^{*++} \\
\pi^{+}p \to \omega^{o}N^{*++} \\
K^{-}p \to K^{*-}p \\
K^{+}p \to K^{o}N^{*++} \\
K^{+}p \to K^{*o}N^{*++} \\
\pi^{-}p \to K^{*+}\Sigma^{-} \\
\pi^{\pm}p \to K^{+}Y^{*\pm} \\
\pi^{-}p \to K^{*+}Y^{*-}
\end{array}\right\}
\qquad
\begin{array}{l}
\text{with the decays:} \\
\rho^{\pm} \to \pi^{\pm}\pi^{o} \\
\rho^{o} \to \pi^{+}\pi^{-} \\
\omega^{o} \to \pi^{+}\pi^{-}\pi^{o} \\
K^{*+} \to K^{o}\pi^{+} \\
K^{*o} \to K^{+}\pi^{-} \\
N^{*++} \to p\pi^{+} \\
Y^{*} \to \Lambda(\Sigma)\pi
\end{array}
\qquad (7)
$$

II. EXPERIMENTAL SEPARATION OF THE REACTIONS a + b → c + d FROM THE BACKGROUND

If one wants to study the reactions (7) experimentally, one has to deal with the following difficulty: due to its short lifetime a resonance does not travel a measurable distance in a bubble chamber but decays "immediately" into the decay products, so only the final state of the reaction is observed experimentally. In the following let us discuss the reactions

$$\pi^{+}p \to \rho^{+}p \qquad (8a)$$

$$\pi^{+}p \to \pi^{o}N^{*++} \qquad (8b)$$

as an example. Both reactions lead to the final state $p\pi^{+}\pi^{o}$. Furthermore, there are $\pi^{+}p$ reactions which proceed directly to this final state ("direct reactions", "background reactions") not going via resonance production. For an individual event one cannot say if it was a direct reaction or a resonance production. How can one then separate the reactions (8) from each other and from the background?

In order to find out how frequently the over-all reaction

$$\pi^{+}p \to p\pi^{+}\pi^{o} \qquad (9)$$

proceeds, e.g. via ρ^{+} production (8a), one plots the <u>effective mass distribution</u> of the $\pi^{+}\pi^{o}$ system. The relativistically invariant effective mass $M_{\pi^{+}\pi^{o}}$ is defined by

$$M^{2}_{\pi^{+}\pi^{o}} = (E_{\pi^{+}} + E_{\pi^{o}})^{2} - (\vec{p}_{\pi^{+}} + \vec{p}_{\pi^{o}})^{2} \quad . \qquad (10)$$

$E_{\pi^{+}} + E_{\pi^{o}}$ is the total energy, $\vec{p}_{\pi^{+}} + \vec{p}_{\pi^{o}}$ the momentum of the $\pi^{+}\pi^{o}$ system. $M_{\pi^{+}\pi^{o}}$ is the total energy of the π^{+} and π^{o} in their c.m.s. (see above). If the π^{+} and π^{o} originate from a ρ^{+} decay the $\pi^{+}\pi^{o}$ c.m.s. coincides with the ρ^{+} rest system. Therefore, due to energy conservation in ρ decay the total $\pi^{+}\pi^{o}$ energy $M_{\pi^{+}\pi^{o}}$ in that system is equal to the total ρ energy in its rest frame, i.e. to the ρ mass. For ρ^{+} productions the quantity $M_{\pi^{+}\pi^{o}}$ has thus

within the decay width Γ_ρ of the ρ meson a definite value equal to the ρ mass (= 750 MeV). So, the over-all $\pi^+\pi^0$ effective mass distribution for reaction (9) will have the shape shown in Fig. 3.

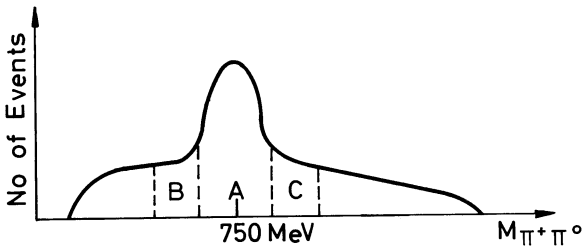

Fig. 3

The distribution consists of a broad background distribution from background events, including reaction (8b), and a bump with a width Γ_ρ around the ρ mass from reaction (8a). From the total number of events and the number of events in the bump, one can then immediately determine the relative frequency of reaction (8a). The same can be done for reaction (8b) by studying the $p\pi^+$ effective mass distribution.

More information is contained in a so-called Dalitz plot in which one plots $M^2_{\pi^+\pi^0}$ versus $M^2_{p\pi^+}$ (one point per event) as shown in Fig. 4. The boundary of the plot as indicated by the curve depends only on the primary momentum.

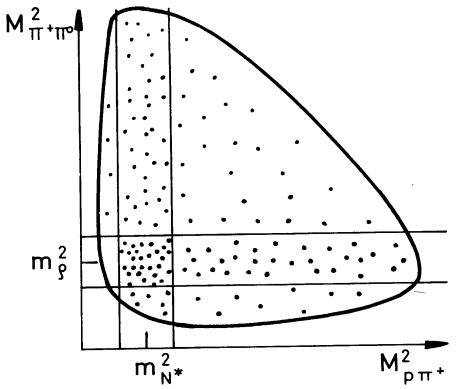

Fig. 4

Now two cases are thinkable:

Case 1: All reactions (9) proceed via ρ or N* production. In this case there will be no points outside the ρ and N* band of Fig. 4. [This situation is realized to a good approximation in the reaction $K^+p \to K^0\pi^+p$ at 3 GeV/c, to which K^{*+} and N^{*++} production contributes $\sim 80\%$ [7)]. The background in the $\pi^+\pi^0$ effective mass distribution then comes only from N^{*++}

events, reaction (8b). One can obtain a pure sample of ρ productions if one takes only events in the ρ band of Fig. 4 outside the N*ρ overlap region, i.e. events for which $M_{p\pi^+}$ is outside the mass region of the N* bump (N* region). However, this sample does not contain those ρ productions for which $M_{p\pi^+}$ falls into the N* region by accident and is, therefore, biased as can be seen from the following consideration:

Figure 5 shows reaction (8a) in the c.m.s. for the dominant case of a small production angle Θ^*. Let us regard, now, those events in which the ρ^+ decays in such a way that in the ρ^+ rest system the decay π^+ goes backward with respect to the incident π^+ (see below, where the decay angle ϑ will be defined). This means since Θ^* is predominantly small, that the decay π^+ travels nearly towards the secondary proton; thus, the effective mass $M_{p\pi^+}$ tends to be small and may therefore fall into the N* mass region. So, if events in this region are not taken the ρ decay angular distribution will be biased.

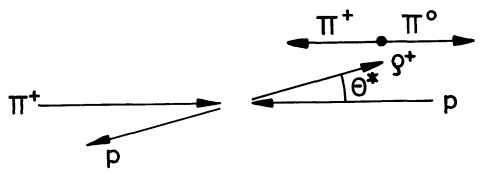

Fig. 5

Since the decay angular distributions play an important role in the framework of the OME model, we discuss here several methods to obtain an unbiased ρ decay distribution:

a) Assuming that the ρ decays symmetrically in the forward and backward hemisphere (as a particle with definite spin should) one takes only those events in the ρ band for which the decay π^+ goes forward and studies only this forward part of the decay distribution. This means that one takes only those events for which $M_{p\pi^+}$ has higher values and does not fall into the overlap region of Fig. 4, so there is no contamination from N* events.

b) One plots the decay angular distribution for the $\pi^+\pi^0$ system for all events with $M_{\pi^+\pi^0}$ in the ρ region A of Fig. 3. This distribution contains background from N* events (overlap region of Fig. 4). If one assumes that the angular distribution for the background $\pi^+\pi^0$ systems does not depend strongly on $M_{\pi^+\pi^0}$ one may represent the background under the ρ peak by the $\pi^+\pi^0$ systems in the regions B and C of Fig. 3 adjacent to the ρ region on the left and right side. So, one also plots the angular distribution for events in the regions B and C, normalizes it to the background under the ρ peak and subtracts it from the over-all angular distribution for region A. The result of this background subtraction method should be the decay angular distribution for the ρ meson only.

c) According to the peripheral model the ρ production (8a) should occur predominantly with small momentum transfer $\Delta^2(p/p)$ between incident and outgoing proton, whereas for N* production (8b) the momentum transfer $\Delta^2(p/p\pi^+)$ between incident proton and outgoing $p\pi^+$ system should be small. Thus, one can hope to obtain a sample of reactions (8a) purified from N* events by taking only those events for which $M_{\pi^+\pi^0}$ is in the ρ band and $\Delta^2(p/p)$ is small (limitation to small Δ^2). In order to examine if this method really works, two checks can be carried out: the $M_{\pi^+\pi^0}$ distribution for events with small $\Delta^2(p/p)$ should have the shape of the ρ resonance. Furthermore, the $M_{p\pi^+}$ distribution for events with $M_{\pi^+\pi^0}$ in the ρ band, and small $\Delta^2(p/p)$, should not show an N* peak.

Since the decay angular distribution, in general, depends on the production angle Θ^* (i.e. on Δ^2) it is a disadvantage of this limitation method that it allows study of the decay only at small Δ^2. The same methods can, of course, be applied for a study of the N* decay angular distribution.

Case 2: In addition to reactions (8a) and (8b), the direct channel contributes appreciably to the whole reaction (9). Since, in the Dalitz plot of Fig. 4, the points from the direct channel are distributed over the whole area inside the kinematical boundary, the ρ and N* resonance bands are contaminated by background events not only in the overlap region but everywhere. In this case one cannot apply method a) in order to obtain, for instance, the ρ decay distribution. Only the subtraction method, and perhaps the limitation to small $\Delta^2(p/p)$, will yield this distribution. Whether the latter method really does strongly reduce the background under the ρ peak must first be checked from a $M_{\pi^+\pi^0}$ distribution for events with small $\Delta^2(p/p)$.

Let us now discuss resonance production in another reaction, namely

$$\pi^+ p \to p\pi^+\pi^+\pi^- \quad . \tag{11}$$

This reaction is more complicated than (9) due to the larger number of secondary particles. Limiting ourselves to N^{*++} and ρ^0 production only and neglecting, for example, N^{*0}, f^0 production, we see that the following four channels can contribute to (11):

$\pi^+ p \to N^{*++}\rho^0$	($N^*\rho$ channel)	(12a)
$\pi^+ p \to N^{*++}\pi^+\pi^-$	(N^* channel; $\pi^+\pi^-$ not resonant)	(12b)
$\pi^+ p \to p\pi^+\rho^0$	(ρ channel; $p\pi^+$ not resonant)	(12c)
$\pi^+ p \to p\pi^+\pi^+\pi^-$	(direct channel; no resonances)	(12d)

Thus, in contrast to reaction (9), two resonances can be produced simultaneously in reaction (11) [channel (12a)].

A further complication in addition to the larger number of channels is the presence of two $\pi^+(\pi_1^+$ and $\pi_2^+)$; in the $p\pi^+$ and $\pi^+\pi^-$ effective mass distributions two combinations enter per event. Thus, even if reaction (11) proceeded, for example, completely via N^{*++} production (12a) and (12b), the $p\pi^+$ effective mass distribution would have many combinations outside the N^* region, since only the π^+ from N* decay gives with the proton an effective mass in the N* region, whereas the effective mass of the proton and the other π^+ may have any value within the kinematical limits.

A useful plot for reaction (11) is a scatter diagram of $M_{p\pi_a^+}$ versus $M_{\pi_b^+\pi^-}$. The boundary of such a plot is given by a triangle, as indicated in Fig. 6. For a given value of $M_{\pi_b^+\pi^-}$ the lower limit of $M_{p\pi_a^+}$ is $m_p + m_\pi$ corresponding to p and π_a^+ being at rest in

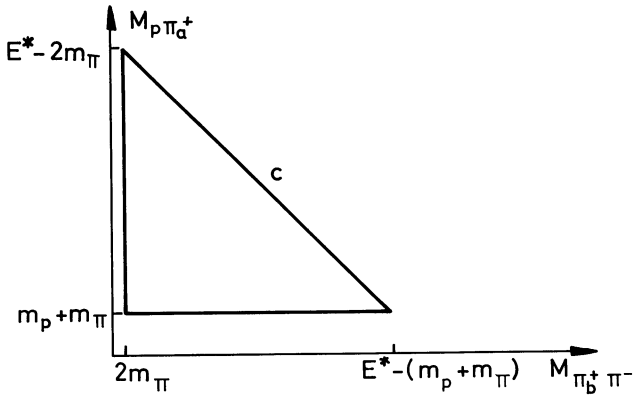

Fig. 6

their c.m.s. The upper limit is

$$M^{max}_{p\pi_a^+} = E^* - M_{\pi_b^+\pi^-} \qquad (13)$$

where E* is the total energy in the over-all c.m.s. This situation corresponds to the $\pi_b^+\pi^-$ system and therefore also the $p\pi_a^+$ system being at rest in the over-all c.m.s. so that all the available energy E* goes into the masses of the two systems. Equation (13) gives the straight line c in Fig. 6. Since the absolute lower limit for $M_{\pi_b^+\pi^-}$ is $2m_\pi$, the absolute upper limit of $M_{p\pi_a^+}$ is $E^* - 2m_\pi$ according to (13).

Figure 7 shows as an example a $M_{p\pi_a^+}$ versus $M_{\pi_b^+\pi^-}$ plot for reaction (11) at a primary momentum of 4 GeV/c [8]. Because of a,b = 1,2 and 2,1 two points enter per event. One observes an accumulation of points in the N* and ρ band, and an additional accumulation in the N*ρ overlap region due to the channel (12a). There are many points outside the two resonance bands. However, even if all reactions proceeded via N* and ρ production (i.e. no contribution from the direct channel) there would be many points outside the two bands because each event contributes two points, one of which must originate from combining the "wrong" particles (π^+ from N* decay combined with π^- and π^+ from ρ decay combined with p). So one cannot rely on the first impression of Fig. 7, and a more careful study of the plot is necessary in order to determine the relative frequencies of the channels (12a) to (12d).

Since we are interested here in quasi-two-body reactions, let us discuss the limitation to small momentum transfers as a method to separate out a rather pure sample of the channel (12a) $\pi^+ p \to N^{*++}\rho^0$. If this process occurs peripherally (Fig. 8) the $\Delta^2(p/p\pi_a^+)$ for the π^+ from N* decay (π_a^+) should predominantly be small, whereas the $\Delta^2(p/p\pi_b^+)$ calculated with the "wrong" π^+ (π_b^+) should have no strong tendency towards small values, so one should obtain a

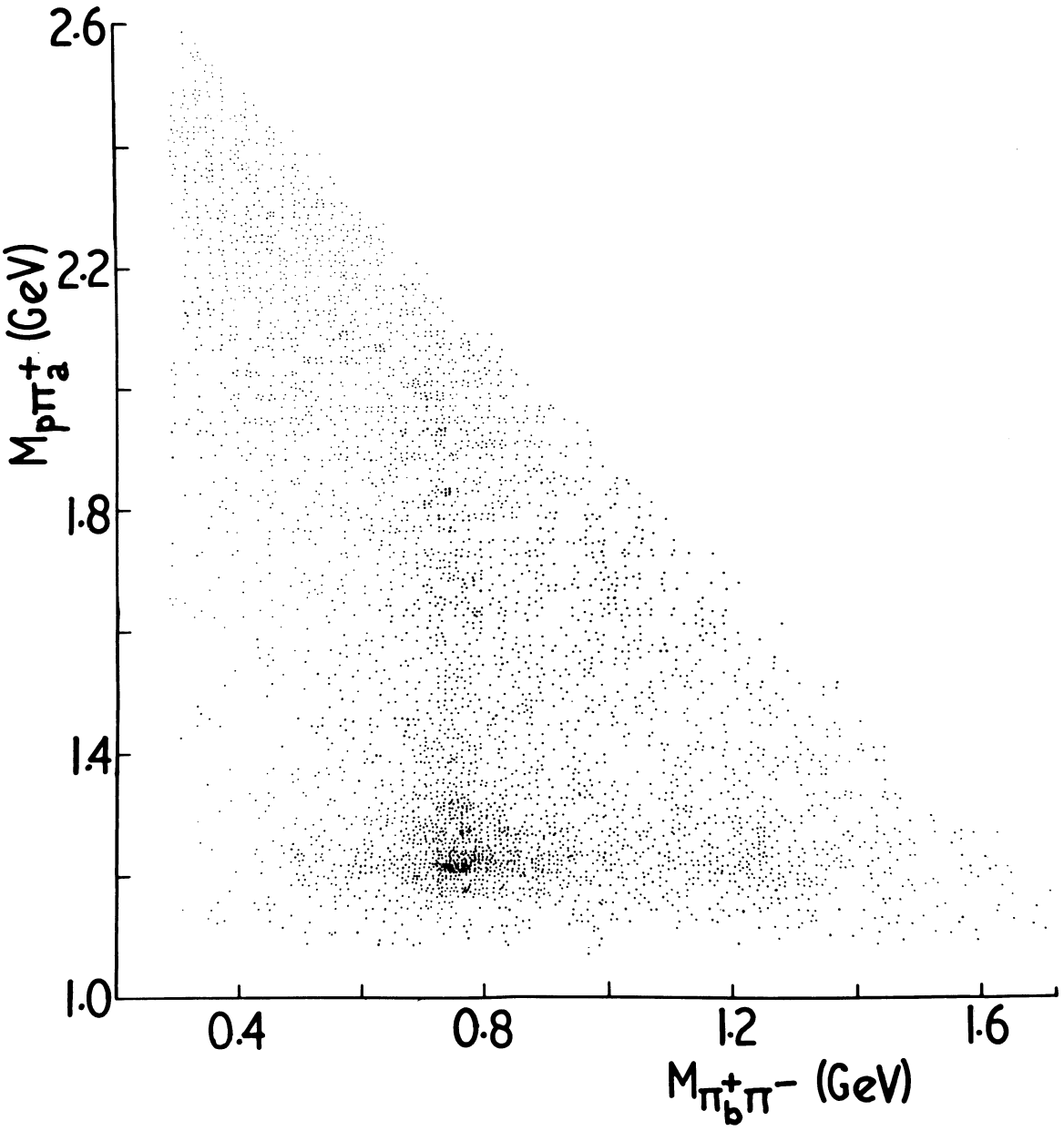

Fig. 7 Scatter diagram of $M_{p\pi_a^+}$ versus $M_{\pi_b^+\pi^-}$ (two points per event) for $\pi^+p \to p\pi^+\pi^+\pi^-$ at 4 GeV/c.

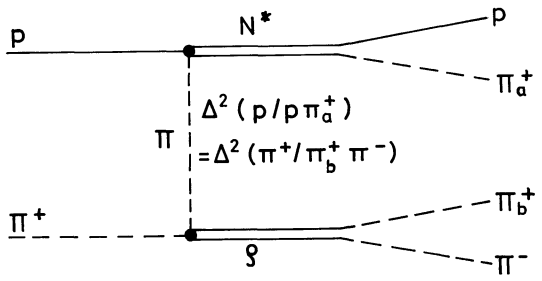

Fig. 8

purified sample of channel (12a) by selecting out those events of type (11) for which one of the two π^+ gives a small $\Delta^2(p/p\pi^+)$. This π^+ then would predominantly be the π_a^+ from N* decay and the other π^+ would be π_b^+ from ρ decay. Figure 9 shows the result of this method when applied to the data of Fig. 7: it shows $M_{p\pi_a^+}$ versus $M_{\pi_b^+\pi^-}$ (one point per event) for events with $\Delta^2(p/p\pi_a^+) < 0.3$ GeV^2. For those few events for which both $\Delta^2(p/p\pi^+)$ were smaller than 0.3 GeV^2, that π^+ was taken to be π_a^+ which gave the smaller Δ^2. One observes the strong purifying effect of the Δ^2 limitation; only in the N*ρ overlap region a strong accumulation of points remains. From the $p\pi_a^+$ and $\pi_b^+\pi^-$ effective mass distributions for events in the ρ and N* band of Fig. 9, respectively (obtained by projecting the number of points in the two bands on the vertical and horizontal scale) one could see that there is very little background left under the N* and ρ peaks. So, the result is: one obtains a rather pure sample of the channel $\pi^+p \to N^{*++}\rho^0$ by taking only those events of type (11) for which $\Delta^2(p/p\pi_a^+)$ is small (e.g. < 0.3 GeV^2), $M_{p\pi_a^+}$ is in the N* mass region and $M_{\pi_b^+\pi^-}$ in the ρ region.

After this discussion on experimental methods of separating out and studying quasi-two-body reactions we return to the OME model.

III. QUANTUM NUMBERS OF THE EXCHANGED PARTICLE

Figure 10 shows the OME diagram for the general two-body reaction (1). From conservation of angular momentum, parity, G-parity, isospin, and strangeness at each vertex of

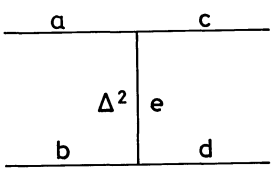

Fig. 10

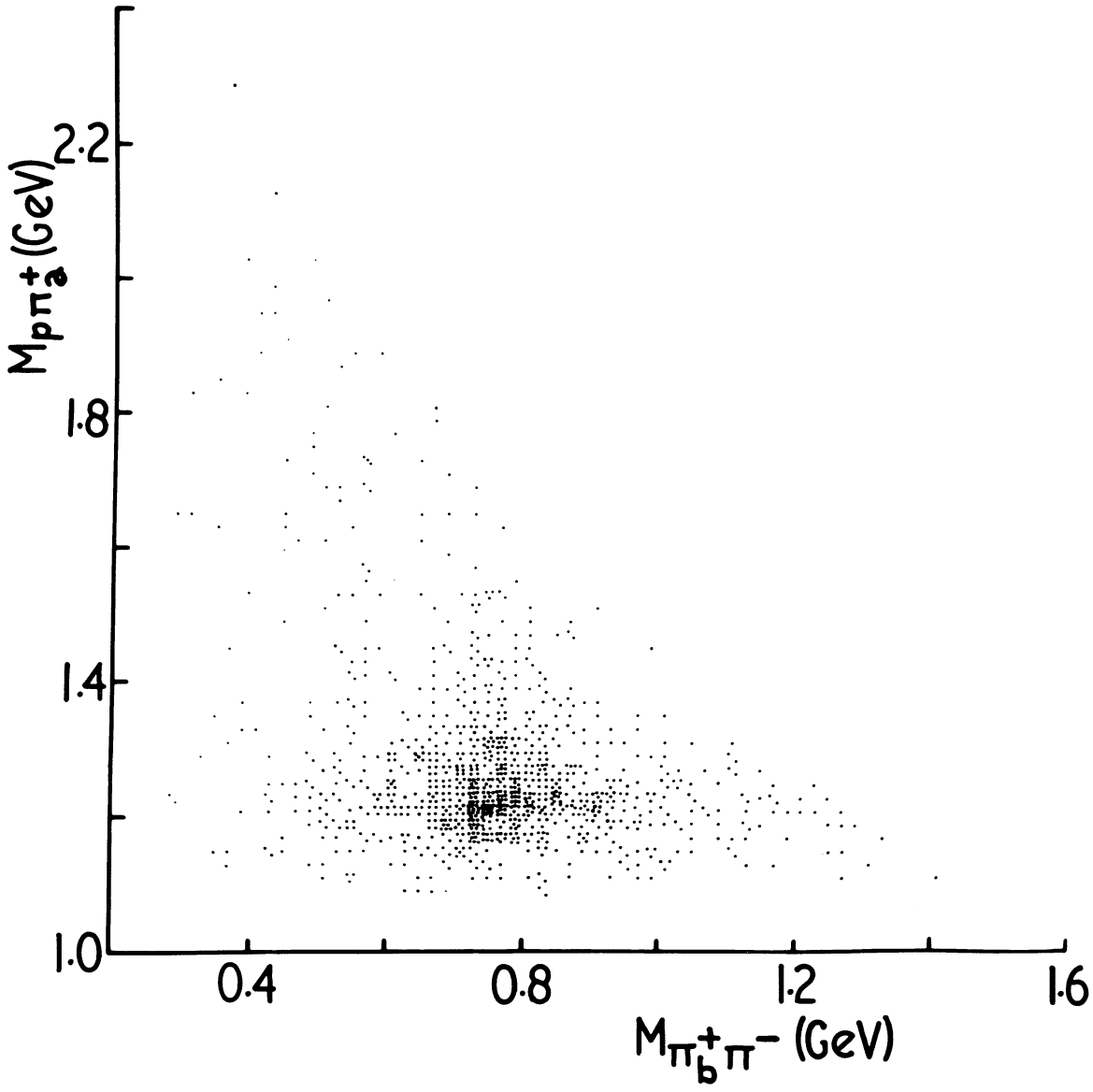

Fig. 9 Scatter diagram of $M_{p\pi_a^+}$ versus $M_{\pi_b^+\pi^-}$ for $\pi^+ p \to p\pi^+\pi^+\pi^-$ at 4 GeV/c with $\Delta^2(p/p\pi_a^+) < 0.3$ GeV^2.

Fig. 10 and from the known quantum numbers of the particles involved, a selection is obtained of what mesons can be exchanged in a given reaction (we do not discuss baryon exchange here). As candidates for the exchanged particle e all known mesons, for which the quantum numbers have definitely been established, are listed in the following list:

$$\pi(10^{--}),\ \eta \text{ and } X_0(00^{-+}),\ \rho(11^{--}),\ \omega \text{ and } \varphi(01^{--}),\ f(02^{++}),\ A_2(12^{+-});$$
$$K(\tfrac{1}{2}0^{-}),\ K^*(\tfrac{1}{2}1^{-}).$$

The numbers and signs in the brackets indicate the isospin I, spin J, parity P, and G-parity G in the form IJ^{PG} for the non-strange mesons (first row) and in the form IJ^{P} for the strange mesons (second row) which do not have a definite G-parity.

Let us now discuss as an instructive example the reaction

$$\pi^+ p \to N^{*++}\pi^0 \qquad (14)$$

in further detail and ask what mesons can be exchanged. Figure 11 shows the OME diagram for this reaction.

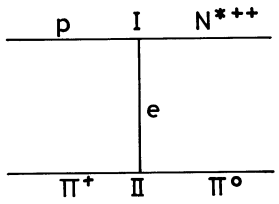

Fig. 11

a) Strangeness

From strangeness conservation at both vertices it follows that e must have strangeness $s_e = 0$.

b) G-parity

The G-parity is a multiplicative quantum number having the values ± 1. Each particle with baryon number zero and strangeness zero is an eigenstate of the G-operator, i.e. has definite G-parity. The pion has G-parity $G_\pi = -1$. From G-parity conservation at the meson vertex II of Fig. 11 where the virtual process

$$\pi + e \to \pi \qquad (15)$$

occurs, it follows that $G_\pi \cdot G_e = G_\pi$ and therefore $G_e = +1$, ruling out π exchange.

c) Angular momentum and parity

The sketch of Fig. 12 illustrates the process (15) in the rest frame of the outgoing π^0. Spin J and parity P of each particle are indicated in the form J^P. L is the relative

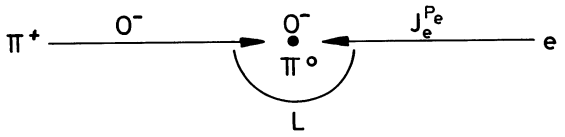

Fig. 12

orbital angular momentum of π^+ and e. Because of angular momentum conservation, the vectors $\vec{L}$ and $\vec{J}_e$ must be added to give the spin zero of the π^0; therefore, $L = J_e$.

Parity conservation yields

$$P_\pi \cdot P_e(-1)^L = P_\pi \quad , \quad \nearrow\!\!\searrow \quad P_e = (-1)^L = (-1)^{J_e} \quad , \quad \text{since } L = J_e \quad .$$

Thus the exchanged particle e must have natural parity (the parity is called natural if $P = (-1)^J$ and unnatural if $P = -(-1)^J$): $J_e^{Pe} = 0^+, 1^-, 2^+ \ldots$. From the baryon vertex I of Fig. 11 no conclusions about J_e^{Pe} can be drawn.

d) Isospin

Isospin conservation at the baryon vertex demands that the isospin I_e of e must be coupled with the nucleon isospin of $1/2$ to give the N* isospin $3/2$. This is feasible with $I_e = 1$ and 2. (From isospin conservation at the meson vertex one obtains only the weaker condition $I_e = 0,1,2.$)

If we search through the above meson list for those mesons which satisfy all these conditions on their quantum numbers, we find that only the ρ meson is left. So, reaction (14) can proceed only via ρ exchange.

In a similar way it is possible to examine which mesons may be exchanged in the other reactions (7). The results are summarized in Table I.

Table I *)

Reaction	s_e	G_e	$J_e^{P_e}$	I_e	known mesons
$\pi N \to \rho N$	0	-1	arbitr., not 0^+	0,1	π, $\omega(\varphi)$, A_2
$\pi N \to \pi N^*$	0	+1	0^+, 1^-, 2^+...	1,2	ρ
$\pi N \to \rho N^*$	0	-1	arbitr., not 0^+	1,2	π, A_2
$\pi N \to \omega N^*$	0	+1	arbitr., not 0^+	1	ρ
$KN \to K^*N$	0	arbitrary	arbitr., not 0^+	0,1	$\pi, \eta(X_0), \rho, \omega(\varphi), f, A_2$
$KN \to KN^*$	0	arbitrary	0^+, 1^-, 2^+...	1	ρ, A_2
$KN \to K^*N^*$	0	arbitrary	arbitr., not 0^+	1	π, ρ, A_2
$\pi N \to \begin{cases} K^*\Lambda \\ K^*\Sigma \end{cases}$	1	/	arbitr., not 0^+	$\begin{cases} 1/2 \text{ for } \Lambda \\ 1/2, 3/2 \text{ for } \Sigma \end{cases}$	K, K*
$\pi N \to KY^*$	1	/	0^+, 1^-, 2^+...	$\begin{cases} 1/2 \text{ for } Y_0^* \\ 1/2, 3/2 \text{ for } Y_1^* \end{cases}$	K*
$\pi N \to K^*Y^*$	1	/	arbitr., not 0^+	$\begin{cases} 1/2 \text{ for } Y_0^* \\ 1/2, 3/2 \text{ for } Y_1^* \end{cases}$	K, K*

IV. DECAY ANGULAR DISTRIBUTIONS

After examining which meson exchanges are allowed, we ask the question, how one can find out experimentally what meson(s) is (are) really exchanged in a given reaction at a given energy? The reaction is, of course, assumed to proceed peripherally as can be checked from the Δ^2 distribution. We assume for the moment the particle d in reaction (1), Fig. 10, to be a resonance with spin J decaying according to

$$d \to \alpha + \beta \qquad (16)$$

into α and β. After its production the particle d is in general in a quantum mechanical mixture of pure spin states. The mixture depends, via the vertex bed (lower vertex of Fig. 10), on the spin and parity $J_e^{P_e}$ of the exchanged particle e, and is described by the $(2J+1)$ dimensional density matrix of d with the elements $\rho_{mm'}$, (m, m' are the magnetic quantum numbers of d running from -J to +J). In general, these matrix elements are functions of the production angle, i.e. of Δ^2 for reaction (1). Properties of the density matrix and predictions on the matrix elements $\rho_{mm'}$ for certain values of $J_e^{P_e}$ will be discussed later. On the other hand,

*) Exercise: check Table I.

the decay angular distribution of d depends on the mixture of spin states of d and, therefore, on some of the density matrix elements. Thus, by measuring the decay distribution of d, one can determine some density matrix elements and find out via these matrix elements which particle e is exchanged in the mechanism producing d.

First we define the decay angles ϑ and φ of the particle d. Figure 13 shows the

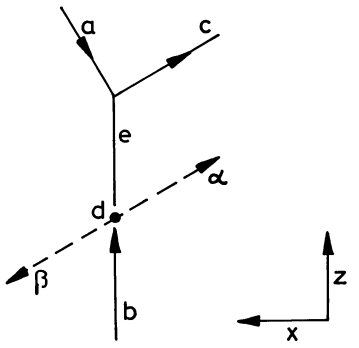

Fig. 13

production process (1) and the decay (16) in the rest frame of d. The momenta of a, c, and b lie in the production plane (paper plane). The momenta of α and β are equal in magnitude and opposite; they usually do not fall into the production plane and are therefore indicated in Fig. 13 by dotted lines. Let us now introduce the following right-handed co-ordinate system xyz: the z axis is along the direction of b, the y axis is along the normal to the production plane defined by $\hat{n} = \frac{\vec{a}\times\vec{c}}{|\vec{a}\times\vec{c}|}$. The unit vector in x direction is then given by $\hat{n}\times\frac{\vec{b}}{|\vec{b}|}$. The decay angles ϑ and φ are the polar and azimuth angle, respectively, of the decay particle α (or β) in that (xyz) system; they are given by the following formulae:

$$\cos\vartheta = \frac{\vec{b}\cdot\vec{\alpha}}{|\vec{b}||\vec{\alpha}|}$$

$$\left.\begin{aligned}\cos\varphi &= \frac{\vec{a}\times\vec{c}}{|\vec{a}\times\vec{c}|}\cdot\frac{\vec{b}\times\vec{\alpha}}{|\vec{b}\times\vec{\alpha}|}\\ \sin\varphi &= \frac{\vec{b}\times(\vec{a}\times\vec{c})}{|\vec{b}\times(\vec{a}\times\vec{c})|}\cdot\frac{\vec{b}\times\vec{\alpha}}{|\vec{b}\times\vec{\alpha}|}\end{aligned}\right\}\ \varphi \text{ between } 0° \text{ and } 360° \ . \qquad (17)^{*)}$$

In these formulae the symbols mean the momenta of the respective particles in the d rest system. Because of the sign one has to be careful to take the momenta in the cross products always in the order indicated by (17). It is seen that φ is zero or 180° in the production plane.

---

*) Exercise: derive formulae (17).

The most frequent cases are the decay of a J = 1 meson resonance into two mesons with $J_\alpha = J_\beta = 0$ (e.g. $\rho \to \pi\pi$, $K^* \to K\pi$) and the decay of a $J = 3/2$ baryon resonance into a $J_\alpha = 1/2$ baryon and a $J_\beta = 0$ meson (e.g. $N^* \to N\pi$, $Y_1^* \to Y\pi$). Thus, we give and discuss below the decay angular distribution

$$W(\cos\vartheta,\varphi) \equiv \frac{\partial\sigma}{\partial \cos\vartheta\, \partial\varphi} \tag{18}$$

in terms of the density matrix elements for these two cases only. The general expression for the decay distribution for any spins can be found in reference 3); its explicit form for a J = 2 resonance decaying into two spin zero mesons (e.g. $f \to \pi\pi$) is given in reference 6). The formula for J = 1 will be derived by Dr. Pilkuhn.

a) $J = 1$, $J_\alpha = J_\beta = 0$

$$W(\cos\vartheta,\varphi) = \frac{3}{4\pi}\left\{\tfrac{1}{2}(1-\rho_{00}) + \tfrac{1}{2}(3\rho_{00}-1)\cos^2\vartheta - \rho_{1,-1}\sin^2\vartheta\cos 2\varphi - \sqrt{2}\,\mathrm{Re}\,\rho_{10}\sin 2\vartheta\cos\varphi\right\}. \tag{19}$$

The normalization constant is chosen such that

$$\int_0^{2\pi} d\varphi \int_{-1}^{+1} d\cos\vartheta\, W(\cos\vartheta,\varphi) = 1 \tag{20}$$

as can be easily checked. It is seen from (19) that by measuring the decay distribution $W(\cos\vartheta,\varphi)$ one can determine the three matrix elements ρ_{00}, $\rho_{1,-1}$, and $\mathrm{Re}\,\rho_{10}$ (ρ_{00} and $\rho_{1,-1}$ are real, see below). Integrating (19) over φ or $\cos\vartheta$ yields the distribution in $\cos\vartheta$ or φ only, respectively:

$$W(\cos\vartheta) = \tfrac{3}{4}\left\{(1-\rho_{00}) + (3\rho_{00}-1)\cos^2\vartheta\right\}$$
$$W(\varphi) = \frac{1}{2\pi}\left\{(1+2\rho_{1,-1}) - 4\rho_{1,-1}\cos^2\varphi\right\}. \tag{21}$$

b) $J = 3/2$, $J_\alpha = 1/2$, $J_\beta = 0$

For this case the normalized decay distribution reads (we now use capital Greek letters for the angles in order to distinguish the decay angles of a baryon resonance from those of a meson resonance):

$$W(\cos\Theta,\Phi) = \frac{3}{4\pi}\left\{\tfrac{1}{6}(1+4\rho_{33}) + \tfrac{1}{2}(1-4\rho_{33})\cos^2\Theta - \frac{2}{\sqrt{3}}\,\mathrm{Re}\,\rho_{3,-1}\sin^2\Theta\cos 2\Phi - \frac{2}{\sqrt{3}}\,\mathrm{Re}\,\rho_{31}\sin 2\Theta\cos\Phi\right\}. \tag{22}$$

(For simplicity the matrix elements are written here in the form $\rho_{2m,2m'}$.) The distributions in cos Θ and Φ alone are given by the formulae

$$W(\cos\Theta) = \tfrac{1}{4}\left\{(1+4\rho_{33}) + (3-12\rho_{33})\cos^2\Theta\right\}$$
$$W(\Phi) = \frac{1}{2\pi}\left\{\left(1+\frac{4}{\sqrt{3}}\,\mathrm{Re}\;\rho_{3,-1}\right) - \frac{8}{\sqrt{3}}\,\mathrm{Re}\;\rho_{3,-1}\cos^2\Phi\right\}. \qquad (23)$$

It should be noted that the validity of the formulae (19) and (22) for the decay distributions is not limited to the OME model. It is more general and valid for the decay of any particle d with a polarization vector which does not have a component in the production plane. This is the case for any strong, i.e. parity conserving two-body production process a + b → c + d with unpolarized incident particles, as will be shown in a moment. The OME model comes in when predictions are made about the density matrix elements (see Section VI).

Figure 14 shows schematically the effect of the parity operation P (space reflection) and of a subsequent rotation D by 180° about the y axis (normal to the production plane) on

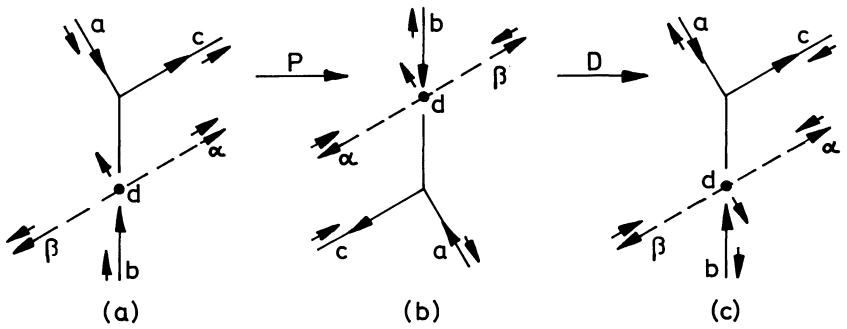

Fig. 14

the process of Fig. 13 with the particles being in definite spin states. These spin states are indicated symbolically in Fig. 14 by the small arrows. Under P the momenta of the particles are reversed, whereas the spins are not affected. The rotation D leads back to the original situation except that:

a) The x and z components of the spins have changed sign, whereas the y components are unchanged.

b) The azimuth angle φ has changed sign.

Since the interaction operator for the process of Fig. 13 is invariant under P and D, the transition matrix elements for Fig. 14a and 14c are the same, except for a phase factor. Since furthermore, due to the incident particles being unpolarized, the initial states of Fig. 14a and 14c occur with equal frequency, also the final states of Fig. 14a and 14c occur equally frequently. This has two immediate consequences:

c) Because of (a) the spin components of d in the production plane cancel; the polarization of d (= expectation value of the spin operator) is perpendicular to the production plane.

d) Because of (b) the relation

$$W(\cos\vartheta,\varphi) = W(\cos\vartheta,-\varphi) \tag{24}$$

holds for the decay distribution.

The application of P to the strong decay process $d \to \alpha + \beta$ interchanges the directions of α and β: $\cos\vartheta \to -\cos\vartheta$, $\varphi \to \pi + \varphi$. From P invariance in the decay one therefore obtains the relation

$$W(\cos\vartheta,\varphi) = W(-\cos\vartheta, \pi+\varphi) \quad . \tag{25}$$

A more mathematical treatment of the P invariance and its consequences can be found, for example, in reference 9).

V. GENERAL PROPERTIES OF THE DENSITY MATRIX OF THE PRODUCED RESONANCE

We list here only briefly those properties of the density matrix which are of importance in our connection. A more detailed discussion of the density matrix can be found, for example, in reference 9).

Let $|\mu\rangle$ be the pure spin states which contribute with weights p_μ to the quantum mechanical mixture of the resonance d. The density operator is then defined by

$$\rho = \sum_\mu |\mu\rangle p_\mu \langle\mu| \qquad \text{with} \sum_\mu p_\mu = 1 \quad . \tag{26}$$

The states $|\mu\rangle$ may be expanded in a complete set of orthogonal and normalized spin states for which we take the $2J+1$ eigenstates $|m\rangle$ of the z component of the spin operator of d. In this representation the ρ operator is a $(2J+1)$ dimensional matrix (density matrix) with the elements

$$\rho_{mm'} = \langle m|\rho|m'\rangle = \sum_\mu \langle m|\mu\rangle p_\mu \langle\mu|m'\rangle \quad . \tag{27}$$

General properties of the density matrix are:

$$0 \le \rho_{mm} = \sum_\mu |\langle m|\mu\rangle|^2 p_\mu \le 1; \quad \rho_{mm} \text{ is real, see (30);} \tag{28}$$

ρ_{mm} is the weight with which the state $|m\rangle$ is contained in the mixture.

$$\sum_m \rho_{mm} = \mathrm{Tr}\ \rho = 1 \quad , \tag{29}$$

$$\rho^+ = \rho, \text{ i.e. } \rho_{mm'} = \rho^*_{m'm} \ (\rho \text{ is Hermitian}). \tag{30}$$

From parity conservation in the production process $a + b \to c + d$ with unpolarized incident particles it follows that

$$\rho_{mm'} = (-1)^{m-m'} \rho_{-m,-m'} \ , \nearrow\searrow \ \rho_{mm} = \rho_{-m,-m} \tag{31}$$

(see Dr. Pilkuhn's lecture). From (30) and (31) one sees immediately that the elements $\rho_{m,-m}$ in the diagonal going from the right upper to the left lower corner of the density matrix are real for integer values of J (mesons) and imaginary for half integer values of J (baryons). Furthermore, from (30) and (31) one obtains the following values for the components of the polarization vector $\vec{P}$ of the particle d:

$$\begin{aligned} P_x &= P_z = 0 \\ P_y &= \sum_m \sqrt{J(J+1) - m(m+1)}\ \mathrm{Im}\ \rho_{m,m+1} \ . \end{aligned} \tag{32}$$

So, the particle d can be polarized only normally to the production plane, as mentioned above.

Exercise: derive equation (32)

Hints for exercise:

(a) $$\vec{P} = \langle \vec{J} \rangle = \mathrm{Tr}(\rho \vec{J}) \quad .$$

In order to obtain the matrix representation of the operators J_x and J_y (J_z is diagonal with its eigenvalues m in the diagonal) introduce

(b) $$\begin{aligned} J_+ &= J_x + iJ_y \\ J_- &= J_x - iJ_y \end{aligned}$$

with the known properties

(c) $$J_\pm |m\rangle = \sqrt{J(J+1) - m(m \pm 1)}\ \ |m \pm 1\rangle \ .$$

Insert matrix elements of J_x, J_y, J_z into (a) and calculate (32).

A $(2J+1)$ dimensional matrix with complex elements has $2(2J+1)^2$ real parameters. Due to the constraints (29), (30) and (31) the number of real independent parameters is

$$\begin{aligned} &2J(J+1) && \text{for integer } J, \text{ and} \\ &2J(J+1)-\tfrac{1}{2} && \text{for half integer } J. \end{aligned} \tag{33}$$

From (29), (30) and (31) it follows that the density matrices for a $J = 1$ meson and a $J = \frac{3}{2}$ baryon have respectively the forms

$$\rho(J=1) = \begin{pmatrix} \frac{1}{2}(1-\rho_{00}) & \rho_{10} & \rho_{1,-1} \\ \rho^*_{10} & \rho_{00} & -\rho^*_{10} \\ \rho_{1,-1} & -\rho_{10} & \frac{1}{2}(1-\rho_{00}) \end{pmatrix} \tag{34}$$

with real ρ_{00} and $\rho_{1,-1}$, and complex ρ_{10} [4 parameters, see (33)], and

$$\rho(J=\tfrac{3}{2}) = \begin{pmatrix} \rho_{33} & \rho_{31} & \rho_{3,-1} & \rho_{3,-3} \\ \rho^*_{31} & \frac{1}{2}-\rho_{33} & \rho_{1,-1} & \rho^*_{3,-1} \\ \rho^*_{3,-1} & -\rho_{1,-1} & \frac{1}{2}-\rho_{33} & -\rho^*_{31} \\ -\rho_{3,-3} & \rho_{3,-1} & -\rho_{31} & \rho_{33} \end{pmatrix} \tag{35}$$

with real ρ_{33}, imaginary $\rho_{1,-1}$, $\rho_{3,-3}$ and complex ρ_{31}, $\rho_{3,-1}$ [7 parameters, see (33)]. These forms of the density matrices have been used in the derivation of the decay distributions (19) and (22).

VI. PREDICTIONS OF THE OME MODEL ON THE DENSITY MATRIX ELEMENTS

From now on we consider the vertex aec of Fig. 10 to be the meson vertex, and the vertex bed to be the baryon vertex. The incident particles a and b are assumed to be a pseudoscalar (0^-) meson (π,K) and a nucleon ($\frac{1}{2}^+$), respectively. This situation is realized in almost all experiments, except for nucleon-nucleon collision which we do not discuss here explicitly. Then from angular momentum and parity conservation at the vertices, predictions about the density matrix elements can be made depending on the spin J_e and parity P_e of the exchanged meson. We derive some of these predictions here although they are modified (often only slightly) when taking into account absorptive effects which lead to a diagram more complicated than the one of Fig. 10 (see Section IX).

Exercise: check equation (33).

1. Vector meson (1^-) production

a) $J_e^{P_e} = 0^-$ (pseudoscalar exchange)

Figure 15 shows the process occurring at the meson vertex in the rest frame of c. L is the relative orbital angular momentum of a and e.

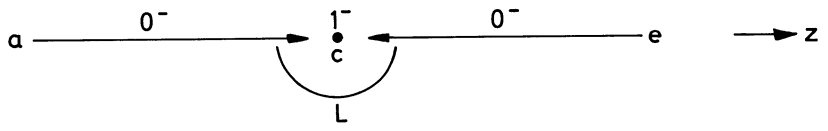

Fig. 15

Angular momentum conservation: $L = 1$ with $L_z = 0$ ($\vec{L}$ has no component along the direction of the incident particles which is, according to Section IV, the direction z of quantization). Parity is then conserved: $P_a P_e (-1) = P_c$ (one sees from here that a 0^+ exchange is forbidden. Conservation of the z component of angular momentum: $m = L_z = 0$, where m is the z component of the spin of c. The states $|m = \pm 1\rangle$ thus do not occur in the mixture consisting of the states $|\mu\rangle$. Therefore, the coefficients $\langle m = \pm 1|\mu\rangle$ vanish and

$$\rho_{\pm 1,m} = \rho_{m,\pm 1} = 0 \qquad (36a)$$

according to (27); only $\rho_{00} \neq 0$ and because of (29):

$$\rho_{00} = 1 \ . \qquad (36b)$$

For this case the decay distributions (19) and (21) of the 1^- meson thus simplify to

$$W(\cos\vartheta,\varphi) = \frac{3}{4\pi}\cos^2\vartheta;\ W(\cos\vartheta) = \tfrac{3}{2}\cos^2\vartheta,\ W(\varphi) = \frac{1}{2\pi} = \text{const.} \qquad (37)$$

b) $P_e = (-1)^{J_e}$, $J_e \geq 1$ (natural parity)

Figure 16 shows the process taking place at the vertex aec for this case.

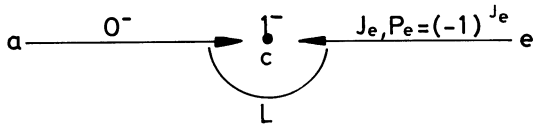

Fig. 16

Angular momentum conservation: $L = J_e - 1,\ J_e,\ J_e + 1$ with $L_z = 0$ (vectors $\vec{L}$ of these magnitudes can be composed with $\vec{J}_e$ to give the spin 1 of the produced vector meson c). Parity conservation: $P_a(-1)^{J_e}(-1)^L = P_c$, $\nearrow\!\!\searrow$ $L + J_e$ is even. Together: $L = J_e$. Conservation of z component of angular momentum: $J_{ez} = m = 0, \pm 1$. However, only the two spin states $|J_e, \pm 1>$ can be coupled with the orbital angular momentum state $|L = J_e, 0>$ to give the states $|J_c = 1, m = \pm 1>$ of c; the two states $|J_e, 0>$ and $|L = J_e, 0>$ cannot be composed to $|J_c = 1, m = 0>$. This is so because the Clebsch-Gordan coefficient $<L = J_e, J_e; 0,0|J_c = 1, m = 0>$ vanishes for odd $L + J_e + J_c$; in the expansion of $|L = J_e, 0>|J_e, 0>$ into eigenstates $|J,0>$ of the total angular momentum only those with even J occur. Thus, it follows that $m = \pm 1$; $|m = 0>$ does not occur in the mixture. Therefore, $<m = 0|\mu> = 0$, and from (27):

$$\rho_{0m} = \rho_{m0} = 0, \quad \text{in particular:} \quad \rho_{00} = 0, \nearrow\!\!\searrow \rho_{11} = \tfrac{1}{2}$$
$$\text{due to (29) and (31);} \quad \rho_{1,-1} \text{ is arbitrary and real.} \tag{38}$$

So the decay distributions (19) and (21) for this case are:

$$W(\cos\vartheta,\varphi) = \frac{3}{4\pi}(\tfrac{1}{2} - \rho_{1,-1}\cos 2\varphi)\sin^2\vartheta$$
$$W(\cos\vartheta) = \tfrac{3}{4}\sin^2\vartheta; \quad W(\varphi) = \frac{1}{4\pi}\left\{(1 + 2\rho_{1,-1}) - 4\rho_{1,-1}\cos^2\varphi\right\}. \tag{39}$$

c) $P_e = -(-1)^{J_e}$, $J_e \geq 1$ (unnatural parity)

Angular momentum conservation: $L = J_e + 1,\ J_e,\ J_e - 1$
Parity conservation $P_a(-1)^{J_e+1}(-1)^L = P_c$, $\nearrow\!\!\searrow$ $L + J_e$ is odd
$\Big\}\nearrow\!\!\searrow\ L = J_e \pm 1.$

In this case all three spin orientations $m = 0, \pm 1$ are allowed, since now $L + J_e + J_c = 2J_e \pm 1 + 1$ is even and the Clebsch-Gordan coefficient $<L,J_e; 0,0|1,0>$ does not vanish. Therefore, in general, all three matrix elements ρ_{00}, $\rho_{1,-1}$, ρ_{10} are different from zero. In particular, one sees that ρ_{10} is different from zero only for the exchange of a particle with unnatural parity and $J_e \geq 1$.

2. Production of a $\frac{3}{2}^+$ baryon resonance

Since the incident nucleon b has spin, the baryon vertex bed cannot be treated as easily as the meson vertex aec; only for $J_e = 0$ predictions about the density matrix elements of the resonance d can be made. For the case of N* production by $\rho(1^-)$ exchange a specific model has been developed by Stodolsky and Sakurai[10].

a) $J_e = 0$

Figure 17 shows the process occurring at the vertex bed in the rest system of d.

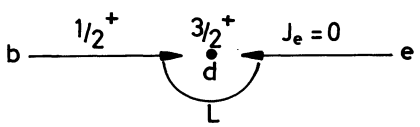

Fig. 17

Angular momentum conservation: $L = 1,2$ with $L_z = 0$ $\Big\}\nearrow\searrow$ $L = 1$ for $P_e = -1$
Parity conservation: $P_b P_e (-1)^L = P_d$, $\nearrow\searrow P_e = (-1)^L$ $\Big\}\nearrow\searrow$ $L = 2$ for $P_e = +1$.

Conservation of the z component of the angular momentum: $m = J_{bz} = \pm \frac{1}{2}$. Thus, the states $|m = \pm \frac{3}{2}>$ do not occur in the mixture of states $|\mu>$ of the resonance d: $<m = \pm \frac{3}{2}|\mu> = 0$. Therefore,

$$\rho_{\pm 3,m} = \rho_{m,\pm 3} = 0, \text{ in particular } \rho_{33} = 0,$$
$$\nearrow\searrow \rho_{11} = \frac{1}{2} \text{ from (29) and (31).} \tag{40}$$

Thus, the decay distributions (22) and (23) simplify to

$$W(\cos\Theta,\Phi) = \frac{1}{8\pi}(1 + 3\cos^2\Theta);$$
$$W(\cos\Theta) = \frac{1}{4}(1 + 3\cos^2\Theta),\ W(\Phi) = \frac{1}{2\pi} = \text{const.} \tag{41}$$

b) N* production by ρ exchange

Since the ρ meson has the same quantum numbers as the γ, Stodolsky and Sakurai[10] have treated the vertex $N\rho N^*$ in analogy to the vertex $N\gamma N^*$ in terms of electromagnetic multipole transitions. This latter vertex occurs in the photoproduction of a pion: $\gamma N \to N^* \to N\pi$. For the magnetic dipole transition M1 which dominates in pion photoproduction, the authors found that the produced N* has only the spin orientations $m = \pm \frac{1}{2}$ normally to the production plane, as Dr. Pilkuhn will show in his lecture. This leads to a decay distribution of the form

$$W(\cos\Theta',\Phi') = \frac{1}{8\pi}(1 + 3\cos^2\Theta') \tag{42}$$

in a co-ordinate system (x' y' z') with z' along the normal to the production plane, and x' and y' in the production plane. The z' axis is thus the y axis defined in Section IV, Fig. 13. Θ' is the angle between the decay nucleon from N* and the normal to the production plane, Φ' the corresponding azimuth angle.

The distribution (42) can be derived as follows: Since the states with $m = \pm \frac{3}{2}$ do not occur, the general spin state of the N* is a linear combination, $a|\frac{3}{2},\frac{1}{2}> + b|\frac{3}{2},-\frac{1}{2}>$, of the two spin states $|J,J_z> = |\frac{3}{2},\pm\frac{1}{2}>$ with

$$|a|^2 + |b|^2 = 1 \tag{43}$$

because of normalization. The decomposition of the spin states into orbital angular momentum states $Y_\ell^m(\cos\Theta',\Phi')$ of the decay nucleon and pion and into the spin states $|\frac{1}{2},\pm\frac{1}{2}>$ of the nucleon reads

$$|\tfrac{3}{2},\pm\tfrac{1}{2}> = \sqrt{\tfrac{2}{3}}Y_1^0|\tfrac{1}{2},\pm\tfrac{1}{2}> + \sqrt{\tfrac{1}{3}}Y_1^{\pm 1}|\tfrac{1}{2},\mp\tfrac{1}{2}> \tag{44}$$

(ℓ = 1 because of parity conservation in N* decay.) Inserting this into the linear combination yields:

$$a\left|\tfrac{3}{2},\tfrac{1}{2}\right\rangle + b\left|\tfrac{3}{2},-\tfrac{1}{2}\right\rangle = \left(\sqrt{\tfrac{2}{3}}\, aY_1^0 + \sqrt{\tfrac{1}{3}}\, bY_1^{-1}\right)\left|\tfrac{1}{2},\tfrac{1}{2}\right\rangle + \left(\sqrt{\tfrac{1}{3}}\, aY_1^1 + \sqrt{\tfrac{2}{3}}\, bY_1^0\right)\left|\tfrac{1}{2},-\tfrac{1}{2}\right\rangle . \tag{45}$$

Remembering that

$$Y_1^0(\cos\Theta',\Phi') = \sqrt{\frac{3}{4\pi}}\cos\Theta', \quad Y_1^{\pm 1}(\cos\Theta',\Phi') = \mp\sqrt{\frac{3}{8\pi}}\sin\Theta'\, e^{\pm i\Phi'} , \tag{46}$$

one obtains with (43)

$$\begin{aligned} W(\cos\Theta',\Phi') &= \left|\sqrt{\tfrac{2}{3}}\, aY_1^0 + \sqrt{\tfrac{1}{3}}\, bY_1^{-1}\right|^2 + \left|\sqrt{\tfrac{1}{3}}\, aY_1^1 + \sqrt{\tfrac{2}{3}}\, bY_1^0\right|^2 \\ &= \frac{1}{8\pi}(1+3\cos^2\Theta') . \end{aligned} \tag{47}$$

This distribution is transformed into the original system xyz by the transformation $z' = y$, $x' = x$, $y' = -z$:

$$\cos\Theta' = \sin\Theta\sin\Phi, \quad \sin\Theta'\cos\Phi' = \sin\Theta\cos\Phi, \quad \sin\Theta'\sin\Phi' = -\cos\Theta . \tag{48}$$

Since the Jacobian for this transformation is unity, one obtains

$$W(\cos\Theta,\Phi) = W(\cos\Theta',\Phi') = \frac{1}{8\pi}(1+3\sin^2\Theta\sin^2\Phi) . \tag{49}$$

Comparing this with the general form (22) one finds the following Stodolsky-Sakurai predictions on the density matrix elements for N* production by ρ exchange in an M1 transition

$$\rho_{33} = \tfrac{3}{8} = 0.375, \quad \mathrm{Re}\,\rho_{3,-1} = \frac{\sqrt{3}}{8} = 0.216, \quad \mathrm{Re}\,\rho_{31} = 0 . \tag{50}$$

VII. EXPERIMENTAL METHODS OF DETERMINING THE DENSITY MATRIX ELEMENTS

1. Method of maximum likelihood

The best method of determining the density matrix elements of a resonance is the maximum likelihood method. Let us assume, as an example, that we have n events in which a ρ meson is produced; for each event the decay angles ϑ_ν and φ_ν are measured. We denote for the moment the three matrix elements ρ_{00}, $\rho_{1,-1}$ and Re ρ_{10} occurring in the decay distribution (19) by x_1, x_2, and x_3. Then the likelihood function for the experiment is defined by

$$\mathcal{L}(x_1,x_2,x_3) = \prod_{\nu=1}^{n} W(\cos\vartheta_\nu,\varphi_\nu;\ x_1,x_2,x_3) . \tag{51}$$

For given sets of values (x_1,x_2,x_3) one calculates with a computer $\mathcal{L}(x_1,x_2,x_3)$ by inserting the experimental values ϑ_ν and φ_ν of the ν-th event into (19) and computing the product (51). By varying (x_1,x_2,x_3) one finds the set (x_1^*,x_2^*,x_3^*) that gives the maximum value of $\mathcal{L}(x_1,x_2,x_3)$. This set is then the best estimate for the matrix elements.

The error matrix $(\overline{\delta x_i\ \delta x_j})$ of the matrix elements $(\Delta x_i = \sqrt{\overline{\delta x_i\ \delta x_i}})$ is (for n not too small) the inverse of the matrix H with the elements

$$H_{ij} = - \frac{\partial^2 \ln \mathcal{L}(x_1,x_2,x_3)}{\partial x_i\ \partial x_j} \Bigg|_{x_{1,2,3} = x^*_{1,2,3}} , \quad \overline{\delta x_i\ \delta x_j} = (H^{-1})_{ij} . \tag{52}$$

The matrix H also can be calculated by computer from the experimental values ϑ_ν, Φ_ν and the best estimates for the matrix elements.

If it is not possible experimentally to obtain a pure unbiased sample of ρ mesons, one should, according to the background subtraction method discussed in Section II, determine the matrix elements x^*_{ia} for all n_a events in the ρ mass region, and then the ones (x^*_{ib}) for events in the adjacent regions representing the background under the ρ peak. From these two sets of matrix elements, and from the number n_b of background events (known from the effective mass distribution) in the ρ region, the matrix elements x^*_i of the ρ can be calculated:

$$x^*_{ia} = \frac{n_b x^*_{ib} + (n_a - n_b)x^*_i}{n_a} . \tag{53}$$

2. Method of moments

The average value $\bar{f}$ of a function $f(\cos\vartheta,\varphi)$ of the decay angles ϑ and φ is given by

$$\bar{f} = \int_0^{2\pi} d\varphi \int_{-1}^{+1} d\cos\vartheta\ f(\cos\vartheta,\varphi)\ W(\cos\vartheta,\varphi) , \tag{54}$$

since $W(\cos\vartheta,\varphi)$ is normalized [see (20)]. Inserting (19) into (54) one finds

$$\begin{aligned} \overline{\cos^2\vartheta} &= \tfrac{1}{5}(1 + 2\rho_{00}) \\ \overline{\sin^2\vartheta\cos 2\varphi} &= -\tfrac{4}{5}\,\rho_{1,-1} \\ \overline{\sin 2\vartheta\cos\varphi} &= -\frac{4\sqrt{2}}{5}\,\mathrm{Re}\,\rho_{10} . \end{aligned} \tag{55}$$

The corresponding formulae for the decay of a $\tfrac{3}{2}$ baryon obtained by inserting (22) into (54) are:

$$\begin{aligned} \overline{\cos^2\Theta} &= -\tfrac{1}{15}(7 - 8\rho_{33}) \\ \overline{\sin^2\Theta\cos 2\Phi} &= -\frac{8}{5\sqrt{3}}\,\mathrm{Re}\,\rho_{3,-1} \\ \overline{\sin 2\Theta\cos\Phi} &= -\frac{8}{5\sqrt{3}}\,\mathrm{Re}\,\rho_{31} . \end{aligned} \tag{56}$$

Thus, from the experimental mean values the corresponding density matrix elements can be obtained by (55) and (56). The error $\Delta\bar{f}$ of $\bar{f}$ is given by

$$\Delta\bar{f} = \sqrt{\frac{1}{n}(\overline{f^2} - \bar{f}^2)} \tag{57}$$

where n is the number of events.

If the sample of resonance events is contaminated by background, the subtraction procedure as described in connection with the maximum likelihood method should be applied.

3. Method of least squares fit

Two of the three matrix elements occurring in the decay distributions can be determined from the experimental distribution in one angle only ($\cos\vartheta,\varphi$; $\cos\Theta,\Phi$). According to (21) and (23) these distributions are all of the form

$$W = A + B\cos^2\Psi \ . \tag{58}$$

A least squares fit of (58) to the experimental distribution yields the values for the coefficients A and B, and the error matrix

$$\begin{pmatrix} \overline{\delta A \delta A} & \overline{\delta A \delta B} \\ \overline{\delta A \delta B} & \overline{\delta B \delta B} \end{pmatrix} \ . \tag{59}$$

From a comparison of (58) with the formulae (21) and (23), one finds that the matrix elements are then given by

$$\begin{aligned} \rho_{00} &= \frac{A_1 + B_1}{3A_1 + B_1} \ , \qquad \rho_{1,-1} = -\tfrac{1}{2}\,\frac{B_2}{2A_2 + B_2} \ , \\ \rho_{33} &= \tfrac{1}{4}\,\frac{3A_3 - B_3}{3A_3 + B_3} \ , \quad \mathrm{Re}\ \rho_{3,-1} = -\frac{\sqrt{3}}{4}\,\frac{B_4}{2A_4 + B_4} \ . \end{aligned} \tag{60}$$

By differentiating these formulae one obtains expressions for the errors of the matrix elements in terms of the elements of the error matrix (59). For instance, the error in ρ_{00} is given by

$$\Delta\rho_{00} = \frac{2}{(3A_1 + B_1)^2}\sqrt{A_1^2\overline{\delta B_1 \delta B_1} + B_1^2\overline{\delta A_1 \delta A_1} - 2A_1B_1\overline{\delta A_1 \delta B_1}} \ . \tag{61}$$

VIII. Δ^2 DISTRIBUTIONS

In the previous sections the angular decay distributions have turned out to be an important tool to study the production mechanism of the process

$$a + b \to c + d \ . \tag{1}$$

A second source of information about this mechanism is the Δ^2 distribution $d\sigma/d\Delta^2$ for reaction (1), as was already briefly outlined in Section I. The Δ^2 distribution is, according to (2), equivalent to the distribution of the production angle. Theoretically, the Δ^2 distribution is given in the peripheral model (Fig. 10) by the Δ^2 dependence of the propagator and of the two vertex functions [formula (4)]. The propagator $1/(\Delta^2 + m_e^2)$ enhances small Δ^2 values. The vertex functions for the vertices aec and bed in Fig. 10 can be calculated in perturbation theory by using the Feynman rules derived from the interaction by which the particles at a vertex are coupled. This will be demonstrated by Dr. Pilkuhn for some examples. It turns out that they are increasing functions of Δ^2; the increase is the stronger the higher the spins are of the particles c and d in the final state. Thus, the fall-off of the Δ^2 distribution as predicted only by the propagator is more or less strongly reduced. Now for all quasi-two-body reactions of type (1) studied so far, it was found that the experimental Δ^2 distribution falls off steeper than the one predicted from the peripheral model of Fig. 10. Thus, one may say that the reactions proceed more peripherally than the peripheral model predicts. As a typical example we show in Fig. 18 the Δ^2 distribution for $\pi^+ p \to \rho^+ p$ at 2.75 GeV/c [7,11]. The curve (A) is calculated from the one-pion exchange formula (the reaction $\pi^+ p \to \rho^+ p$ was found to proceed practically completely via π exchange); it does not fit the data at all.

Two approaches have been used to overcome the discussed difficulty of the peripheral model:

a) The first approach is mainly due to Ferrari and Selleri [12,13]: For each of the two vertex functions and for the propagator of Fig. 10, a Δ^2 dependent form factor has been introduced by which the vertex function and the propagator, as calculated from perturbation theory, is to be multiplied. Thus, in the matrix element (4) for the peripheral diagram of Fig. 10 there occurs a product $F(\Delta^2)$ of three form factors. The vertex form factors are supposed to take into account higher order effects due to which the vertices have an internal structure. Similarly, the propagator form factor is a correction to the perturbative form $1/(\Delta^2 + m_e^2)$ of the propagator. Since the coupling constant occurring in a vertex function is defined such that it gives the value of the vertex function at the pole $\Delta^2 = -m_e^2$, the corresponding form factor is unity for $\Delta^2 = -m_e^2$. The same holds for the form factor of the propagator. Thus, $F(-m_e^2)$ should be unity.

Until now no theory exists which allows one to calculate form factors. Therefore, the function $F(\Delta^2)$ occurring in the theoretical expression of a Δ^2 distribution has been parameterized in a more or less arbitrary fashion, and the parameters have then been adjusted to the experiments. Since the experimental Δ^2 distributions fall off more rapidly than the peripheral model without form factors predicts, agreement between experiment and theory is restored with functions $F(\Delta^2)$ which decrease with increasing Δ^2. It was found that the experimental Δ^2 distributions for several one-pion exchange reactions, such as $NN \to NN\pi$, $\pi N \to \rho N$, $\pi N \to N\pi\pi\pi$, at various primary energies could well be reproduced theoretically by the introduction of one empirical form factor of the form [14]

$$F(\Delta^2) = \frac{0.72}{1 + \frac{\Delta^2 + \mu^2}{4.73\,\mu^2}} + \frac{0.28}{1 + \left(\frac{\Delta^2 + \mu^2}{32\,\mu^2}\right)^2} \quad , \quad [F(-\mu^2) = 1,\ \mu = \text{pion mass}] \quad . \quad (62)$$

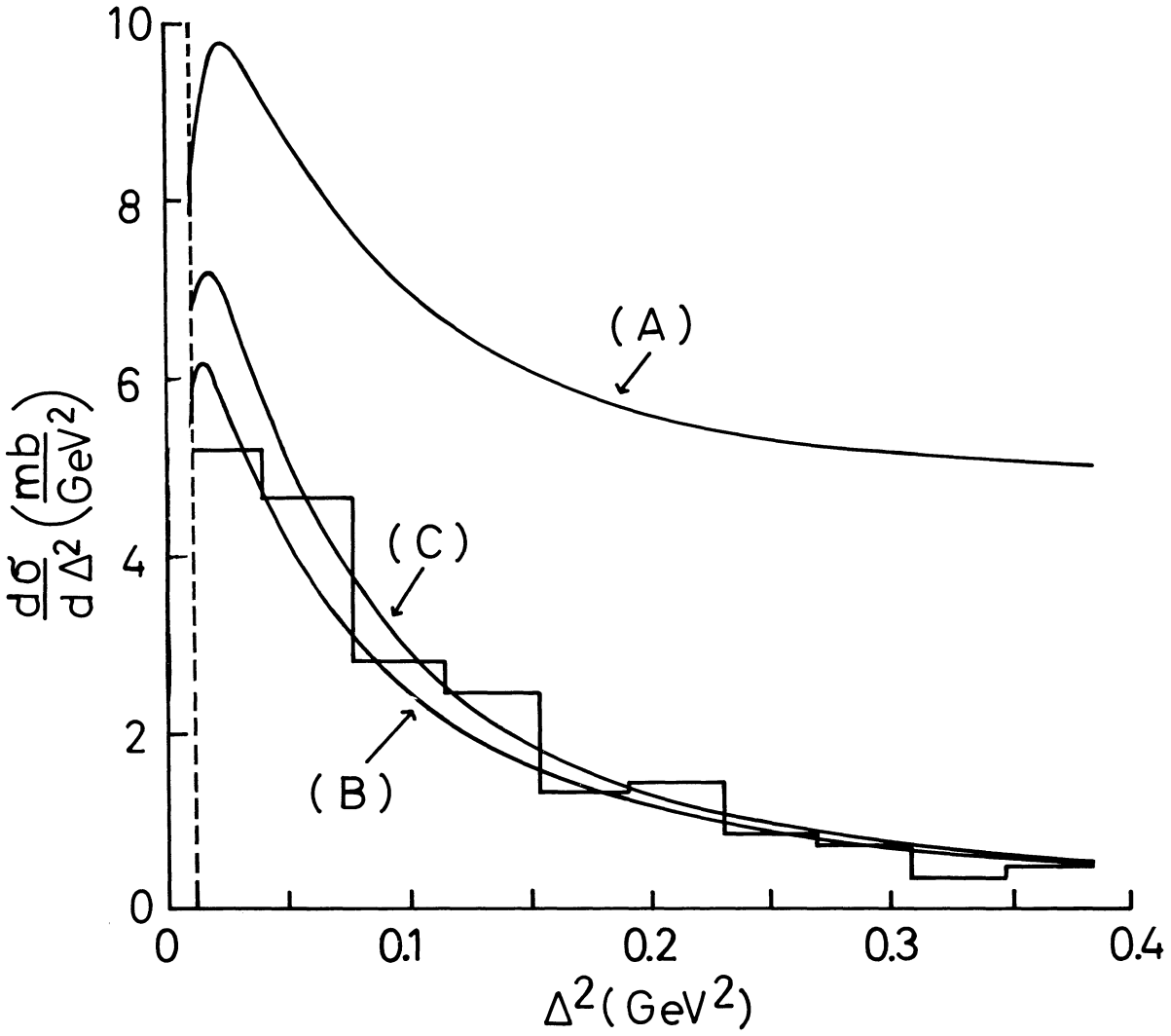

Fig. 18 Δ^2 distribution for the reaction $\pi^+ p \to \rho^+ p$ at 2.75 GeV/c. The curves show the predictions (A) of the unmodified OPE model, (B) of the OPE model with the Amaldi-Selleri form factor, and (C) of the absorptive OPE model.

As an example the curve (B) in Fig. 18 shows the prediction of the one-pion exchange formula, including the form factor (62).

On the other hand, the study of reactions for which π exchange is forbidden has led to much less satisfactory results: in order to fit, for example, the experimental Δ^2 distribution for the reaction $\pi N \to \pi N^*$ which can proceed only via ρ exchange (see Table I), a form factor $F(\Delta^2)$ had to be introduced which depends rather strongly on Δ^2, so that the Δ^2 dependence of the propagator is masked. Furthermore, in order to fit the reaction $\pi N \to \pi N^*$ at different primary energies a "form factor" $F(\Delta^2)$ was needed which depends on the primary energy[15], whereas a genuine form factor should be a function of Δ^2 only. So at least for non-π exchange reactions there are heavy doubts as to whether the "form factors" have any physical meaning, i.e. whether they are more than just arbitrary fitting functions which allow a fit of the theoretical formulae to the experimental Δ^2 distribution. So we will not discuss the form factor approach any further.

b) Because of the rather unsatisfactory results of the form factor approach, one has tried another method to reconcile the peripheral model with the experiments[5,7,16,17]: the absorptive model has been developed which can be regarded as a refinement of the simple peripheral model. The absorptive model is briefly sketched in the next section; a more rigorous treatment is given by Dr. Pilkuhn.

IX. THE ABSORPTIVE MODEL

The idea of the absorptive model is the following: in the collision of the particles a and b there are at higher energies many inelastic open channels which all contribute to the total inelastic cross-section. These channels compete with each other and suppress each other in frequency. In particular, the quasi-two-body reaction is reduced by the presence of the other absorptive channels. This absorptive effect is the stronger, the closer the incident particles get together in the collision, i.e. the smaller their impact parameter b is. In other words, one would expect mainly the partial waves with small orbital angular momentum l to contribute to the absorption, since l and b are related by the well-known relationship

$$\hbar^2 l(l+1) = (pb)^2 \qquad (63)$$

where p is the c.m.s. momentum of the incident particles. Thus, mainly the contribution of the low partial waves to the quasi-two-body channel is suppressed by the occurrence of the absorptive processes; the suppression is the stronger, the smaller l is. On the other hand, the collisions in the lower angular momentum states, i.e. with small impact parameter, lead to larger scattering angles, i.e. to higher values of Δ^2 for the reaction $a+b \to c+d$. (For s-wave scattering the angular, and therefore the Δ^2, distribution is isotropic!) Thus, by reducing the contribution of the low partial waves, the absorptive effects suppress the frequency of reactions with higher Δ^2; the Δ^2 distribution falls off more sharply than the simple peripheral model, without absorption, predicts. This is in at least qualitative agreement with the experimental observation.

The quantitative formulation of the idea of the absorptive model starts from the diagram of Fig. 19, which replaces the simpler purely peripheral diagram of Fig. 10.

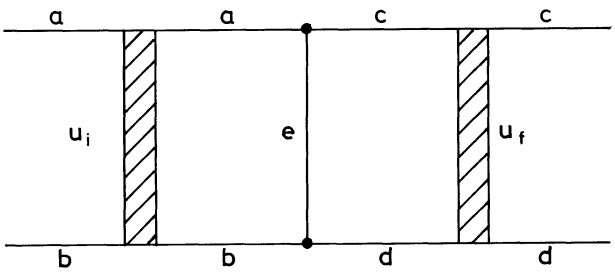

Fig. 19

The absorptive effects are taken into account by an interaction U_i and U_f of the particles in the initial and final state, respectively. Dr. Pilkuhn will say more about the nature of this interaction and about the theoretical treatment of the absorptive model.

There are two main results of the model:

a) The theoretical Δ^2 distribution is collimated towards small values, as has already been discussed.

b) The predictions on the density matrix elements are modified. They are no longer as simple as discussed in Section VI, but depend now on the production angle, i.e. on Δ^2. That the matrix elements are changed can be understood qualitatively from the following consideration: let us assume the particle c to be a resonance, the density matrix elements of which are to be predicted. In Section VI, the predictions were made from angular momentum and parity conservation at the vertex aec of Fig. 10, in the rest frame of c with the direction of a as the axis of quantization. In the absorptive model of Fig. 19, however, the experimentally observed rest system of c after the final state interaction U_f is no longer the rest system of c when it emerges from the vertex aec. Furthermore, due to the interaction U_i in the initial state, the known direction of a before the interaction U_i is not the direction of a at the vertex aec. Therefore, since the decay angular distribution and thereby the matrix elements of c are measured in the rest frame of c <u>after</u> the interaction U_f with respect to the direction of a <u>before</u> the interaction U_i, the predictions on these matrix elements made for the process at the vertex aec in the rest frame of c and with respect to the direction of a <u>at that vertex</u> are no longer strictly valid. Since the predictions of the simple peripheral model (Fig. 10) on the matrix elements are often modified by the absorption only slightly (especially for small Δ^2), nevertheless, it was worth while to discuss them in Section VI.

The modified predictions of the absorptive model for various cases will be discussed in the following section in connection with the experimental results.

X. EXPERIMENTAL RESULTS AND COMPARISON WITH THEORY

We do not intend to give in this section a complete review of all experiments on resonance production in quasi-two-body reactions. Only typical experiments on the following seven reactions will be discussed in some detail although some interesting points (e.g. determination of coupling constants) will be left out:

$$\pi^{\pm} p \to \rho^{\pm} p \tag{64}$$

$$\pi^{+} p \to \pi^{0} N^{*++} \tag{65}$$

$$\pi^{+} p \to \rho^{0} N^{*++} \tag{66}$$

$$\pi^{+} p \to \omega^{0} N^{*++} \tag{67}$$

$$K^{\pm} p \to K^{*\pm} p \tag{68}$$

$$K^{+} p \to K^{0} N^{*++} \tag{69}$$

$$K^{+} p \to K^{0*} N^{*++} \tag{70}$$

1. $\pi^{\pm} p \to \rho^{\pm} p$

The Δ^2 distribution for this reaction at 2.75 GeV/c has already been shown up to $\Delta^2 = 0.4$ GeV^2 in Fig. 18. The curve (C) in this figure is the theoretical distribution as predicted by the absorptive model for pure π exchange without any form factor[7]. It fits the experimental histogram rather well. It should be mentioned that the theoretical distribution can be calculated in absolute scale since the $N\pi N$ and the $\pi\pi\rho$ coupling constants which enter the theoretical formula are known; the latter coupling constant is known from the mass and the decay width of the ρ decaying into two pions[4]. The absorptive model was first applied by Gottfried and Jackson[5] to the reaction $\pi^- p \to \rho^- p$ at 4 GeV/c [18]. Also at this momentum the experimental Δ^2 distribution was reproduced well in shape and absolute magnitude by the absorptive model.

Figure 20 shows the distributions of the ρ^+ decay angles $\cos\vartheta$ and φ for the reaction $\pi^+ p \to \rho^+ p$ at 4 GeV/c with $\Delta^2 < 0.3$ GeV^2 [19]. The distributions were obtained by the background subtraction method discussed in Section II. The curves show least squares fits of the form (58). From these fits and from the average value of $\sin 2\vartheta \cos\varphi$, the ρ^+ density matrix elements ρ_{00}, $\rho_{1,-1}$, Re ρ_{10} were determined according to (60) and (55) for $\Delta^2 < 0.3$ GeV^2. The experimental values are tabulated in Table II.

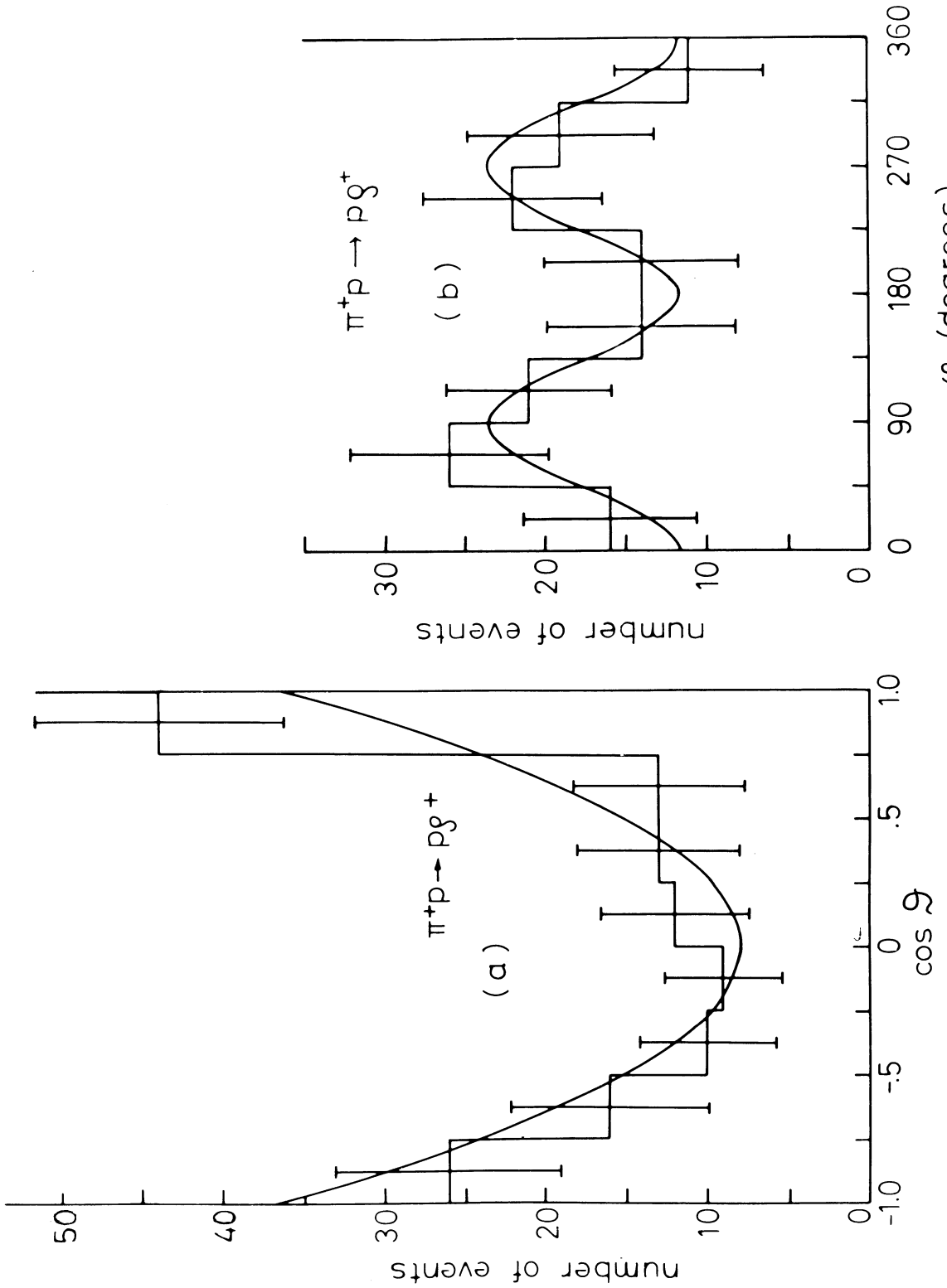

Fig. 20 Distributions of the ρ^+ decay angles (a) cos ϑ and (b) φ for reaction $\pi^+p \to \rho^+p$ at 4 GeV/c with $\Delta^2 < 0.3$ GeV^2. The curves are least squares fits of the form $A + B\cos^2\vartheta$ and $A + B\cos^2\varphi$, respectively.

Table II

Density matrix elements of resonances produced in π^+p collisions at 4 GeV/c

Reaction	vector meson (ρ,ω)			baryon (N*)			Δ^2 range (GeV^2)
	ρ_{00}	$\rho_{1,-1}$	Re ρ_{10}	ρ_{33}	Re $\rho_{3,-1}$	Re ρ_{31}	
$\pi^+p \to \rho^+p$	0.70 ± 0.08	0.17 ± 0.08	-0.074 ± 0.070				< 0.3
$\pi^+p \to \pi^0N^{*++}$				0.40 ± 0.06	0.21 ± 0.08	-0.026 ± 0.072	< 0.3
$\pi^+p \to \rho^0N^{*++}$	0.77 ± 0.04	-0.044 ± 0.035	-0.062 ± 0.025	0.077 ± 0.028	0.011 ± 0.030	-0.013 ± 0.028	< 0.3
$\pi^+p \to \omega^0N^{*++}$	0.47 ± 0.05	0.13 ± 0.05	-0.10 ± 0.03	0.15 ± 0.04	0.035 ± 0.040	-0.048 ± 0.038	< 0.6

Figure 21 shows the ρ^+ density matrix elements as functions of Δ^2 for four Δ^2 intervals below 1 GeV^2. The curves are the theoretical predictions of the absorptive model for pure π exchange. Their agreement with the experimental points is satisfactory; the experimental errors are unfortunately rather large.

Thus from the Δ^2 distribution, as well as from the density matrix elements, it seems that the reaction $\pi^\pm p \to \rho^\pm p$ proceeds via pure π exchange. No evidence was found for a contribution of ω (or A_2) exchange (see Table I).

2. $\pi^+p \to \pi^0N^{*++}$

In the same way the density matrix elements ρ_{33}, Re $\rho_{3,-1}$, Re ρ_{31} of the N^{*++} produced in the reaction $\pi^+p \to \pi^0N^{*++}$ at 4 GeV/c [19] were determined from the experimental distributions of the N^{*++} decay angles cos Θ and Φ, and from the average value of sin 2Θ cos Φ, using the formulae (60) and (56). The experimental values for the Δ^2 range below 0.3 GeV^2 are listed in Table II. It is seen that the results are in very good agreement with the Stodolsky-Sakurai prediction (50) for ρ exchange in an M1 transition at the baryon vertex.

Figure 22 shows the N^{*++} matrix elements for three Δ^2 intervals below 0.3 GeV^2. Above 0.3 GeV^2 there were only very few events so that the matrix elements could not be determined there. So far, the predictions of the absorptive model on these matrix elements have not yet been published. They probably will not deviate strongly from the Stodolsky-Sakurai values. Also, the absorptive model prediction on the Δ^2 distribution for reaction (65) is not yet available in the literature.

The reaction (65) has also been studied at various other primary momenta: 1.59 GeV/c [20], 2.75 GeV/c [21], 3.54 GeV/c [22]. At all momenta the N^{*++} decay distributions were found to agree with the Stodolsky-Sakurai predictions for ρ exchange in an M1 transition.

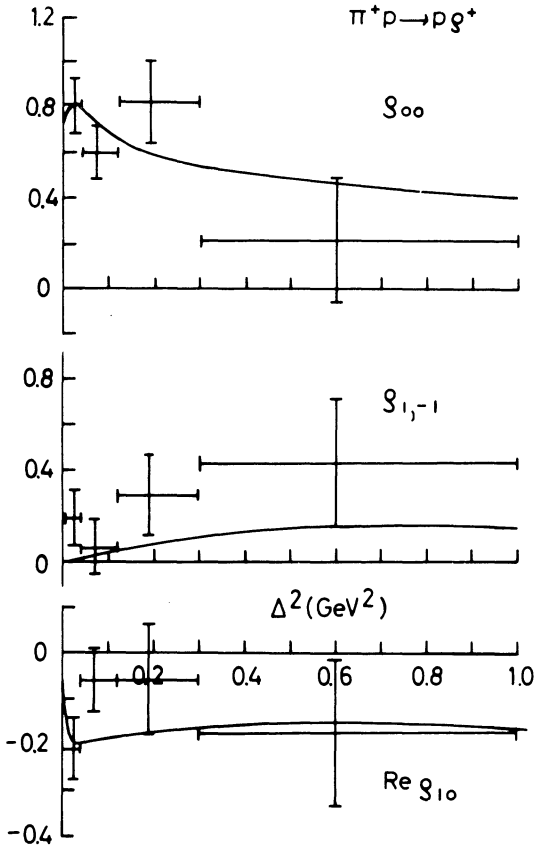

Fig. 21 Density matrix elements of ρ^+ from $\pi^+p \to \rho^+p$ at 4 GeV/c as functions of Δ^2. The curves show the predictions of the absorptive model for OPE.

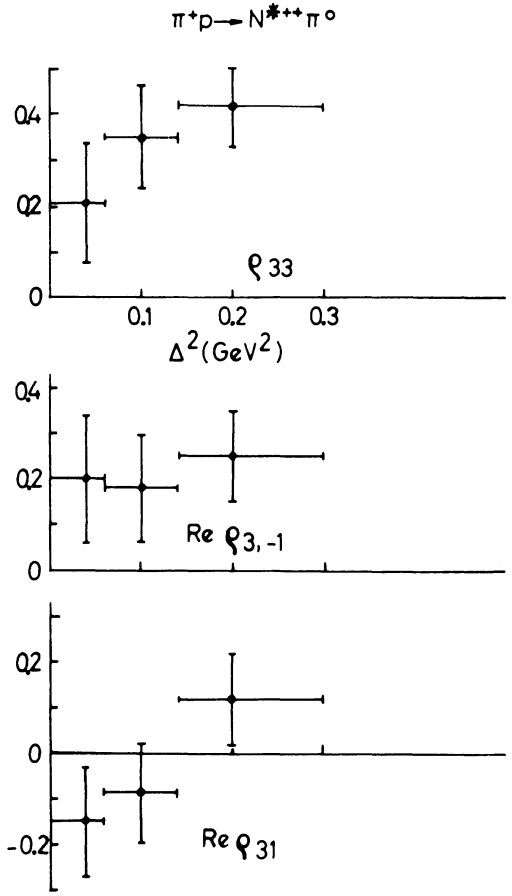

Fig. 22 Density matrix elements of N^{*++} from $\pi^+p \to \pi^0N^{*++}$ at 4 GeV/c as functions of Δ^2.

3. $\pi^+ p \to \rho^0 N^{*++}$

In Section II (Figs. 7 and 9) a method (limitation to small Δ^2) has been discussed by which a rather pure sample of reaction (66) could be isolated from events of the type $\pi^+ p \to p\pi^+\pi^+\pi^-$ at 4 GeV/c [8,23]. From the ρ^0 and N^{*++} decay angular distributions, and from the average values of $\sin 2\vartheta \cos\varphi$ and $\sin 2\Theta \cos\Phi$, the ρ^0 and N^{*++} density matrix elements were determined for $\Delta^2 < 0.3$ GeV^2. The experimental values are listed in Table II.

Figures 23 and 24 show the density matrix elements of ρ^0 and N^{*++}, respectively, for five Δ^2 intervals. The points for the highest Δ^2 region (0.3 GeV^2 to 0.8 GeV^2) have to be taken with caution since the events there were contaminated by background. The curves show the predictions of the absorptive model for pure π exchange [7]. Apart from a few points lying outside the general trend of the experimental Δ^2 dependence, the agreement with the theoretical curves is not bad.

The experimental Δ^2 distribution for reaction (66) could be reproduced in its shape but not in absolute magnitude by the absorptive model [7]; the theoretical distribution was too high by a factor of about three.

The reaction $\pi^+ p \to \rho^0 N^{*++}$ has also been investigated at 3.65 GeV/c [24].

4. $\pi^+ p \to \omega^0 N^{*++}$

As in the case of reaction $\pi^+ p \to \rho N^*$ a pure sample of reaction (67) at 4 GeV/c was obtained from events of the type $\pi^+ p \to p\pi^+\pi^+\pi^-\pi^0$ by limitation to small Δ^2 (< 0.6 GeV^2) [8,23]. Since the ω^0 decays according to

$$\omega^0 \to \pi^+\pi^-\pi^0 \qquad (71)$$

into three pions, the ω decay angles ϑ and φ cannot be defined in the same way as for a resonance decaying into two particles by the formulae (17). It can be shown, however, that for the ω meson (as for any vector meson decaying into three pions) the decay distribution is given by (19) if one takes ϑ to be the angle between the incident π^+ and the normal

$$\hat{m} = \frac{\vec{\pi^-} \times \vec{\pi^0}}{|\vec{\pi^-} \times \vec{\pi^0}|} \qquad (72)$$

to the ω decay plane in the ω rest system; φ is then the corresponding azimuth angle. The ω decay angles ϑ and φ are thus obtained from the formulae (17) if one replaces in them $\vec{\alpha}$ by $\hat{m}$.

From the ω^0 and N^{*++} decay angular distributions, and from the average values of $\sin 2\vartheta \cos\varphi$ for the ω and $\sin 2\Theta \cos\Phi$ for the N^{*++}, the density matrix elements for the two resonances were obtained. The values are listed in Table II for $\Delta^2 < 0.6$ GeV^2.

Figures 25 and 26 show the density matrix elements of the ω^0 and N^{*++} for five Δ^2 intervals. The curves are the theoretical predictions of the absorptive model for ρ exchange by an M1 transition at the baryon vertex [25]. Their agreement with the experimental points is not very good, but within the rather large experimental errors the results may be consistent with ρ exchange.

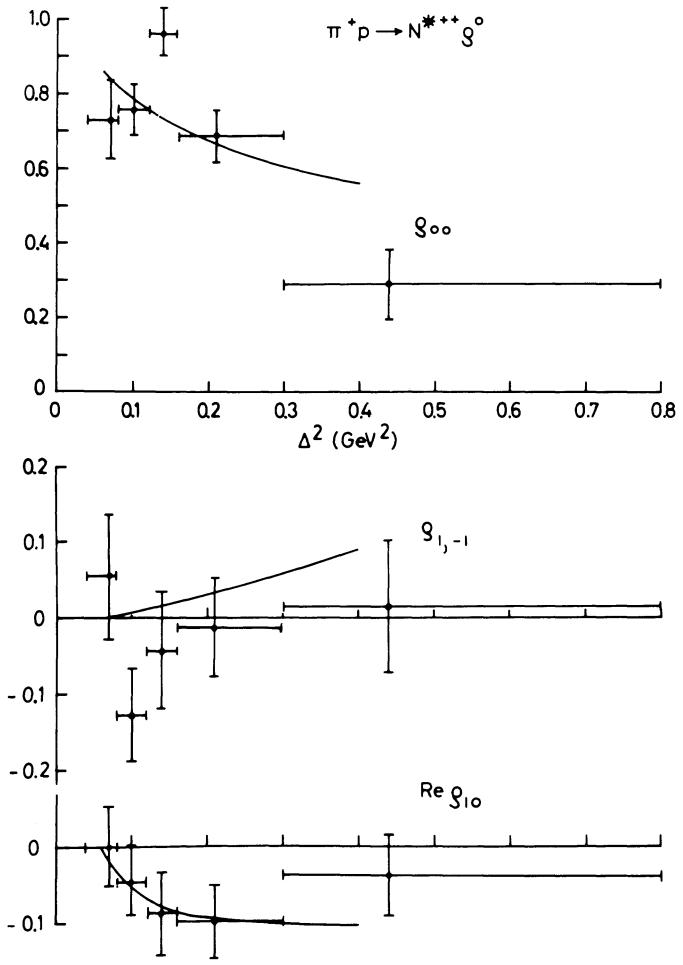

Fig. 23 Density matrix elements of ρ^0 from $\pi^+ p \to \rho^0 N^{*++}$ at 4 GeV/c as functions of Δ^2. The curves show the predictions of the absorptive model for OPE.

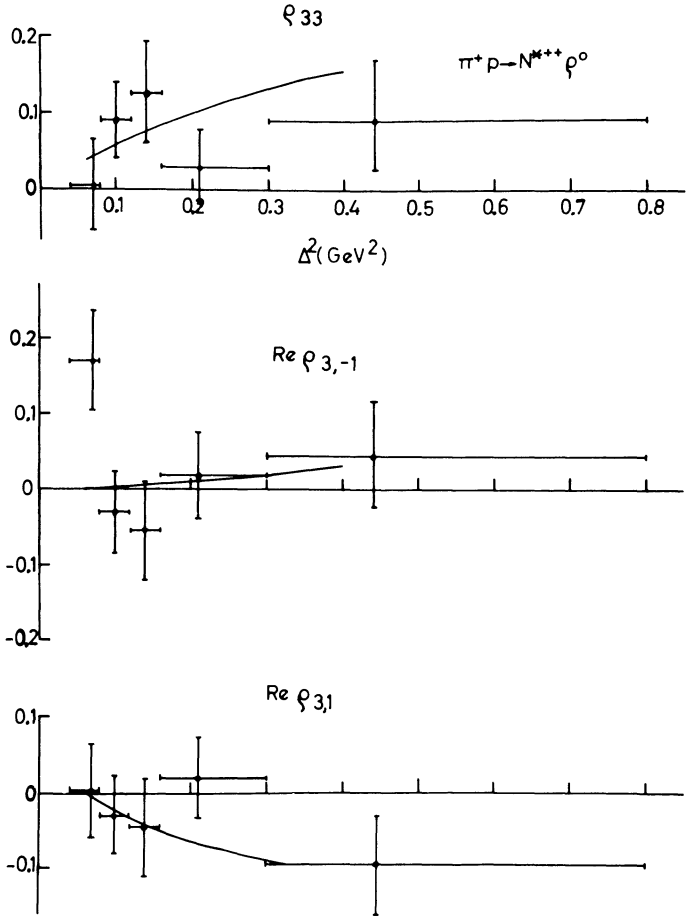

Fig. 24 Density matrix elements of N^{*++} from $\pi^+ p \to \rho^0 N^{*++}$ at 4 GeV/c as functions of Δ^2. The curves show the predictions of the absorptive model for OPE.

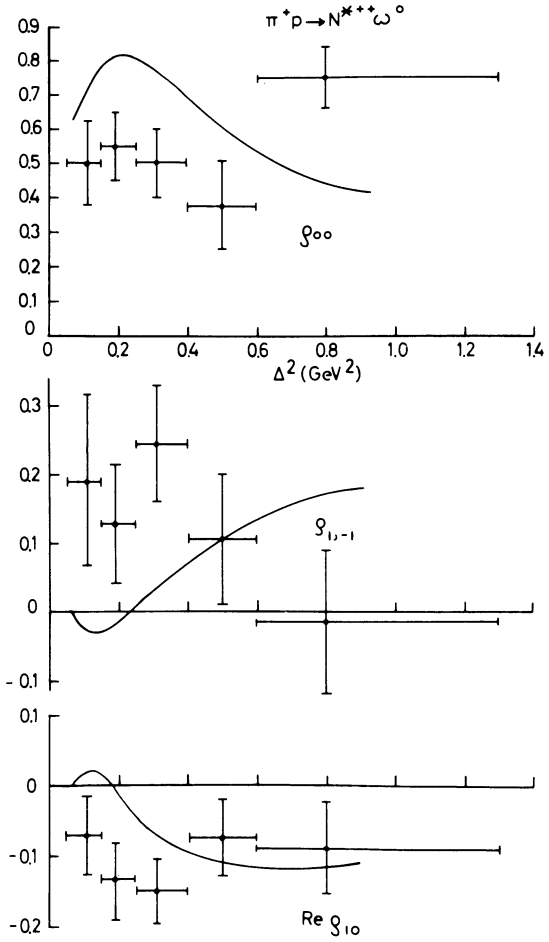

Fig. 25 Density matrix elements of ω^0 from $\pi^+p \to \omega^0 N^{*++}$ at 4 GeV/c as functions of Δ^2. The curves show the predictions of the absorptive model for ρ exchange by M1 transition.

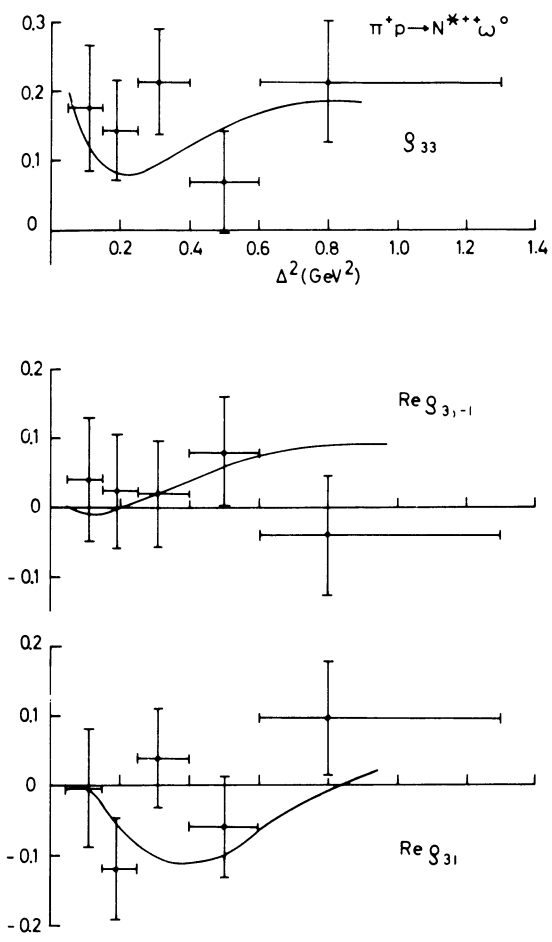

Fig. 26 Density matrix elements of N^{*++} from $\pi^+p \to \omega^0 N^{*++}$ at 4 GeV/c as functions of Δ^2. The curves show the predictions of the absorptive model for ρ exchange by M1 transition.

The experimental Δ^2 distribution of reaction (67) could not be fitted well by the absorptive model for ρ exchange without form factor. However, agreement between the experimental distribution and the absorptive model is restored, when one introduces a form factor of the form

$$F(\Delta^2) = F(0)e^{-0.5\ \Delta^2/GeV^2} \qquad (73)$$

which does not depend very strongly on Δ^2 [25].

5. $K^{\pm}p \rightarrow K^{*\pm}p$

The reaction $K^+p \rightarrow K^{*+}p$ has been studied mainly at the following three primary momenta: 1.45 GeV/c [26], 1.96 GeV/c [27], 3.0 GeV/c [28,29]. We discuss here briefly the experiment at 3.0 GeV/c [see also references (7) and (30)]. Figure 27 shows the experimental Δ^2 distribution up to $\Delta^2 = 0.8$ GeV^2. The π exchange contribution to reaction (68) can be calculated in absolute magnitude from the absorptive model since the $N\pi N$ and $K\pi K^*$ coupling constants are known [the latter is known from the mass and the decay width of the K* decaying into K and π [4]]. Thus, the dashed curve in Fig. 27 shows the prediction of the absorptive model for π exchange only. It is seen that π exchange alone cannot account for the whole cross-section for reaction (68). Therefore, Gottfried, Jackson, and Svensson [7,30] have included vector-meson exchange in their absorptive model calculation, and have adjusted its amount to the experimental Δ^2 distribution and to the experimental values for the K* density matrix elements (see below; the amount of vector-meson exchange is adjustable since the coupling constants for this exchange are not known a priori). The solid curve in Fig. 27 shows the resulting theoretical distribution.

In Fig. 28 the experimental values for the K^{*+} density matrix elements are plotted as functions of Δ^2. The curves show the predictions of the absorptive model for a mixture of π and vector-meson exchange.

It should be noted that the reaction

$$K^+n \rightarrow K^{*0}p \qquad (68a)$$

seems to proceed via π exchange only [7,31]. The difference between this reaction and reaction

$$K^+p \rightarrow K^{*+}p \qquad (68b)$$

is that in (68a) the exchanged particle is charged, whereas it is neutral in (68b). Thus, the vector-meson exchanged in reaction (68b) seems to occur only in the neutral charge state; otherwise its exchange would also contribute to reaction (68a). Therefore, it has isospin zero and must be the ω or φ meson; the ρ meson is excluded.

The reaction $K^-p \rightarrow K^{*-}p$ has been investigated at 3 GeV/c [32], and at 3.5 GeV/c [33]. The density matrix elements of K^{*-} were very similar to those of the K^{*+} from reaction (68b).

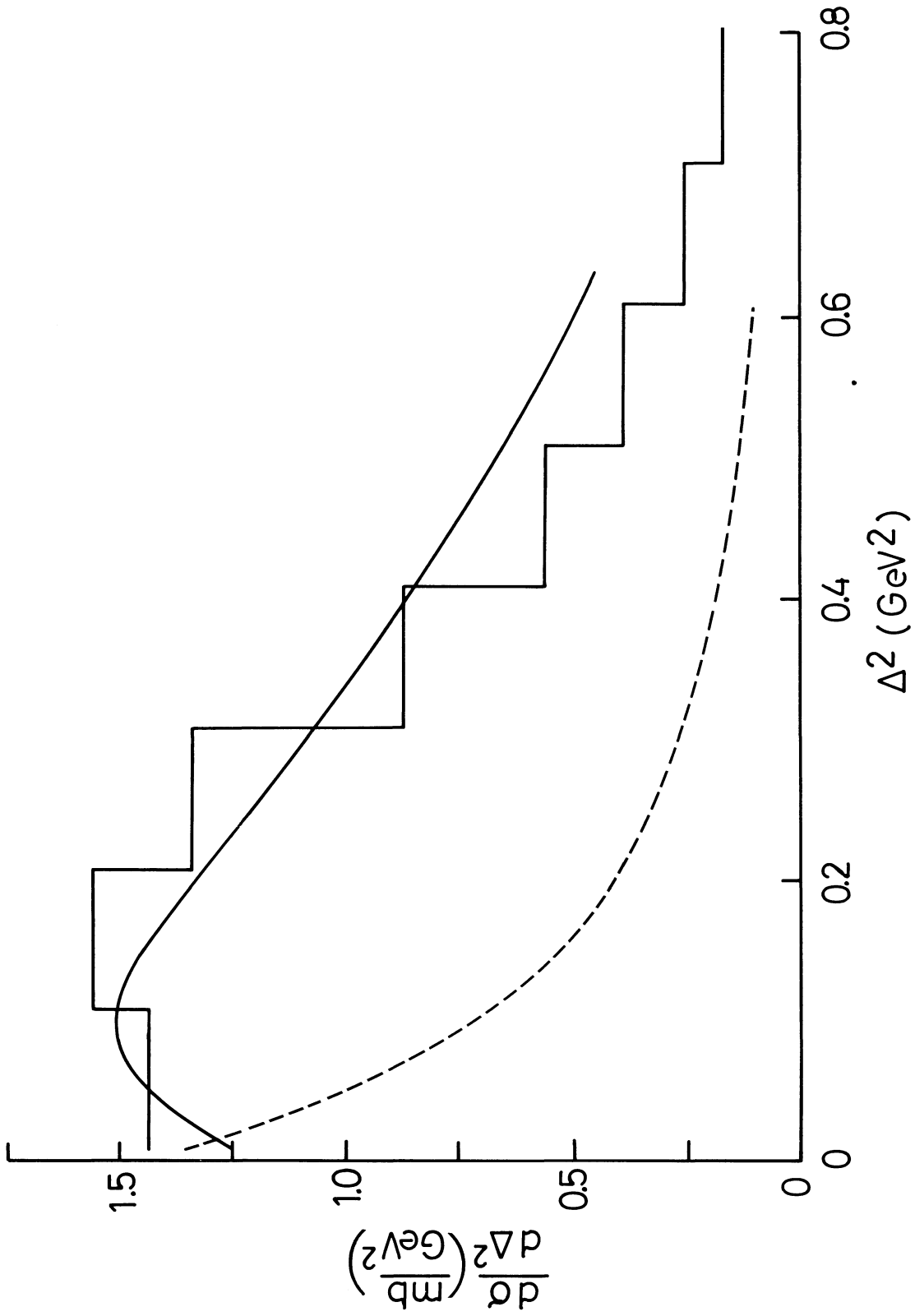

Fig. 27 Δ^2 distribution for $K^+p \to K^{*+}p$ at 3 GeV/c. The dashed curve is the prediction of the absorptive model for pure OPE; the solid curve is the prediction for a combination of π and vector-meson exchange.

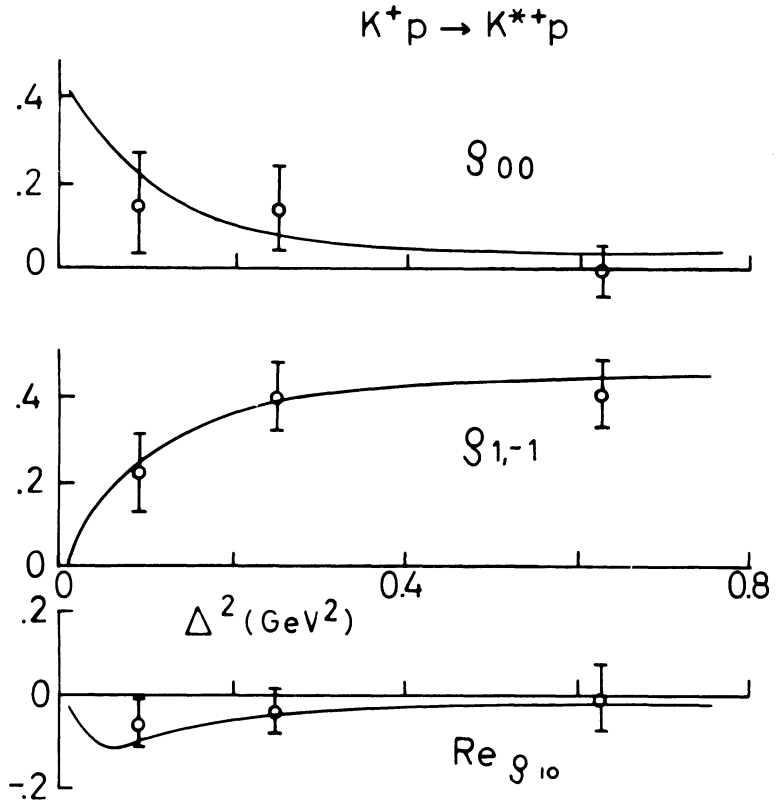

Fig. 28 Density matrix elements of K^{*+} from $K^+p \to K^{*+}p$ at 3 GeV/c as functions of Δ^2. The curves show the predictions of the absorptive model for a mixture of π- and vector-meson exchange.

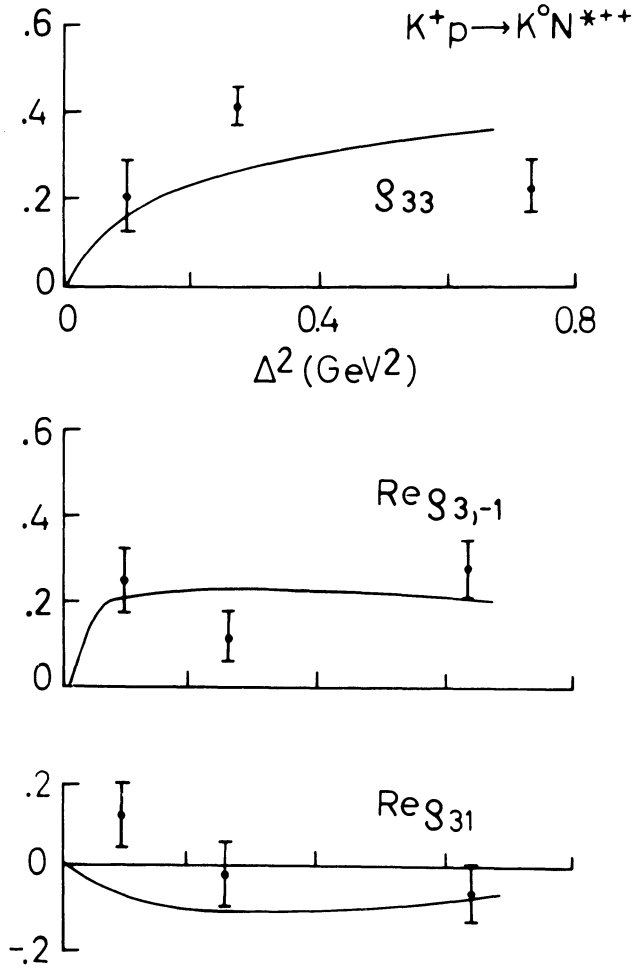

Fig. 29 Density matrix elements of N^{*++} from $K^+p \to K^0N^{*++}$ at 3 GeV/c as functions of Δ^2. The curves show the predictions of the absorptive model for ρ exchange by M1 transition.

6. $K^+p \to K^0N^{*++}$

This reaction has been studied at primary momenta of 0.91 GeV/c [34], 1.14 GeV/c [35], 1.45 GeV/c [26], 1.96 GeV/c [27], 3.0 GeV/c [29]. Figure 29 shows the N^{*++} density matrix elements as functions of Δ^2 from the experiment at 3.0 GeV/c. The experimental points are in reasonable agreement with the theoretical Stodolsky-Sakurai values (50) for ρ exchange by an M1 transition at the baryon vertex. When absorption is taken into account, the theoretical predictions are somewhat modified, as exhibited by the curves in Fig. 29 [30]. The curves fit the experimental data rather well. Also at the other primary momenta, the N^{*++} decay distributions were found to agree with the Stodolsky-Sakurai predictions.

The experimental Δ^2 distribution falls off a little steeper than is expected from the absorptive model[30].

7. $K^+p \to K^{*0}N^{*++}$

This reaction has been investigated at 1.96 GeV/c [36], 3.0 GeV/c [29], and 3.5 GeV/c [37]. It was found from the decay angular distributions that it proceeds predominantly via π exchange.

REFERENCES

1) G.F. Chew and F.E. Low, Phys.Rev. 113, 1640 (1959).

2) G. Puppi, Ann.Rev.Nucl.Sci. 13, 287 (1963).

3) K. Gottfried and J.D. Jackson, Nuovo Cimento 33, 309 (1964).

4) J.D. Jackson and H. Pilkuhn, Nuovo Cimento 33, 906 (1964); Nuovo Cimento 34, 1841 (1964).

5) K. Gottfried and J.D. Jackson, Nuovo Cimento 34, 735 (1964); Nuovo Cimento 34, 1843 (1964).

6) J.D. Jackson, Nuovo Cimento 34, 1644 (1964).

7) J.D. Jackson, Revs.Modern Phys., in print.

8) Aachen-Berlin-Birmingham-Bonn-Hamburg-London-München Collaboration, Phys.Rev., in print.

9) W. Koch, Proc. of the 1964 Easter School at Herceg-Novi, CERN 64-13, Vol. II, p.113.

10) L. Stodolsky and J.J. Sakurai, Phys.Rev.Letters 11, 90 (1963).

11) Saclay-Orsay-Bari-Bologna Collaboration, to be published.

12) E. Ferrari and F. Selleri, Nuovo Cimento 21, 1028 (1961); Nuovo Cimento Suppl. 24, 453 (1962); Nuovo Cimento 27, 1450 (1963).

13) F. Selleri, Physics Letters 3, 76 (1962).

14) U. Amaldi and F. Selleri, Nuovo Cimento 31, 360 (1964).

15) Aachen-Berlin-Birmingham-Bonn-Hamburg-London-München Collaboration, Physics Letters 10, 229 (1964).

16) N.J. Sopkovich, Nuovo Cimento 26, 186 (1962).

17) L. Durand and Y.T. Chiu, Phys.Rev.Letters 12, 399 (1964); Phys.Rev.Letters 13, 45 (1964).

18) Aachen-Birmingham-Bonn-Hamburg-London-München Collaboration, Nuovo Cimento 31, 729 (1964).

19) Aachen-Berlin-Birmingham-Bonn-Hamburg-London-München Collaboration, Nuovo Cimento 34, 495 (1964).

20) A. Daudin, M.A. Jabiol, C. Kochowski, C. Lewin, S. Mongelli, A. Romano and P. Waloschek, Proc. of the 1964 International Conference on High Energy Physics at Dubna, in print. Physics Letters 7, 125 (1963).

21) Saclay-Orsay-Bari-Bologna Collaboration, Physics Letters 13, 341 (1964).

22) M.A. Abolins, D.D. Carmony, D.N. Hoa, R.L. Lander, C. Rindfleisch and N. Xuong, Phys.Rev. 136, B195 (1964).

23) Aachen-Berlin-Birmingham-Bonn-Hamburg-London-München Collaboration, Nuovo Cimento 35, 659 (1965).

24) G. Goldhaber, Proc. of the Conference on Particle and High Energy Physics at Boulder (1964), in print.

25) B. Svensson, preprint (1964).

26) C.B. Chadwick et al., Physics Letters 6, 309 (1963).

27) S. Goldhaber, Proc. of the Athens Topical Conference on Recently Discovered Particles, p.92 (1963).

28) R. Lynch, M. Ferro-Luzzi, R. George, Y. Goldschmidt-Clermont, V.P. Henri, B. Jongejans, D.W.G. Leith, F. Muller and J.M. Perreau, Physics Letters 9, 359 (1964).

29) M. Ferro-Luzzi, R. George, Y. Goldschmidt-Clermont, V.P. Henri, B. Jongejans, D.W.G. Leith, G.R. Lynch, F. Muller and J.M. Perreau, Proc. of the Sienna International Conference on Elementary Particles, Vol. I, p.189 (1963); Nuovo Cimento 36, 1101 (1965).

30) K. Gottfried, J.D. Jackson and B. Svensson, Proc. of the 1964 International Conference on High Energy Physics at Dubna, in print.

31) S. Goldhaber, I. Butterworth, G. Goldhaber, A.A. Hirata, J.A. Kadyk, T.A. O'Halloran, B.C. Shen and G.H. Trilling, Proc. of the 1964 International Conference on High Energy Physics at Dubna, in print. UCRL 11465 (1964).

32) R. Barloutand et al., Physics Letters 12, 352 (1964).

33) N. Haque et al., Physics Letters 14, 338 (1965).

34) B. Kehoe, Phys.Rev.Letters 11, 93 (1963).

35) E. Boldt et al., Phys.Rev. 133, B220 (1964).

36) G. Goldhaber, W. Chinowsky, S. Goldhaber, W. Lee and T.A. O'Halloran, Physics Letters 6, 62 (1963).

37) J. Debaisieux, F. Grard, J. Henghebaert, L. Pape and R. Windmolders, Proc. of the 1964 International Conference on High Energy Physics at Dubna, in print.

THE PERIPHERAL MODEL

H. Pilkuhn,
Theory Division, CERN.

I. THE BORN TERM MODEL

1. Definition of the BTM

At this CERN School, experimental information on peripheral collisions has been discussed by Schmitz, who also explained the main physical ideas leading to the peripheral model. Consequently, I shall concentrate in these two lectures on the mathematical formulation of the various versions of the peripheral model.

Since no generally accepted definition of "the peripheral model" exists, I shall avoid this term altogether. Also, I shall restrict my discussion to reactions of the type

$$a + b \to c + d \quad , \tag{1}$$

where the outgoing particles c and d are either stable or else resonances with definite spin, parity and isospin quantum numbers (quasi-two-particle reactions).

First, let me define the Born Term Model (hereafter abbreviated as BTM). In this model, the scattering amplitude $T(s,t)$ is given by the sum of all possible Born terms, calculated by means of the Feynman rules in lowest (i.e. second) order perturbation theory:

$$T(s,t) = B_{\pi}(s,t) + B_{v}(s,t) + B_{b}(s,t) + \dots \quad , \tag{2}$$

where s = (c.m.s. energy)^2, $t = -\Delta^2$ = -(four momentum transfer)^2, and π = pion, v = vector meson, b = baryon indicate the quantum numbers of the exchanged particle e (see Fig. 1). As Schmitz told you, in each specific reaction most of the Born terms are forbidden by selection rules. If, for example, the outgoing particles c and d carry different strangeness than the ingoing particles a and b, then the exchanged particle in each of the contributing Born terms has to carry strangeness (K, K* and hyperons).

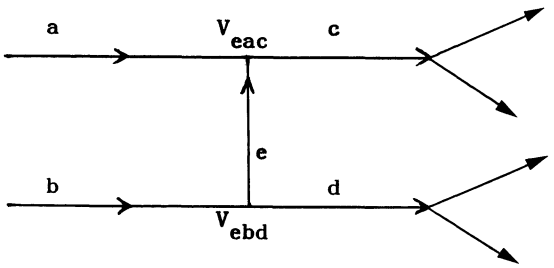

Fig. 1

The general forms of the Born terms for exchange of spin zero and one are:

$$B_\pi = V_{\pi ac} \frac{1}{\Delta^2 + m_\pi^2} \cdot V_{\pi bd} \quad , \tag{3}$$

$$B_v = V^\mu_{vac} \frac{g_{\mu\nu} + e_\mu e_\nu / m_v^2}{\Delta^2 + m_v^2} \cdot V^\nu_{vbd} \quad , \tag{4}$$

where the vertex factors V contain one coupling constant each, and a few more factors which follow from the Feynman rules (examples are given in this section, paragraph 5). When particles b and d represent baryons, V^ν_{vbd} generally contains more than one term, corresponding to the different couplings (vector, tensor, etc.). In that case B_v is strictly a sum of several Born terms.

The baryon exchange B_b is allowed in most reactions, but is nevertheless neglected (except in antinucleon annihilation and in meson-nucleon backward scattering). If the BTM as defined in (2) is to be consistent, one should of course verify by calculation that the contribution of B_b to some forward peaked reaction is really small, especially in reactions where it would give rise to an interference term with some pseudoscalar or vector exchange. I say this as a warning to the younger experimentalists, because on their question concerning the "exchange mechanism" they might get as an answer not just a single graph, but a sum of squares and interference terms.

The connection between the differential cross-section $d\sigma/dt$ and the scattering amplitude T is

$$d\sigma_2(s,t) = \frac{1}{16\pi q^2 s} \cdot \tfrac{1}{2} \sum_{\text{spins}} |T(s,t)|^2 \, dt \tag{5}$$

where q = initial c.m.s. momentum, and the index 2 on $d\sigma$ indicates that there are two outgoing particles. If one of the particles in the final state is a resonance with appreciable width, particle d, say, then (5) is modified into[1-4]

$$d\sigma = d\sigma_2(s,t,s_d) \cdot \frac{1}{\pi} \frac{M_0 \, \Gamma(s_d) \, ds_d}{(s_d - M_0^2)^2 + M_0^2 \Gamma^2(s_d)} \quad , \tag{6}$$

where s_d is the square of the invariant mass of the decay products of d, and M_0 and $\Gamma(s_d)$ denote the mass and width of the resonance, respectively. This modification comes from the propagator of the unstable particle, $[s_d - M^2]^{-1}$, $M \equiv M_0 - i\Gamma/2$. It is important for the exact shape and position of the resonance; in the following I shall omit it.

2. Pion-exchange Born terms and their relation to the pole approximation

As you know, many reactions are dominated by one-pion-exchange, which means that the sum, (2), reduces to the single term B_π, which is of the general form (3). In the BTM, this can have three reasons:

i) In a few reactions the exchange of a particle other than a pion is forbidden by selection rules, as discussed by Schmitz.

ii) The vertex factors $V_{\pi ac}$ and $V_{\pi bd}$ may be much larger than those of the remaining Born terms.

iii) $m_\pi^2 \ll m_V^2$, which makes the denominator in (3) much smaller than the denominator in (4), at least for $\Delta^2 < m_V^2$.

Whereas points (i) and (ii) occur accidentally, (iii) is true for all reactions where π exchange can occur, and is the origin of the peripheral model[5-10] invented around 1958. At that time, of course, one knew little about vector mesons, so instead of B_V one had the "exchange of more than one pion". Also, at that time one had few quasi-two-particle reactions, and one wanted to apply the model to more general reactions, where c and d in (1) simply meant two groups of uncorrelated particles, one going forward, the other going backward in the c.m.s.[9]. Since, for such processes, one knew nothing about the vertex factors $V_{\pi ac}$ and $V_{\pi bd}$, they were expressed in terms of the cross-sections $\sigma_{\pi ac}$ and $\sigma_{\pi bd}$ by relations of the type:

$$d\sigma_{\pi ac} = \frac{1}{\text{flux}} |V_{\pi ac}|^2 \, d(\text{phase-space element}) \ . \qquad (7)$$

This is the so-called pole approximation (this term derives from dispersion theory). Since (7) holds true for a real incident pion, the approximation is

$$V_{\pi ac}(\Delta^2) \approx V_{\pi ac}(-m_\pi^2) \ . \qquad (8)$$

When one applies the pole approximation to a quasi-two-particle reaction and compares the result with the BTM, one finds[10,4]

$$d\sigma \approx \left(\frac{P_{off}}{P_{on}}\right)^{2\ell_{\pi ac}}_{\pi ac} \cdot \left(\frac{P_{off}}{P_{on}}\right)^{2\ell_{\pi bd}}_{\pi bd} \cdot d\sigma_{pole} \ , \qquad (9)$$

where $\ell_{\pi ac}$ and $\ell_{\pi bd}$ denote the relative orbital angular momenta for pion absorption at the two vertices πac and πbd, respectively, and P_{off}, P_{on} = pion momentum in resonance rest frame taken at Δ^2 and $-m_\pi^2$, respectively:

$$\left(\frac{P_{off}}{P_{on}}\right)^2_{\pi ac} = \frac{(s_c - m_a^2 + \Delta^2)^2 + 4m_a^2\Delta^2}{(s_c - m_a^2 - m_\pi^2)^2 - 4m_a^2 m_\pi^2} \ . \qquad (10)$$

Equation (9) is exactly correct for the mesonic vertex, whereas at the baryonic vertex the Feynman rules give rise to small extra terms.

3. Form factors

As you heard from Schmitz, the sad fact about the BTM is that $d\sigma/dt$ falls off too slowly at high Δ^2. There is usually a peak at small Δ^2, due to the factor $[\Delta^2 + m^2]^{-2}$ (deriving from the square of the propagator), but then at large Δ^2 the curve starts rising

again due to the various factors $(P_{off})^2$ which increase like $(\Delta^2)^2$. [Although (9) is meaningful for π exchange only, the argument on the powers of Δ^2 is true in general.]

This shows that the BTM is wrong, except maybe at the smallest values of Δ^2. This is not surprising since nobody would expect lowest order perturbation theory to give good results in strong interactions. I shall discuss three possible improvements of the BTM in my second lecture. There is, however, one rather trivial improvement, namely a form factor, $F(\Delta^2)$, which is independent of s. In field theory such a factor would arise from the higher order corrections to a one-particle exchange graph, but since these corrections cannot be calculated, $F(\Delta^2)$ is really arbitrary. It should however be real, and for $\Delta^2 = m_e^2$ it should reproduce the Born term:

$$F(-m_e^2) = 1 \quad . \tag{11}$$

For pion exchange, Ferrari and Selleri used a form factor that goes like

$$\frac{\alpha^2 - m_\pi^2}{\alpha^2 + \Delta^2} \quad . \tag{12}$$

Schmitz has given you the later version of Amaldi and Selleri[11] which contains one more denominator with one more power of Δ^2. I can recommend to you the exponential form factor[12]

$$\exp \lambda(-m_e^2 - \Delta^2) \quad , \tag{13}$$

which will kill the Δ^2 increase of $(P_{off})^{2\ell}$ for any value of ℓ. The value $\lambda = 2.5$ GeV^2 gives a reasonable fit to both pion and vector-meson exchange for most meson-nucleon reactions up to 3 or 4 GeV/c, but this number should, of course, be modified when other improvements of the BTM are introduced.

In a loose way I shall continue to speak about the "BTM", even when I admit the inclusion of a form factor. As a better term, let me suggest the name "reduced BTM", since in the physical region of Δ^2 the form factor always reduces the matrix element to a smaller value.

4. Decay distributions

When one of the outgoing particles is a resonance, the distribution of its decay vector gives information about the production amplitudes. Let me first discuss the more complicated case where you have two resonances in the final state, for example

$$\pi^+ + p \to \rho^0 + N^* \tag{14}$$

and suppose one wants the joint decay distribution[13] $W(s,\Delta^2,\hat{\alpha},\hat{\beta})$, where $\hat{\alpha}$ and $\hat{\beta}$ are the decay directions of the ρ^0 and N*, respectively. Problems of this type occur again and again [see for example, W. Koch in the Proceedings of the 1964 CERN Easter School[14]]. We are interested in the general result independent of the BTM.

The spin summation of (5) for reaction (14) reads explicitly

$$\sum_{mn\lambda} |\langle mn|T|\lambda\rangle|^2 \qquad (15)$$

where m and n are the z components of the ρ and N* spins, and λ that of the proton spin. In order to arrive at $W(\hat{\alpha},\hat{\beta})$ (dropping the variables s and t for this section), one cannot use (15). Instead, one has to multiply each $\langle mn|T|\lambda\rangle$ by the angular-dependent parts of the ρ and N* decay matrix elements, which I shall denote by $M^1_m(\hat{\alpha})$ and $M^{3/2}_n(\hat{\beta}\ \lambda')$, respectively. (The index λ' stands for the polarization of the decay proton from N*.) Then one has to sum these products of amplitudes over m and n, then to <u>square the sum</u>, and finally to sum the squared sums over the remaining polarization indices λ and λ'. The first double sum is

$$\langle\lambda'|M(\hat{\alpha},\hat{\beta})|\lambda\rangle = \sum_{m,n} M^1_m(\hat{\alpha}) \cdot M^{3/2}_n(\hat{\beta},\lambda') \cdot \langle mn|T|\lambda\rangle \ , \qquad (16)$$

and the sum of the squares is

$$W(\hat{\alpha},\hat{\beta}) = \sum_{\lambda\lambda'} |\langle\lambda'|M(\hat{\alpha},\hat{\beta})|\lambda\rangle|^2 \ . \qquad (17)$$

Once you understand these two equations the rest is trivial. Interchanging the order of summations, (17) becomes

$$W(\hat{\alpha},\hat{\beta}) = \sum_{\substack{mm'\\nn'}} M^1_m M^{1,*}_{m'} \left(\sum_{\lambda'} M^{3/2}_n M^{3/2,*}_{n'} \right) \cdot \rho^{mm'}_{nn'} \ , \qquad (18)$$

where

$$\rho^{mm'}_{nn'} = \sum_{\lambda} \langle mn|T|\lambda\rangle\langle m'n'|T|\lambda\rangle^* \qquad (19)$$

is the joint density matrix acting in both the ρ-meson spin space and the N* spin space. If you want the distribution of the N* decay alone, you integrate (18) over $\hat{\alpha}$. For the M^1_m you have to insert the spherical harmonics Y^1_m. Since these are orthonormal,

$$\int M^1_m(\hat{\alpha}) \cdot M^{1,*}_{m'}(\hat{\alpha})\ d\Omega_\alpha = \delta_{mm'} \ , \qquad (20)$$

you simply obtain

$$W(\hat{\beta}) = \sum_{nn'} \left(\sum_{\lambda'} M^{3/2}_n M^{3/2,*}_{n'} \right) \cdot \rho_{nn'} \ , \qquad (21)$$

where

$$\rho_{nn'} = \sum_{m} \rho^{mm}_{nn'} \tag{22}$$

is the density matrix of N* alone. In the same way, the ρ-meson decay distribution $W(\hat{\alpha})$ is obtained by integrating (18) over $\hat{\beta}$:

$$\int \sum_{\lambda'} M^{3/2}_{n}(\hat{\beta},\lambda')\; M^{3/2*}_{n'}(\hat{\beta},\lambda')\; d\Omega_{\beta} = \delta_{nn'} \;, \tag{23}$$

$$W(\hat{\alpha}) = \sum_{mm'} M^{1}_{m}(\hat{\alpha}) \cdot M^{1,*}_{m'}(\hat{\alpha}) \cdot \rho^{mm'} \;, \tag{24}$$

$$\rho^{mm'} = \sum_{n} \rho^{mm'}_{nn} \;. \tag{25}$$

If you integrate over both decay directions, you rediscover (15):

$$\int W(\hat{\beta})\; d\Omega_{\beta} = \int W(\hat{\alpha})\; d\Omega_{\alpha} = \sum_{m,n} \rho^{mm}_{nn} = (15) \;. \tag{26}$$

Usually this sum is normalized to one:

$$\sum_{m} \rho^{mm} = \sum_{n} \rho_{nn} = \sum_{m,n} \rho^{mm}_{nn} = 1 \;. \tag{27}$$

In the explicit expressions for $W(\hat{\alpha})$ and $W(\hat{\beta})$ in paragraph 5 of this section, I shall assume this normalization.

For the explicit construction of the joint decay distribution (18), one simplifies the summations over m, m', n, n' by using the hermiticity

$$\rho^{mm'}_{nn'} = \rho^{m'm*}_{n'n} \tag{28}$$

and the symmetry following from parity conservation

$$\rho^{-m,-m'}_{-n,-n'} = (-1)^{m-m'+n-n'} \cdot \rho^{mm'}_{nn'} \;. \tag{29}$$

The hermiticity follows trivially from (19), whereas (29) holds true only when the spin quantization axis (z axis) lies in the production plane. One may choose different quantization axes for ρ and N*; a useful choice is the incident pion momentum direction in the ρ rest frame for the ρ decay, and the initial proton momentum direction in the N* rest frame for the N* decay.

In the literature[13,15], (29) is proven for helicity eigenstates, with reference to (44) of Jacob and Wick[16]. This is an unnecessary complication since we want to prove (29) for the peculiar quantization axes which I just mentioned, which are not helicity eigenstates. The direct argument goes as follows:

i) Apply a momentum inversion (parity operation). Neglect intrinsic parities since they will drop out in (19). This operation does not affect the spin states.

ii) Rotate by 180° around the normal to the production plane, taken as y axis. This sends the momenta back to their old positions. Moreover, with both z axes in the production plane, this transforms the spin states according to

$$|s,m> \rightarrow (-1)^{s-m} \; |s,-m> \quad , \tag{30}$$

because of

$$\left(e^{-i\pi J_y}\right)^{s}_{m'm} = d^{s}_{m'm}(\pi) = (-1)^{s-m} \, \delta_{m',\,-m} \quad . \tag{31}$$

The total effect on $<mn|T|\lambda>$ is thus

$$<mn|T|\lambda> \rightarrow (-1)^{\pm(\frac{1}{2}-\lambda) \pm (1-m) \pm (\frac{3}{2}-n)} \; <-m,-n|T|-\lambda> \quad , \tag{32}$$

where the sign of each bracket in the exponent does not matter since the bracket is an integer number. Taking the upper signs in (32) and the lower signs in the corresponding transform of $<m'n'|T|\lambda>^*$, multiplying together and summing over λ gives one equation (29).

With (28) and (29), the general forms of the single-particle density matrices reduce to

$$\rho^{mm'} = \begin{bmatrix} \rho^{11} & \rho^{10} & \rho^{1-1} \\ \rho^{10*} & \rho^{00} & -\rho^{10*} \\ \rho^{1-1} & -\rho^{10} & \rho^{11} \end{bmatrix} \quad ; \quad \rho_{nn'} = \begin{bmatrix} \rho_{33} & \rho_{31} & \rho_{3-1} & \rho_{3-3} \\ \rho^{*}_{31} & \rho_{11} & \rho_{1-1} & \rho^{*}_{3-1} \\ \rho^{*}_{3-1} & -\rho_{1-1} & \rho_{11} & -\rho^{*}_{31} \\ -\rho_{3-3} & \rho_{3-1} & -\rho_{31} & \rho_{33} \end{bmatrix} \tag{33}$$

for the ρ meson and N*, respectively. Hermiticity requires that all diagonal elements are real, and that in addition ρ^{1-1} is real, and that ρ_{3-3} and ρ_{1-1} are purely imaginary.

The explicit result for $W(\hat{\alpha},\hat{\beta})$ has been given in reference 13; it is rather lengthy. The forms of $W(\hat{\alpha})$ for the ρ meson alone and $W(\hat{\beta})$ for the N* alone are by now well known[15]:

$$W(\hat{\alpha}) = \frac{3}{4\pi}(\rho^{11} \sin^2\Theta + \rho^{00} \cos^2\Theta - \rho^{1,-1} \sin^2\Theta \cos 2\varphi - \sqrt{2}\,\mathrm{Re}\,\rho^{10} \sin 2\Theta \cos\varphi) \quad , \tag{34}$$

$$W(\hat{\beta}) = \frac{3}{4\pi}\left[\rho_{33}\sin^2\Theta + \rho_{11}(1+\tfrac{1}{3}\cos^2\Theta) - \frac{2}{\sqrt{3}}\,\mathrm{Re}\,\rho_{3-1}\sin^2\Theta\cos 2\varphi - \frac{2}{\sqrt{3}}\,\mathrm{Re}\,\rho_{31}\sin 2\Theta\cos\varphi\right], \tag{35}$$

where Θ and φ stand for polar and azimuthal angles as usual. Let me just indicate how (34) is derived from (24), using the symmetry properties (33): as mentioned before, $M^1_m(\hat{\alpha}) = Y^1_m(\Theta,\varphi)$, or explicitly

$$Y^1_0 = \tfrac{1}{2}\sqrt{\frac{3}{\pi}}\cos\Theta,\quad Y^1_{\pm 1} = \mp\tfrac{1}{2}\sqrt{\frac{3}{2\pi}}\sin\Theta\, e^{\pm i\varphi}\ . \tag{36}$$

The coefficient of ρ^{11} is $\frac{4}{3}\pi(|Y^1_1|^2 + |Y^1_{-1}|^2)$, that of Re ρ^{10} is $\frac{4}{3}\pi(Y^1_1 Y^1_0 + Y^1_0 Y^{1*}_1 - Y^1_{-1} Y^1_0 - Y^1_0 Y^{1*}_{-1})$, and so on.

It is generally true that the decay distributions of resonances depend on the real part of the density matrix only, if the decays conserve parity. The imaginary part is measured in polarization experiments. An important property of most peripheral models is that they predict that <u>all polarizations are strictly zero</u>, simply because all density matrix elements are real. This is true for the BTM without and with form factor, and also for the absorption model, but not for the unitary models like the K-matrix model and the N/D method.

5. Vertex factors

Consider first a 3-meson vertex. Let <u>a</u> be the incident pseudoscalar meson, π or K. If the outgoing meson c is pseudoscalar too, then π exchange is forbidden, whereas vector-meson exchange gives

$$V^{\mu}_{vpp'} = ig(a+c)^{\mu}\ . \tag{37}$$

For an outgoing vector-meson resonance one can have both π and v exchange:

$$V_{\pi pv'} = ig(a-e)\cdot\epsilon^{*(m)}\ , \tag{38}$$

$$V^{\mu}_{vpv'} = \frac{f}{m_c}\,\epsilon^{\mu\nu\rho\sigma}a_\nu e_\rho \epsilon^{*(m)}_\sigma\ , \tag{39}$$

where $\epsilon^{(m)}$ is the polarization vector of the resonance. (The complex conjugate ϵ^* has to be taken for outgoing particles.)

In the c rest frame,

$$\epsilon^{(+)} = \frac{1}{\sqrt{2}}\begin{pmatrix}-1\\-i\\0\end{pmatrix},\quad \epsilon^{(-)} = \frac{1}{\sqrt{2}}\begin{pmatrix}1\\-i\\0\end{pmatrix},\quad \epsilon^{(0)} = \begin{pmatrix}0\\0\\1\end{pmatrix} \tag{40}$$

are the polarization vectors for m = +1, -1, and 0, respectively. The time components of all three ϵ vectors are zero in the c rest frame. In any system, $c^{\mu}\epsilon^{(\lambda)}_{\mu} = 0$. From $e = c - a$ and $c\cdot\epsilon = 0$ one rewrites (38) as:

$$2iga \cdot \epsilon^{*(m)} = 2iga_c \, \epsilon_3^{*(m)} \quad , \tag{41}$$

where a_c is the magnitude of $\vec{a}$ in the c rest frame, and the 3-axis is taken along $\vec{a}$. From (40) we see that $\epsilon^{(o)}$ is the only polarization vector with a non-vanishing 3-component, and therefore

$$\rho^{mm'} = \delta_{mo} \, \delta_{m'o} \quad , \tag{42}$$

and $W(\hat{\alpha}) = \frac{3}{4\pi} \cdot \cos^2 \Theta$, independent of the azimuth.

For the vector exchange (39), the antisymmetry property of $\epsilon^{\mu\nu\rho\sigma}$ this time allows one to replace e by c, and (39) becomes $f \cdot \epsilon^{\mu 34\nu} \cdot \epsilon_\nu^{*(m)}$, which shows that $\epsilon_3^{(m)}$ will not contribute, thence $\rho^{io} = 0$.

On the nucleon side there are more couplings and their evaluation is more complicated. The $\pi NN'$ coupling is conveniently written as

$$V_{\pi NN'} = G\bar{u}(d,\lambda')\gamma_5 \, u(b,\lambda) \quad . \tag{43}$$

There are two different vNN' couplings, which are conveniently written as

$$V^{\nu}_{vNN'} = \bar{u}(d,\lambda') \left[(G_v + G_t) \, \gamma^{\nu} + 2i \, \frac{G_t}{m_b + m_d} \, d^{\nu} \right] u(b,\lambda) \quad , \tag{44}$$

where G_v and G_t are the vector and tensor coupling constants, respectively.

For the N* finally, a vector spinor $u_\mu(d,\lambda'')$ is used[17]. It is constructed from the spinor $u(d,\lambda')$ and polarization vectors ϵ by means of C-G coefficients:

$$u_\mu(d,3/2) = u(d,1/2) \cdot \epsilon_\mu^{(+)} \quad , \tag{45}$$

$$u_\mu(d,1/2) = \frac{1}{\sqrt{3}} \, u(d,-1/2) \cdot \epsilon_\mu^{(+)} + \sqrt{2/3} \, u(d,1/2) \cdot \epsilon_\mu^{(o)} \quad . \tag{46}$$

The remaining two vector spinors $u_\mu(d,-3/2)$ and $u_\mu(d,-1/2)$ are obtained from (45) and (46) simply by replacing

$$u(d,1/2) \Leftrightarrow u(d,-1/2), \quad \epsilon_\mu^{(+)} \Leftrightarrow \epsilon_\mu^{(-)} \quad . \tag{47}$$

With the vector spinor, the πNN^* vertex reads

$$V_{\pi NN^*} = \frac{G^*}{m_\pi} \, \bar{u}_\mu(d,\lambda'') \, b^\mu \cdot u(b,\lambda) \quad , \tag{48}$$

and the vNN* coupling reads

$$V^{\mu}_{vNN^*} = i\bar{u}_{\nu}(d,\lambda'')\left[G_1 g^{\mu\nu} - i\frac{G_2}{m_b+m_d}e^{\nu}\gamma^{\mu}\right]\gamma_5\, u(b,\lambda) \quad . \qquad (49)$$

In the last formula a possible term proportional to $e^{\nu}\, b^{\mu}\, \gamma_5$ is omitted. Still, equation (49) becomes practicable only for $G_1 = G_2$, which is the Stodolsky-Sakurai model[18].

6. The Stodolsky-Sakurai model

An important prediction of this model is that the decay distribution of N* with respect to the production normal is approximately $1+3\cos^2\Theta$, independent of the azimuth. Schmitz has discussed how this follows from the absence of states with $\lambda'' = \pm 3/2$ (quantization axis = normal to the production plane). The absence of these states follows from the picture of magnetic dipole absorption[18,22], but for those who are not familiar with this picture I shall show by explicit calculation under which conditions

$$T(\lambda'' = 3/2,\ \lambda = 1/2) = \bar{u}_{\nu}(d,3/2)\left[G_1 A^{\nu} - i\frac{G_2}{m_b+m_d}e^{\nu}\gamma\cdot A\right]\gamma_5\, u(b,\pm 1/2) \approx 0 \ , \qquad (50)$$

where A^{ν} is the product of the V propagator and V^{μ}_{vac}. An exact treatment shows that (50) is only approximately true, therefore we can put $m_b = m_d \equiv M$ and obtain, by inserting the Hermitian conjugate of equation (45),

$$T(3/2,\pm 1/2) = \frac{1}{\sqrt{2}}\,\bar{u}(d,1/2)\left[G_1 A_- - i\frac{G_2}{2M}e_-\gamma\cdot A\right]\gamma_5\, u(b,\pm 1/2) \quad , \qquad (51)$$

where we have abbreviated

$$A_- = -(A_x - iA_y), \quad e_- = -(e_x - ie_y) \quad . \qquad (52)$$

With $\gamma_5 = -\begin{pmatrix} 0 & I \\ I & 0 \end{pmatrix}$ and

$$u(b,1/2) = \begin{pmatrix} 1 \\ 0 \\ \frac{\vec{\sigma}\cdot\vec{b}}{2M}\begin{pmatrix}1\\0\end{pmatrix} \end{pmatrix} = \begin{pmatrix} 1 \\ 0 \\ 0 \\ \frac{-1}{2M}\,b_+ \end{pmatrix} \qquad (53)$$

we get

$$\gamma_5\, u(b,1/2) = \begin{pmatrix} 0 \\ b_+/2M \\ -1 \\ 0 \end{pmatrix}, \quad \gamma_5\, u(b,-1/2) = \begin{pmatrix} b_-/2M \\ 0 \\ 0 \\ -1 \end{pmatrix} \quad . \qquad (54)$$

Similarly, we have in the approximation $m_b = M$

$$\bar{u}(d,1/2) = (1,0,0,d_-/2M) \quad . \qquad (55)$$

Next, we go to a co-ordinate system (for example the lab. system) in which both $d_+/2M$ and $b_+/2M$ are so small that we can work in lowest non-vanishing order of $1/2M$ (such a system exists only when Δ^2 is small). Due to the factor γ_5 in (51), this is the first order in $1/2M$. Inserting equation (55) into equation (51), we get

$$\bar{u}(d,\tfrac{1}{2})\left[G_1 A_- - i\,\frac{G_2}{2M}\,e_-\gamma A\right] = \left[G_1 A,\ 0, -\frac{G_2}{2M}\,e_- A_z,\ \frac{A_-}{2M}(G_2 e_- + G_1 d_-)\right] . \qquad (56)$$

Dotting this spinor into $\gamma_5\, u(b,\tfrac{1}{2})$ gives zero if

$$A_z = 0 \ , \qquad (57)$$

and dotting it into $\gamma_5\, u(b,-\tfrac{1}{2})$ gives

$$\frac{1}{2M}[b_+ A_- - A_-(G_2 e_- + G_1 d_-)] = 0 \quad \text{for } G_1 = G_2 \ . \qquad (58)$$

To complete the proof, I should show that the matrix elements for $\lambda'' = \pm\,\tfrac{1}{2}$ do not vanish to order $1/2M$, and that $A_z = 0$ for the reactions in which we are interested. For the vertex (37) $A_z = 0$ holds because the z axis is the normal to the production plane. For vertex (39), A_z becomes approximately zero for high meson energies.

II. MODIFICATIONS OF THE BORN TERM MODEL

1. What is wrong with the Born term model?

Schmitz has already told you the main physical arguments, so let me again restrict my arguments to the formal theoretical points.

The first point is unitarity of the S matrix:

$$S^\dagger S = 1 \ , \qquad (59)$$

where "1" means a big unit matrix. Putting

$$S = 1 + iT \ , \qquad (60)$$

and taking T as a symmetric matrix (which is possible whenever S is time-reversal invariant), unitarity reads

$$2\,\mathrm{Im}T = T^\dagger T \ . \qquad (61)$$

In the BTM, $T = \Sigma B$. Since Born terms are real, the left-hand side of (61) is zero. In quantum electrodynamics, B is proportional to the small fine structure constant α, and the right-hand side is then, in fact, zero too, to lowest order in α. (You can also invert this argument to prove that B has to be real.) But in strong interactions the coupling constants are large,

and so is $T^\dagger T$. Since the perturbation theory of strong interactions does not converge, one has to modify the Born terms in a non-perturbative way in order to get a unitary model.

Two such "unitarizers" are the K-matrix[19,20] and the N/D[21] methods. The latter method is superior to the K-matrix method in the low-energy region, for bound states, etc., but is difficult to apply at high energies where many channels are open.

Then there are approximate methods, among which the absorption model[22] has reached the greatest practical importance. In the approximate methods elastic scattering plays a special role. To see the reason for this, put some indices onto (61), i,m, and f for initial, intermediate, and final states, respectively:

$$2 \text{ Im } T_{if} = \sum_m T^*_{im} T_{mf} \quad . \tag{61'}$$

Then for f = i, you have a sum of absolute squares, which is certainly larger than any sum with $i \neq f$. Therefore, at high energies where the number of contributing channels is large, the absorption model takes T_{ii} as purely imaginary, and the remaining T_{if} as purely real, hoping that many terms in the sums for $i \neq f$ somehow cancel each other.

Now you understand why the BTM is not applied to elastic scattering: it would give a purely real amplitude.

The second, and probably more serious, difficulty arises when one considers the exchange of particles with spin: for exchange of a particle of spin j, the amplitude B(s,t) diverges like s^j as $s \to \infty$. This will be briefly discussed under paragraph 4.

2. Absorption model

In the absorption model the Born terms are modified by elastic scattering in the initial and final states. This has to be done for each value of J, the total angular momentum. The transition from $T(s,\Theta)$ to $T^J(s)$ is conveniently done in the helicity representation of Jacob and Wick[16],

$$\langle \lambda_c \lambda_d | T(\Theta) | \lambda_a \lambda_b \rangle = \sum_J (J + \tfrac{1}{2}) \langle \lambda_c \lambda_d | T^J | \lambda_a \lambda_b \rangle \cdot d^J_{\lambda\mu}(\Theta) \quad , \tag{62}$$

where Θ denotes the c.m.s. scattering angle. The magnetic quantum numbers of the d functions are

$$\lambda = \lambda_a - \lambda_b, \quad \mu = \lambda_c - \lambda_d \quad . \tag{63}$$

The inverse formula of (62) will be needed for the Born terms:

$$\langle \lambda_c \lambda_d | B^J | \lambda_a \lambda_b \rangle = 2\pi \int_{-1}^{1} d \cos\Theta \, \langle \lambda_c \lambda_d | B(\Theta) | \lambda_a \lambda_b \rangle \cdot d^J_{\lambda\mu}(\Theta) \quad . \tag{62'}$$

The absorption model consists of putting

$$\langle\lambda_c\lambda_d|T^J|\lambda_a\lambda_b\rangle = e^{i\delta cd(J)}\,\langle\lambda_c\lambda_d|\Sigma B^J|\lambda_a\lambda_b\rangle\,e^{i\delta ab(J)}\ , \tag{64}$$

where δ_{ab} and δ_{cd} are the elastic scattering phase shifts in the initial and final states. At high energies, the complex number $\delta(J)$ has a large positive imaginary part, as can be seen from (61′), so that in (64) each Born term is "damped" by a factor $\exp[-2\bar{\delta}(J)]$, where $\bar{\delta}(J)$ is the average imaginary part of initial and final states.

There exist two derivations of equation (64), one in potential scattering[23,24], the other in S-matrix theory, using the eigenphases of the S matrix[25]. Both derivations involve so many assumptions that at present it appears to be more appropriate to assume (64) as an elegant ansatz, which is justified by its practical success.

The darkest point in both derivations concerns the range of the interactions: except when $\delta_{ab} = \delta_{cd}$, one has to assume that $\delta(J)$ extends to much larger values of J than does B^J. But at least for pion exchange, the long range of B_π is the very basis of the peripheral model, so there is a plain contradiction. (I should, however, mention that in the case of antiproton-proton scattering it appears that $\delta(J)$ does extend further in J than does B_π.)

Nevertheless, let me at least indicate how (64) is derived in potential scattering. Instead of J, one uses the impact parameter b, and writes[26]

$$T_{if} = \int d^2b \int_{-\infty}^{\infty} dz\ e^{i(\underline{q}-\underline{q}')\underline{b}}\ B(\underline{b}+\underline{k}\cdot z)\ e^{+i\delta_i(\underline{b},z)}\cdot e^{i\delta_f(\underline{b},z)}\ . \tag{65}$$

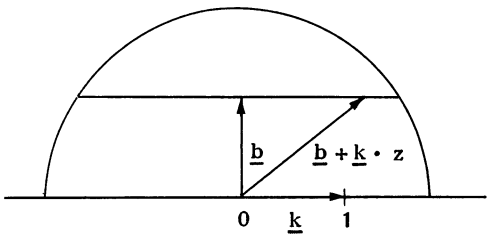

Fig. 2

Here $\underline{q}$ and $\underline{q}'$ denote the incident and outgoing momentum, respectively, $\underline{k}$ is a unit vector in the direction of $\underline{q}+\underline{q}'$, and the impact parameter vector $\underline{b}$ is perpendicular to $\underline{k}$. The indices i and f on the phase shifts stand for initial and final state:

$$\begin{aligned}\delta_i(\underline{b},z) &= -\frac{1}{v_i}\int_{-\infty}^{z} u_i(\underline{b}+\underline{k}\cdot z')\,dz' \\ \delta_f(\underline{b},z) &= -\frac{1}{v_f}\int_{z}^{\infty} u_f(\underline{b}+\underline{k}\cdot z')\,dz'\ ,\end{aligned} \tag{66}$$

where u is the optical potential. This is Glauber's[26] approximation to the DWBA, valid at high energies and small scattering angle. Because Θ is supposed to be small, $\underline{q}, \underline{q}'$ and $\underline{k}$ are nearly parallel, and $\underline{b} + \underline{k} \cdot z'$ is the straight line on which a classical particle of impact parameter $\underline{b}$ would move (see Fig. 2) and δ_i is the phase shift characteristic of that path, ending at the point $\underline{b} + \underline{k} \cdot z$, where the Born term induces the transition to the final state.

Notice that (64) implies that the elastic scattering does not change the helicities. This assumption is always made in high-energy scattering. Also, it is customary to take δ purely imaginary (the real part does not contribute to the "damping" anyway). If the elastic scattering is described by an exponential which goes through the optical point,

$$\frac{d\sigma}{d\Delta^2} = \frac{\sigma_{total}^2}{16\pi} \exp\left(-\frac{R^2}{4}\Delta^2\right) , \tag{67}$$

then

$$e^{i\delta(J)} = \left[1 - \frac{\sigma_{total}}{\pi R^2} \exp\left(\frac{-2J^2}{R^2 q^2}\right)\right]^{1/2} . \tag{68}$$

Since (68) is a real quantity, no polarizations can occur. Instead of J one should have the orbital angular momentum L, but for high values of L the two quantities become equal, since in most reactions they differ by $\pm \frac{1}{2}$ only. In fact, in the applications (62) is approximated by the integral

$$\langle \lambda_c \lambda_d | T(\Theta) | \lambda_a \lambda_b \rangle \approx \int J dJ \, \langle \lambda_c \lambda_d | T^J | \lambda_a \lambda_b \rangle \cdot J_n\left(2J \sin\frac{\Theta}{2}\right) , \tag{69}$$

where J_n is the Bessel function of the first kind of order $n = \mu - \lambda$. This approximation should be regarded with suspicion, since it turns out that the largest part of the absorption occurs in the 3-4 lowest partial waves.

How does the model compare with experiment? In meson-nucleon scattering $\sigma_{total}/\pi R^2$ is of the order of 0.75. For production processes the final-state scattering is unknown, and therefore $(\sigma_{total})_f$ and R_f^2 are parameters whose values are determined by the differential production cross-section. The range of these parameters is, however, somewhat limited: because of (68), $\sigma_{total}/\pi R^2$ should not be greater than one. As a rule, no fit is obtained when this ratio is smaller than one, therefore

$$(\sigma_{total})_f = \pi R_f^2 \tag{70}$$

is the "standard choice". The only remaining parameter is then R_f^2/R_i^2. In meson-nucleon collisions, $R_f^2/R_i^2 \approx 2 - 3$. These numbers imply that both σ_{total} and $\sigma_{elastic}$ in all final states are systematically three or four times bigger than in the initial state. This is a somewhat unpleasant result, especially for charge exchange reactions where $\sigma_i = \sigma_f$ follows from Pomeranchuk's theorem. In antiproton annihilation, $(\sigma_{total})_i \approx \pi R_i^2$, and the situation is somewhat better. When the outgoing particles carry high spin, the absorption model gives a poor fit to the differential production cross-section. This seems again to be connected with the factors $(P_{off})^{2\ell}$, which diverge like $(\Delta^2)^{2\ell}$ as $\Delta^2 \to \infty$.

By increasing the parameter λ in the form factor (13), one can get arbitrarily steep differential cross-sections. The reason why one cannot get the same result by increasing R_f^2 follows from (68): for big R^2, the exponent varies too slowly for those values of J for which the Born term is non-zero, and (64) does not decrease rapidly enough as a function of J. From the theoretical point of view this is no criticism of the absorption model, it merely shows that the Born term is wrong. This is confirmed by the K-matrix calculation, to be discussed below.

In addition to the differential cross-section, the density matrix elements are also changed by the absorption. This might appear surprising since δ_i and δ_f do not depend on the helicities. But they do depend on J, which means that the Born term no longer "sees" the original incident plane wave, but a distorted wave.

The agreement with experiment is usually good[22,27], although the significance of this agreement is not easily judged. For the K-matrix model, the situation is the same[28]. The experimental points have large error flags.

3. K-matrix model

In the K-matrix model one writes

$$S = \frac{1 + iK}{1 - iK} = (1 + 2iK - K^2)(1 + K^2)^{-1} \quad , \tag{71}$$

and for K one puts

$$K = \tfrac{1}{2}\Sigma B \quad , \tag{72}$$

which automatically leads to a strictly unitary S matrix. This is so because the Born terms are real and symmetric, which are exactly the requirements K has to fulfil.

Remember that all terms in (71) are again matrices, therefore you have to do matrix inversion. This inversion is practically possible only when you invent a clever way of handling the three-and more-particle states which enter the quasi-two-particle reactions only indirectly through the unitarity conditions. This can be done by assuming that for given J the elements of K corresponding to $2 \to 3$ and to $3 \to 3$ transitions are distributed statistically around zero mean[28]. In that case K^2 becomes diagonal in the quasi-particle number, such that for the calculation of S_{22} only K_{22} and $(K^2)_{22}$ are needed.

The final result for $T = \frac{1}{i}(S - 1) = \frac{2K}{1 - iK}$ is

$$T_{22} = 2\,\frac{K_{22} + iK_{22}^2 + ib(b + 1)}{(1 + b)^2 + K_{22}^2} \tag{73}$$

where

$$b = iK_{23} \cdot \frac{1}{1 - iK_{33}} \cdot K_{32} \tag{74}$$

is a multiple of the unit matrix. All this holds true for a given partial wave J.

Because of the non-linear coupling between the different channels any unitary theory is necessarily much more complicated than the absorption model, say, where one can treat one channel at a time. Also, you have to insert the Born terms for such reactions as $\pi + N^* \to \rho + N^*$, which involve the unknown $N^*N^*\pi$ coupling constant.

On the other hand, you can, of course, calculate what you want: elastic scattering, charge exchange, real and imagainary parts of elastic amplitudes, decay distributions, polarizations, etc.

How does the model compare with experiment? Well, one can get good agreement for the inelastic processes, but then the total scattering comes out too big by a factor of 3 (for K^+p interactions at 3 GeV/c), and the elastic cross-section is too big by a factor 5 - 10. This is rather similar to the situation found in the absorption model.

We are led to the following tentative conclusions:

i) The unmodified Born terms are so enormously big that a unitary theory will give a strong damping in the low partial waves.

ii) This implies an imaginary amplitude in the elastic channel which is much too big.

iii) In many cases the damping is still too weak to give a good fit to $d\sigma/d\Delta^2$. Additional damping is provided by the unitary effects of the three-and more-particle states. This, however, makes the amplitude in the elastic channel even bigger.

4. High-energy behaviour and Regge poles

The most serious difficulty with Born terms other than spin-zero exchange is the high-energy behaviour of these terms. For vector-meson exchange, $B(s,t)$ diverges like s as $s \to \infty$. This is due to the metric tensor $g_{\mu\nu}$ in the vector-meson propagator, which contracts external momenta from both vertices. Generally, the exchange of a spin-j particle gives rise to a term proportional to s^j.

In the partial wave decomposition, B^J will increase like s^{j-1} simply because

$$\frac{d\sigma}{d\Delta^2} = \frac{1}{2qq'} \frac{d\sigma}{d \cos \Theta} \quad . \tag{75}$$

In the absorption model, T^J could increase more slowly than B^J if the absorption increases with energy. But for some reactions like charge exchange (where the exchanged particle has to be a ρ meson), we need $T^J \to 0$ as $s \to \infty$. This is only possible if $R^2 \to \infty$, which means that σ_{total} goes to infinity too! This follows from (70). Also $\sigma_{elastic}$ will become infinite in this case by integration of (67): $\sigma_{elastic} \approx \frac{1}{4}\sigma_{total}$.

The situation becomes even worse for spin-2 exchange (f_0 particle). Here $R^2 \to \infty$ is already necessary in order to avoid that T^J increases beyond the unitary limit $|T^J| = 2$.

In the K-matrix model, T^J will not exceed the unitary limit for the exchange of any spin. This is simply due to the exact construction of unitarity, and holds true in the N/D method too. Unfortunately, the requirement of unitarity is not enough for a good description

of high-energy physics. Let us consider the case of spin-2 exchange again. Here $T^J = 2i$ follows for the elastic channel by neglecting anything but K_{22}^2 in (73), provided that terms of order s^2 occur in the diagonal elements of K_{22}^2 only. This implies that the inelastic scattering in each partial wave goes to zero, despite the fact that the Born term for one inelastic process becomes infinite. (However, it does not imply that the total inelastic scattering goes to zero, since the number of partial waves increases, too.) To say the least is that we do not expect such high-energy behaviour merely because there happens to exist a resonance in a spin-2 state [there appear, in fact, to be rather strict conditions on the magnitudes of the K-matrix elements[28] for which (73) makes sense].

It appears, therefore, that at high energies one has to start with something else than the usual Born terms. At present, the only model for this purpose seems to be the Regge pole model[29]. There, one would replace j by the "Regge trajectory" $\alpha(\Delta^2)$, with $\alpha(-m_V^2) = j$. The real part of α decreases as Δ^2 increases towards positive values. The factor s^j of the BTM would be replaced by $s^{\alpha(\Delta^2)}$, which increases less than s^j, for all physical values of Δ^2.

It is unlikely that a Regge pole model could dispense with a unitarization procedure. The difference between peripheral proton and antiproton interactions, for example, seems to be a direct consequence of absorption. But one has to take care that the amplitudes have qualitatively correct s and t dependence <u>before</u> one starts unitarizing them, otherwise one is wasting a good procedure on a bad object.

Except for Δ^2 of the order of a few m_π^2, the peripheral model is still rudimentary. This need not surprise us: if we knew what is going on at $\Delta^2 = 1\ \mathrm{GeV}^2$ (at high energies this is still in the forward cone), we would have a <u>theory</u> of strong interactions.

REFERENCES

1) S. Bergia, F. Bonsignori and A. Stanghellini, Nuovo Cimento 16, 1073 (1960).

2) G. Bordes and B. Jouvet, C.R.Acad.Sc. Paris 257, 1007 (1963); see also B. Jouvet, J.M. Abillon and G. Bordes, Physics Letters 6, 273 (1963).

3) R.F. Christy, as quoted by M. Bloch and M. Sands, Phys.Rev. 113, 305 (1959).

4) J.D. Jackson, Nuovo Cimento 34, 1644 (1964).

5) C.J. Goebel, Phys.Rev.Letters 1, 337 (1958).

6) G.F. Chew and F.E. Low, Phys.Rev. 113, 1640 (1959).

7) F. Bonsignori and F. Selleri, Nuovo Cimento 15, 465 (1960).

8) S.D. Drell, Phys.Rev.Letters 5, 342 (1960); Revs.Modern Phys. 33, 458 (1961).

9) F. Salzman and G. Salzman, Phys.Rev.Letters 5, 377 (1960); Phys.Rev. 120, 599 (1960); 121, 1541 (1961).

10) E. Ferrari and F. Selleri, Nuovo Cimento Suppl. 24, 453 (1962), see Appendix IV for further references.

11) U. Amaldi and F. Selleri, Nuovo Cimento 31, 360 (1964).

12) J.D. Jackson and H. Pilkuhn, Nuovo Cimento 33, 906 (1964).

13) H. Pilkuhn and B.E.Y. Svensson, Nuovo Cimento (in press), contains references to earlier work on joint decay distributions.

14) W. Koch, CERN Report 64-13, Vol II (1964).

15) K. Gottfried and J.D. Jackson, Nuovo Cimento 33, 309 (1964).

16) M. Jacob and G.C. Wick, Ann.Phys. 7, 404 (1959).

17) W. Rarita and J. Schwinger, Phys.Rev. 60, 61 (1961);
S. Kusaka, Phys.Rev. 60, 61 (1961).

18) L. Stodolsky and J.J. Sakurai, Phys.Rev.Letters 11, 90 (1963);
L. Stodolsky, Phys.Rev. 134, B.1099 (1964).

19) W. Heitler, Proc. Cambridge Phil.Soc. 37, 291 (1941); The Quantum Theory of Radiation, Oxford University Press, New York 1944, 2nd edition, Sec. 25.

20) R.H. Dalitz, Revs.Modern Phys. 33, 471 (1961).

21) G.F. Chew and S. Mandelstam, Phys.Rev. 119, 467 (1960).

22) The absorption model has recently been reviewed by J.D. Jackson, Revs.Modern Phys. (in press).

23) N.J. Sopkovich, Nuovo Cimento 26, 186 (1962).

24) K. Gottfried and J.D. Jackson, Nuovo Cimento 34, 735 (1964).
L. Durant, III, and Y.T. Chiu, Phys.Rev.Letters 12, 399 (1964); Phys.Rev. 137, B 1530 (1965).

25) R. Omnes, UCRL-11601 (1964).

26) R.J. Glauber, Lectures in Theoretical Physics, Vol. I, 1958, ed. by W.E. Brittin, B.W. Downs and J. Downs (Interscience, N.Y. 1959).

27) J.D. Jackson, J.T. Donohue, K. Gottfried, R. Keyser and B.E.Y. Svensson, Phys.Rev. (to be published).

28) K. Dietz and H. Pilkuhn, Nuovo Cimento (in press), and to be published.

29) M.M. Islam, Nuovo Cimento 30, 579 (1963).
M.M. Islam and R. Piñon, Nuovo Cimento 30, 837 (1963).
K. Gottfried and J.D. Jackson, Physics Letters 8, 144 (1964).

HIGH-ENERGY ELASTIC SCATTERING

A.M. Wetherell,
Nuclear Physics Division, CERN.

I. INTRODUCTION

In this talk on the elastic scattering of the strongly interacting elementary particles at energies up to about 30 GeV, I shall give a general picture of the established experimental results in the field, and describe the current problems and the probable future directions for research.

One of the main current interests in elastic scattering, namely the behaviour at very small angles, has been studied recently at the CERN Proton Synchrotron and a discussion of this work will form a substantial part of this report.

We may begin by asking the question, at a fundamental level, what do we expect to learn from studying the elastic scattering of hadrons? Possible answers might be:

i) the shape of the strongly interacting charge distribution;

ii) something about the internal structure of the particles;

iii) the mechanism of scattering or the way in which momentum is transferred from one colliding particle to another.

Such answers might be expected to result from a study of the scattering amplitude, and experimentally one sets out to learn about that by performing angular distribution and polarization measurements over the complete range of scattering angle available which is, of course, 0 to π for unlike particles, but only 0 to $\pi/2$ for like particles. From the results of such measurements one would hope to determine the structure of an amplitude, which in general will be complex

$$F(s,t) = D(s,t) + iA(s,t) = F_0(s,t) \exp i\,\varphi(s,t)$$

and spin dependent

$$D = D(\vec{\sigma}_1, \vec{\sigma}_2)$$

$$A = A(\vec{\sigma}_1, \vec{\sigma}_2) \quad .$$

The kinematic variables here are s, which is the square of the total energy, and t the four-momentum transfer squared.

$$t = -2\bar{p}^2(1 - \cos\bar{\Theta}) \approx -p^2\Theta^2 \quad \text{(for small angles)}.$$

These variables are often convenient to use rather than momentum (or wave number) and scattering angle, but I shall use all of them, as in some circumstances one set of variables suits the discussion better than the other.

At the GeV energies we are considering, the elastic scattering angular distributions are dominated by a very strong forward peak. The peak can be mainly explained by diffraction resulting from the absorption of the incident waves by the many open inelastic interaction channels. In these circumstances one may believe, for small-angle scattering, that the imaginary, or absorptive part of the scattering amplitude, A, is larger than the real, or dispersive part, D.

A simple optical model of diffraction scattering[1], which will be useful as a phenomenological guide during my discussion, can be written down as follows. Spin is completely ignored.

The scattering amplitude may be expanded in partial waves

$$f(\Theta) = \sum_{\ell} (2\ell + 1)\, f_\ell P_\ell(\cos\Theta) \quad . \tag{1}$$

As a physical assumption let us take

$$\begin{aligned} f_\ell &= \tfrac{i}{2k}[1 - \eta_\ell \exp(2i\delta_\ell)] \quad \text{for } \ell \leq L \\ f_\ell &= 0 \qquad\qquad\qquad\quad \text{for } \ell > L \quad . \end{aligned} \tag{2}$$

The waves for which $\ell \leq L$ are equally absorbed and for which $\ell > L$ do not interact at all, in other words an absorbing disc model is what we are discussing. In these terms we may write $L = kR$, where k is the wave number of the incident wave and R the maximum impact parameter, or radius.

As a physical approximation, based on ignorance, we now put

$$f_\ell = \tfrac{i}{2k}(1 - \eta) \qquad \text{for } \ell \leq L \quad . \tag{3}$$

This is merely to say that a sort of average over the absorbed amplitudes has been made. Then,

$$f(\Theta) = \tfrac{i}{2k}(1 - \eta) \sum_{\ell=0}^{L} (2\ell + 1)\, P_\ell(\cos\Theta) \quad , \tag{4}$$

and this can be written <u>exactly</u>

$$f(\Theta) = \tfrac{i}{2k}(1 - \eta) \left[P'_L(\cos\Theta) + P'_{L+1}(\cos\Theta) \right] \quad , \tag{5}$$

the primes indicating differentiation with respect to $\cos\Theta$. This form of the partial wave optical model amplitude is rarely used; mathematically it is valid at all angles.

An approximation valid at small angles may be written as follows. Consider $L = kR >> 1$ so that the scattering is confined mainly to small angles. Then,

$$\sum_{\ell=0}^{kR} (2\ell + 1)\, P_\ell(\cos\Theta) \approx 2 \int_0^{kR} \ell\, J_0(\ell\Theta)\, d\ell = (K^2R^2) \left[\frac{2\, J_1(kR\Theta)}{kR\Theta}\right] . \tag{6}$$

Hence, in this approximation

$$f(\Theta) = \frac{i}{2k}(1 - \eta)(k^2R^2) \left[\frac{2\, J_1(kR\Theta)}{kR\Theta}\right] . \tag{7}$$

The cross-section is obtained from both (5) and (7) by

$$\frac{d\sigma}{d\Omega}(\Theta) = |f(\Theta)|^2 . \tag{8}$$

From (7) therefore the angular distribution is

$$\frac{d\sigma}{d\Omega}(\Theta) = \tfrac{1}{4}(1 - \eta)^2\, k^2R^4 \left[\frac{2\, J_1(kR\Theta)}{kR\Theta}\right]^2 . \tag{9}$$

The characteristic oscillatory Bessel function angular distribution (9) is, of course, just that first given by Airy in 1835 in discussions of the diffraction of light. It has been much used in nuclear physics since the original discussion of Fernbach, Serber and Taylor[2].

A further mathematical approximation to the Airy formula valid within the first minimum of (9) may be made using

$$\left(\frac{2\, J_1(x)}{x}\right) \approx \exp -\left(\frac{x}{2}\right)^2 . \tag{10}$$

For a diffracting radius of ≈ 0.9f the first minimum is at $t \approx -0.7$ GeV^2/c.

In this approximation a neat formula for the forward diffraction peak may be written in terms of the variable $t(\approx -p^2\Theta^2)$; this is

$$\left(\frac{d\sigma}{dt}\right) = \left(\frac{d\sigma}{dt}\right)_0 \exp\left[-\left(\frac{R}{2}\right)^2 |t|\right] \tag{11}$$

where

$$\left(\frac{d\sigma}{dt}\right)_0 = \frac{\sigma^2 tot}{16\pi} . \tag{12}$$

Thus, the forward diffraction peak on this model is exponential in $|t|$ with a shape depending only on the size of the diffracting object. There is no energy dependence in the shape of the diffraction peak.

It is interesting to note that in this optical model the assumptions which lead to a forward diffraction peak also give a peak in the backward direction. This point was originally discussed by Blokhintsev[3] and further by Perl et al.[4].

Putting $\Theta' = \pi - \Theta$ in equation (5) and applying the same approximations as for (6) one finds

$$\frac{d\sigma}{d\Omega}(\Theta') = (1-\eta)^2 R^2 \left[J_0(kR\Theta') \right]^2 . \qquad (13)$$

This angular dependence gives a peak steeper than that of the forward one and also much smaller ($1/L^2$) in intensity.

These optical model formulae are, of course, specific to the model adopted, [equation (2)]. A useful general quantum mechanical result which allows one, from experiment, to say something about the phase and/or spin dependence of the scattering amplitude is the optical theorem[5] which states that

$$\frac{d\sigma}{d\Omega}(\Theta = 0) \geq \left(\frac{k\sigma_{tot}}{4\pi} \right)^2 , \qquad (14)$$

where the equality holds for a purely imaginary scattering amplitude without spin dependence. If, in a measurement of scattering at very small angles, it is found that the differential cross-section extrapolates to a value greater than the optical theorem value, it can immediately be said that there is a real part in the scattering amplitude and perhaps also a spin dependence. In this sense, then, small-angle measurements are sensitive to the phase of the amplitude: we shall see later how other possibilities arise in this context.

So far, we have discussed a model for the imaginary part, which gives specific ideas about diffraction scattering. For contributions from real part or as it is sometimes called dynamical scattering, one may suppose that the particle exchange mechanisms, π, ρ, etc., which form the basis of nuclear force considerations will play a role at high energies. Field theoretical and dispersion theoretical considerations lead, however, to the expectation that such mechanisms should decrease relative to the diffraction processes at very high energies. Let us now leave these preliminary remarks and look at some interesting elastic scattering data collected during the past two years.

II. EXPERIMENTAL RESULTS ON THE DIFFRACTION PEAK AND LARGE-ANGLE SCATTERING

Beginning at the low end of the GeV range, some measurements of Damouth et al.[6] on $\pi^{\pm}$-p scattering at 2 GeV/c using optical spark chambers, exhibit interesting features relevant to our discussion of diffraction. Figure 1 shows their angular distributions, which were measured over the complete angular range. Outside of the sharp forward peak some structure in the angular distribution is evident. The peak at $\cos \bar{\Theta} \approx 0.2$ was at first tentatively related

to the bump (resonance) found in the π^--p total cross-sections at 2.08 GeV/c by Diddens et al.[7]. Another explanation has been given by Simmons[8] who has fitted the angular distributions rather well by the simple optical model discussed in the Introduction.

Using equation (5) with L = 3 the fits shown in the figure were obtained, the bump at $\cos\bar{\Theta} \approx 0.2$ coming out simply as a secondary diffraction maximum. Perl et al.[9] have recently looked critically at the available $\pi^{\pm}$-p data and find that the secondary diffraction maximum is evident, but more weakly, up to about 4 GeV/c. In terms of the variable t it peaks at $t \approx -1.2\,(\mathrm{GeV/c})^2$. Moreover, taking the diffracting radius to be 0.9 f, the secondary maximum, using the high-energy form of our optical model (9), should be exactly at this momentum transfer.

Much of the data is from bubble chamber measurements and is weak statistically; future high-energy π-p counter and spark chamber measurements should have interesting angular distributions with which to deal.

It is at least amusing that discontinuities in the π-p angular distributions outside the main diffraction peak can be qualitatively but naturally explained by the simple optical model.

Information on the existence of a backward peak in $\pi^{\pm}$-p scattering has been obtained from bubble chamber measurements by Aderholz et al.[10] at 4 GeV/c, and by Deutschmann et al.[11] at 8 GeV/c. Figure 2 shows the angular distributions with a distinct backward peak at 4 GeV/c. At 8 GeV/c and at the enormous momentum transfer of $\approx 14\ (\mathrm{GeV/c})^2$ the CERN group found two events exactly in the backward direction. Whether this behaviour in the backward hemisphere can be characterized by an optical description is as yet impossible to say, but again the fact an optical model can give some such behaviour leads to a hope that it may provide some sort of phenomenological description even outside the forward peak.

Returning to the region of the main diffraction peak and looking at higher energies, detailed and extensive results on p-p, $\bar{p}$-p, $\pi^{\pm}$-p, and $K^{\pm}$-p scattering have been obtained[12] by a Brookhaven group using elaborate counter hodoscopes with computer on-line. Similar experiments[13] on p-p and $\pi^{\pm}$-p scattering have been performed by a CERN-collaboration group using optical spark chambers.

The general appearance of the results of the BNL p-p experiment are shown in Fig. 3, which gives the data taken at 6.8 and 19.6 GeV/c. The noticeable qualitative features are that the differential cross-section fall almost three decades in a range of t of $-0.9\ (\mathrm{GeV/c})^2$. There is a distinct energy dependence, shown by the splitting of the curves for $-t > 0.3\ (\mathrm{GeV/c})^2$, and considerable curvature at each energy. The energy dependence, the famous shrinking of the p-p diffraction peak, and the departure from a pure exponential t dependence are, of course, subtle features which are not obtained from the simple optical model. To discuss these features the experimenters fitted the curves empirically with the formula

$$\frac{d\sigma}{dt} \sim \exp(a + bt + ct^2) \quad , \qquad (15)$$

the departure from a pure exponential coming from the t^2 term and the energy dependence showing up in the variation of the coefficients b and c with energy. One may note

in passing that $b/c > 1$, and more strongly $b^2/c >> 1$. Some $\pi^{\pm}$-p results are shown in Fig. 4. The immediate striking feature is the difference from the p-p data in that there is no shrinking. This result demolished the initial wave of enthusiasm for Regge pole theories of scattering. The range of t covered in Fig. 4 does not extend, unfortunately, over the region of the second diffraction maximum, but there is no clear sign of a minimum or change of slope at $-t \approx 0.7$ (GeV/c)^2. The results of this work on the other particles may be stated briefly as follows:

i) $\bar{p}$-p shows an energy variation opposite to the p-p, in other words an expansion of the diffraction pattern;

ii) K^+-p exhibits a shrinking but at a rate, with respect to energy, less than the p-p; for K^--p no definite conclusion can be reached.

Further statements from these experiments are that the p-p and π^+-p angular distributions show a +10% deviation from the optical theorem value when extrapolated to the forward direction. Evidence for a considerable real part in the p-p and π^+-p, and possible spin dependence in the p-p scattering, is thus offered by this experiment.

The form of the diffraction peak angular distributions found in these high-energy experiments has been discussed by Van Hove[14] in a phenomenological calculation of the shadow scattering induced by the production of secondary particles. An interesting conclusion of this discussion is that the momentum transfer dependence of the angular distributions (15) can be accounted for if the secondaries created are numerous and emitted with weak dynamic correlations.

At momentum transfers larger than 1 GeV/c no extensive survey work has yet been done apart from that of the Cornell-BNL group on p-p scattering[15]. Differential cross-sections were measured, using counters, at scattering angles up to 90° (c.m.s.), and at energies up to 30 GeV. Systematic angular distribution measurements at fixed energy were not made due to practical difficulties caused by the use of the internal beam of the accelerator. The results of the large angle p-p measurements are shown in Fig. 5. An impressive feature is the enormous range (a factor $\sim 10^6$) of cross-section covered. The dashed lines show the trend of fixed energy angular distributions from which it is clear that while the t dependence slows down (as it must towards 90° c.m.s. for like particle systems) the energy dependence or shrinking is rather strong. Several attempts[15-18] have been made to fit this large-angle data with a simple empirical formula. A fit of Orear[18] is shown in Fig. 6 in which a form

$$\frac{d\sigma}{d\Omega} = \frac{A}{S} \exp - (ap_\perp) \qquad (16)$$

where $p_\perp = p \sin \Theta$

has been used. The fit was achieved with

$$A = 595 \pm 135 \text{ GeV}^2 \text{ mb/sr, and } \frac{1}{a} = 158 \pm 3 \text{ MeV/c} .$$

Considering the range of variation of the cross-section in Fig. 6 the fit is remarkably good.

Various interpretations of these results have been discussed and are listed in reference 15. The optical model which we have seen to show interesting possibilities for π-p scattering at lower energies has been extended by Serber[19] for the conditions of the p-p experiment. While the over-all rapid decrease with momentum transfer ($\sim t^{-6}$) is reproduced by Serber's model, the energy dependence is not, and in this sense the optical description fails. A statistical model for the large-angle scattering has been also discussed[20]. In this model the emission of two particles at large angles is supposed to result from the decay of a compound state formed in the collision. The calculations using this model have been performed in two ways. Hagedorn, Jones and Fast used the results of computer calculations of phase space for particle production estimates, while the other authors in reference 20 discussed the problem using thermodynamic arguments. It was found that the statistical model gave a rather good description of the energy dependence of the very wide angle (90°) proton scattering data; the angular dependence outside of the diffraction peak is not well explained, however.

A nice physical picture of collisions, which in a general way brings together the various points of view, has been presented by Wu and Yang[21]. They remark that if the proton is pictured as an extended object containing characteristic frequencies largely in the region of $\sim$ 100 MeV, then it is clear that a very rapid decrease of elastic cross-section with transverse momentum is to be expected as it is difficult to accelerate pieces of the nucleon violently without breaking it up. Exchange of pieces of nucleon matter longitudinally can be rather easily made, however, as the internal motion in the nucleon leads to large longitudinal components of momentum in the laboratory system.

So far extensive work on wide-angle very high-energy π-p scattering has not been published; it will be interesting to see whether the general behaviour is similar to that of the p-p scattering. Already we have seen a difference in the diffraction peak, namely the non-shrinking of the π-p. Also, the existence of secondary diffraction maxima in the lower energy π-p data seems to constitute a difference from the p-p behaviour.

To summarize the above experimental results we may say that:

i) the π-p and p-p scattering amplitude at momentum transfer less than 1 GeV/c is largely imaginary but a certain amount of real amplitude is probably present;

ii) the scattering amplitude, in the main diffraction peak region, has an energy dependence which depends on the particle system;

iii) the π-p scattering appears to show secondary diffraction maxima up to about 4 GeV/c;

iv) the wide angle (90° c.m.) p-p scattering appears to behave statistically rather than optically.

It is clear that the over-all situation is quite complicated and that only rather qualitative statements have been made, for example no definite phase for, say, the p-p scattering amplitude has been given. This problem has been taken up in the last year in measurements of p-p and π-p scattering at very small angles.

III. SCATTERING EXPERIMENTS AT VERY SMALL ANGLES

A general method to find the phase of a high-energy charged particle scattering amplitude at small momentum transfers is to measure the interference between the essentially real Coulomb scattering amplitude and the real part of the strong interaction amplitude. The cross-section can be written simply, ignoring spin complications and small correction terms, as

$$\frac{d\sigma}{d\Omega} \sim |C + D + iA|^2 \qquad (17)$$

in which C is the Coulomb amplitude. Then,

$$\frac{d\sigma}{d\Omega} \sim C^2 + A^2 + D^2 + 2CD \ . \qquad (18)$$

After removing the known Coulomb contribution C^2 the two last terms in (18) give:

i) a deviation from the optical theorem value, and

ii) a characteristic shape in the angular distribution.

The interference term varies essentially as Θ^{-2} so that an experiment detecting such a contribution to an angular distribution would give a direct measurement of the real part of the scattering amplitude. This method works well at lower energies and Fig. 7 shows a p-p angular distribution measured at about 0.8 GeV/c by Fischer and Goldhaber[22], using nuclear emulsions in a forward camera-type of experiment. Figure 7 gives an idea of how destructive Coulomb interference with the real nuclear amplitude can appear. As the Coulomb force in a p-p system is repulsive, the destructive interference terms show that the nuclear force corresponding to the real part is attractive at this energy.

At energies above, say, 5 GeV, the main experimental difficulties in detecting the scattered particle arise from the very small laboratory angles at which measurements in the Coulomb interference region have to be made; for example at 19 GeV/c the differential cross-section has to be well measured at angles below 5-6 mrad. Another possibility is to detect the recoil proton which emerges at almost 90° (lab. system), but then a problem is presented by the very low energy of the particle.

The recoil kinetic energy is:

$$T_{rec} = \frac{|t|}{2M} \approx \frac{p^2\Theta^2}{2M} \ , \qquad (19)$$

so that for 19 GeV/c and a scattering angle of 2 mrad the recoil energy is only about 0.8 MeV.

The recoil proton method has been much used by the workers at Dubna[23] in p-p measurements, using the very simple system shown in Fig. 8.

The internal beam of the accelerator is incident on a very thin foil hydrocarbon target, and particles emitted at essentially 90° were detected by nuclear emulsions in which the angle and energy can be well measured. A similar experiment has been performed[24] at CERN, at 24 GeV/c, using an extracted beam and a H_2 gas target. Recently, the Dubna workers have applied solid-state detectors to this type of experiment, which seems to be a progressive and interesting development.

Experiments detecting the fast scattered particle have been recently done at CERN[25], at Brookhaven[26], and at the Rutherford Laboratory in England[27]. The CERN and the British experiments measured p-p scattering using sonic spark chambers, while the BNL group measured both π-p and p-p scattering with elaborate counter hodoscopes.

The layout of the CERN experiment is shown in Fig. 9. An elastically scattered beam of protons from the accelerator was used. The directions and momenta of incident and scattered protons were measured by a system of five thin-plate sonic spark chambers S_1 to S_5, a small counter C_1, and four magnets. The amount of stray material in the beam was kept to a minimum to reduce multiple scattering and background. The angular resolution of the system was $\sim$ 1/10 mrad and the momentum resolution $\sim$ 1/2%. This good resolution was possible because of the accurate location ($\sim$ 1/2 - 1 mm) of particles in the spark chambers; for hodoscopes the precision is generally not better than 1/2 cm.

In the original runs of the spark chamber experiments the digitized time-of-flight information from the chambers was recorded on magnetic tape at a rate of 1-2 per synchrotron cycle. More recently, a small (4K memory) fast computer has been put on-line, and rates up to $\sim$ 10 per pulse can be achieved by using the computer memory as a store during the data acquisition cycle and writing on tape between cycles. Moreover, the computer checks the data and signals faulty operation of the spark chamber system. The calculations of momenta, scattering angles, and cross-sections are always performed by a large central computer from the filled magnetic tapes acquired during data taking periods.

In this respect, the BNL hodoscope system using an on-line computer is more advanced as it provides immediately fully computed results from a sample of the raw material taken.

The angular distributions found in the CERN p-p experiment at 10, 19, and 26 GeV/c are shown in Fig. 10, and clear deviations of the cross-section above the optical theorem value are seen. For a quantitative discussion the cross-sections were analysed using two models. First, fits were made on the assumption of a complex spin independent scattering amplitude f_n using the relations:

$$f_n = \left(\frac{\sigma_{tot}}{4\pi n}\right)\left[\rho(t)\ \exp(\tfrac{1}{2}A_R t) + i(\exp\ \tfrac{1}{2}A_I t)\right] \qquad (20)$$

$$f_c = \frac{-2e^2}{\beta c|t|}\ (1 + i\epsilon) \qquad (21)$$

$$\epsilon = 0.0073\ \ln\frac{0.0437}{t} \qquad (22)$$

$$\frac{d\sigma}{d\Omega} = p^2\,|f_n + f_c|^2 + \text{corrections} \qquad (23)$$

in which t is in units of $(GeV/c)^2$, β is the laboratory velocity, and σ_{tot} is the strong interaction total cross-section. For the very small values of t involved, the electromagnetic form factor of the proton has been taken equal to unity. The expression for the Coulomb amplitude was taken from the discussion of Bethe[28] and contains a small imaginary part ϵ. The interference of the latter with the large imaginary nuclear amplitude is always small and contributes, for example, at $t = -1.8 \cdot 10^{-3}$ $(GeV/c)^2$, 2.3% to $d\sigma/d\Omega$. At larger momentum transfers this contribution is even smaller.

In the evaluation the following simplifications were made: $A_1 = A_R = A$, and $\rho(t) = \rho$ independent of t. Corrections amounting to about 1% were made to take account of multiple scattering in the hydrogen target and the presence of small non-additive Coulomb terms[29].

The good fits found using this model are shown on the left-hand side of Fig. 10 with an angle scale as abscissa. The amount of real part found over this energy range is substantial, about 30-40% of the imaginary. The sign of the interference here is positive, corresponding to a repulsive force and opposite to that which we saw at 0.8 GeV/c in Fig. 7.

In the second model the characteristic shapes of the angular distributions were attributed to spin dependence of the p-p interaction. Pure imaginary singlet-triplet spin amplitude fits were made using the amplitude term:

$$f_n = i \left(\frac{\sigma_{tot}}{4\pi\hbar} \right) \left[\sqrt{\frac{3}{4}} \frac{(3 + \vec{\sigma}_1 \cdot \vec{\sigma}_2)}{4} a_3 \exp(\tfrac{1}{2} A_3 t) + \sqrt{\frac{1}{4}} \frac{(1 - \vec{\sigma}_1 \cdot \vec{\sigma}_2)}{4} a_1 \exp(\tfrac{1}{2} A_1 t) \right] , \quad (24)$$

and the optical theorem constraint (because both amplitudes are imaginary)

$$\tfrac{3}{4} a_3 + \tfrac{1}{4} a_1 = 1 . \quad (25)$$

The exponential slopes A_1 and A_3 for the singlet and triplet states, and the amplitude coefficients a_1 and a_3 were varied to fit the experimental points.

The fits obtained are given in the right-hand side of Fig. 10, where the abscissa is the four-momentum transfer squared. In this section of Fig. 10 the Coulomb cross-section has been subtracted. The rapidly decreasing initial part of the angular distribution has then to be fitted using a very steeply falling imaginary triplet amplitude. It was found that the fits obtained from this model were not very good. In any case, the steep initial slope exhibited by the data would appear to be most plausibly Coulomb-like in origin.

It was concluded, therefore, that a complex spin independent amplitude explains the data better, although of course a more complicated situation, such as complex spin dependent amplitudes, could not be ruled out. Polarization measurements of various kinds must be made to study this possibility.

Some π^--p data obtained between about 8 and 12 GeV/c in the BNL experiment are shown in Fig. 11. A distinct destructive Coulomb interference is manifest in these curves. Spin dependence can be essentially ruled out at very small angles in the π-p system as the only possible spin dependent term approaches zero with scattering angle. The real part inducing

a destructive Coulomb interference in the π^--p system corresponds, as in the p-p case, to a repulsive force. The same is found to be true for π^+-p at around 10 GeV/c and the ratio of real and imaginary parts for both π^+ and π^- is $\approx$ 25%.

Figure 12 shows the ratios of real to imaginary amplitudes (ρ or D/A) for forward p-p scattering which were obtained from the various experiments. The interesting qualitative features are the rapid switch from positive to negative values (attractive to repulsive) in the region (1 - 1.5 GeV/c) of the steep rise in the p-p total cross-section and the rather constant behaviour up to 26 GeV/c. This general sort of behaviour was found by Söding[30] from an evaluation of the nucleon-nucleon dispersion relations of Goldberger, Nambu and Oehme[31]. Figure 13 shows the results of Södings computation on a logarithmic momentum scale. The trend of the experimental points is well reproduced; on the same basis the prediction is that the $\bar{p}$-p will show a much smaller negative D/A above 5 GeV/c. This will be an important experiment to check on this application of the dispersion relations. The extension of these studies to the 100 GeV region, in the rather distant future, also presents fascinating possibilities. In Söding's evaluation D/A is set equal to zero and $\sigma^+_{tot} = \sigma^-_{tot}$ at extremely high energies; indications as to whether or not this is possible might be forthcoming in the 100 GeV region. The Coulomb interference experiments will be difficult at these very large energies, but it is worth noting, in passing, that the present CERN small-angle experiment could rather readily measure the diffraction peak region (say $-t \lesssim 0.5$ GeV/c^2) at energies between 100 and 300 GeV. The angular ranges would be about 7 and 2.5 mrad, respectively.

To summarize this brief discussion of the phase problem we can say that:

i) the p-p scattering amplitude has a considerable ($\approx$ 30%) repulsive real part at momenta between about 7 and 26 GeV/c;

ii) at around 10 GeV/c both π^+ and π^--p amplitudes have repulsive real parts about 25% of the imaginary;

iii) the p-p measurements show no strong evidence for spin dependence.

Point (iii) is a rather negative statement about such an interesting problem, and the next section discusses briefly experiments on polarization which aim to find out about spin effects.

IV. POLARIZATION EXPERIMENTS

The scattering matrix for a spinless meson and a nucleon has the general form:

$$M = N + F\vec{\sigma}\cdot\vec{n} \quad , \tag{26}$$

where $\vec{n} = \vec{k}_i \times \vec{k}_f$ (normal to the scattering phase). The two pieces of the matrix correspond to non-spin flip and spin flip, respectively. For very small scattering angles $\vec{\sigma}\cdot\vec{n} \to 0$ and, as remarked in the last section, the interesting small-angle effects in π-p scattering must be caused by Coulomb interference with a real amplitude.

For nucleon-nucleon scattering the situation is more complicated. Dalitz[32], Wolfenstein and Ashkin[33] have given the general form of the scattering matrix as:

$$M = A + B(\vec{\sigma}_1 \cdot \vec{\sigma}_2 - 1) + C(\vec{\sigma}_1 + \vec{\sigma}_2) \cdot \vec{n} + D(\vec{\sigma}_1 - \vec{\sigma}_2) \cdot \vec{n} + E(\vec{\sigma}_1 \cdot \vec{K})(\vec{\sigma}_2 \cdot \vec{K}) + F(\vec{\sigma}_1 \cdot \vec{P})(\vec{\sigma}_2 \cdot \vec{P}) \ , \tag{27}$$

where

$$\vec{K} = \vec{k}_i - \vec{k}_f, \text{ and } \vec{P} = \vec{k}_i + \vec{k}_f \ .$$

As the scattering angle approaches zero, terms drop out and one is left with:

$$M \sim f_1 + f_3 + S\ \vec{\sigma}_1 \cdot \vec{\sigma}_2 \tag{28}$$

which is ordinary singlet and triplet (complex) amplitudes and a spin flip amplitude, which does not necessarily approach zero in the forward direction. As we have seen in the last section, the possibility of complex singlet and triplet amplitudes operating in the p-p small-angle scattering could not be excluded, and absolutely no information exists on the spin flip term. A possible way to study these spin effects which may be present at small angles is to measure the scattering of polarized beam protons on the polarized target. Up to now only the latter exists; as yet no degree of polarization is known to exist in any GeV proton beam.

The p-p experiments which have recently measured polarization effects, away from the forward direction, where $\vec{\sigma} \cdot \vec{n}$ terms operate, have been done in two ways:

i) the degree of polarization of the recoil proton produced in an elastic scattering has been analysed by the asymmetry in a second scatter[34];

ii) the scattering on a polarized hydrogen target has been measured[35].

The second method offers by far the best possibilities and a series of measurements between about 0.33 and 6.15 GeV has been made by the Berkeley group using this technique. They measured:

$$\left(\frac{d\sigma}{d\Omega}\right)_{pol} = \left(\frac{d\sigma}{d\Omega}\right)_{unpol} [1 + P(\Theta)\ P_T]$$

where P_T is the target polarization ($\sim$ 30%). At GeV energies $P(\Theta)$ is found to peak at $t \approx -0.3$ GeV/c^2, and Fig. 14 shows the maximum value of $P(\Theta)$ as a function of energy. The highest energy point on this graph is from a Dubna measurement using the double scattering method.

It is interesting to see in Fig. 14 that the polarization rises to a maximum of $\sim$ 50% at $\sim$ 1 GeV and then falls slowly to $\sim$ 10% at $\sim$ 9 GeV. One may note also that the maximum occurs in the region of the steep rise of the p-p total cross-section and the slow decrease on the flat plateau region of the cross-section. We have already noted the change in the behaviour of the real part at around 1 GeV/c; this multiple production threshold region seems to be very interesting and would be worth some study with the smaller proton machines working now.

The behaviour of $P(\Theta)$ at 10 GeV/c and above also presents an important challenge to the experimenters and one would hope that in the next year some data will be produced.

To summarize the GeV energy polarization data, one can only say that up to $\sim$ 10 GeV spin effects can manifest themselves in a non-negligible way for angles away from the forward direction. It is not yet clear how to fit this information into any complete description of the scattering amplitude.

V. PROTON-NUCLEAR SCATTERING AT HIGH ENERGIES

In this section I shall describe briefly some new results on proton-nuclear scattering at 19.3 GeV/c which were obtained using the CERN sonic spark chamber set-up. The only essential difference from the p-p experiments was the change of target.

The elastic momentum peaks obtained at each scattering angle measured contained contributions both from coherent scattering and from quasi-elastic scattering; the ratio of the two would be expected to be large at the very small angles studied. Also it should be stressed that the energy resolution of the system was, of course, not sufficient to distinguish scattering with nuclear excitation.

The angular distribution found for Pb and for Cu are shown in Fig. 15. The experimental points are plotted in $\frac{1}{2}$ mrad intervals. A striking oscillatory behaviour is evident in Fig. 15. The curve drawn on the Pb graph is the Airy diffraction pattern, equation (9) of the Introduction, which, with a nuclear radius of 7.5 f reproduces very well the periodicity of the angular distribution. It may be concluded, therefore, that three subsidiary diffraction maxima are visible in the Pb angular distribution. In the Cu only a secondary peak is seen as the angular range available in the experiment did not fully cover the tertiary maximum. It should be said that these data are quite preliminary; it is possible that the diffraction minima evident in Fig. 15 are really deeper and more data will be taken with improved resolution (less multiple scattering in the target) to study this question. For lighter nuclei the subsidiary maxima occur at larger angles outside of the experimental range and, moreover, they are probably overwhelmed by the dominance of quasi-elastic scattering. The reason that the structure is so evident for the Pb and Cu nuclei also depends on the fact that the edge or transition layer ($\sim$ 1.5 - 2f) covers considerably less space than does the body of the nucleus itself, $R \approx 7.50$ and 5.55 f for Pb and Cu, respectively.

These elegant results on nuclear scattering also suggest that secondary diffraction maxima in elementary particle interactions may be masked by the way in which the angular distribution falls off at larger angles, and an application of this way of thinking may be for the π-p and p-p systems.

VI. CONCLUSION

During the course of this talk it will have become evident that the physics available from elastic scattering measurements is both extensive and complicated.

With respect to the questions asked in the Introduction, we can probably say that the proton exhibits a rather extended loosely bound structure, without any profound momentum components. An essential mechanism of high-energy scattering is diffraction but the dynamical scattering manifested in the existence of the real part of scattering amplitudes is unexplained.

With the advent of the very small angle scattering measurements the quantitative study of the scattering amplitudes has really begun. As will have become apparent, the completion of the task over the presently available energy range will present interesting work for many in the next years.

REFERENCES

1) K.R. Greider and A.E. Glassgold, Ann.Phys. 10, 100 (1960).

2) S. Fernbach, R. Serber and T.B. Taylor, Phys.Rev. 75, 1352 (1949).

3) D.I. Blokhintsev, Nuovo Cimento 23, 1061 (1962).

4) M.L. Perl, L.W. Jones and C.C. Ting, Phys.Rev. 132, 1252 (1963).

5) G.C. Wick, Phys.Rev. 75, 1459 (1949).

6) D.E. Damouth, L.W. Jones and M.L. Perl, Phys.Rev.Letters 11, 287 (1963).

7) A.N. Diddens, E.W. Jenkins, T.F. Kycia and K.F. Riley, Phys.Rev.Letters 10, 262 (1963).

8) L.M. Simmons, Phys.Rev.Letters 12, 229 (1964).

9) M.L. Perl, Y.Y. Lee and E. Marquit, SLAC-PUB-58, Nov. 1964.

10) Aachen, Berlin, Birmingham, Bonn, Hamburg, Imperial College, Munich collaboration, Physics Letters 10, 248 (1964).

11) M. Deutschmann, D. Kropp, S. Nagel, H. Weber, I. Woischnig, C. Grote, J. Klugow, S. Nowak, S. Brandt, V.T. Cocconi, O. Czyzewski, J. Danysz, P. Dalpiaz, G. Kellner and D.R.O. Morrison, presented at the Int.Conf. on High-Energy Physics (1964) Dubna.

12) K.J. Foley, S.J. Lindenbaum, W.A. Love, S. Ozaki, J.J. Russell and L.C.L. Yuan, Phys.Rev.Letters 10, 376 (1963); 10, 543 (1963); 11, 425 (1963); 11, 503 (1963).

13) D. Harting, P. Blackall, B. Elsner, A.C. Helmholtz, W.C. Middelkoop, B. Powell, B. Zacharov, P. Zanella, P. Dalpiaz, M.N. Focacci, G. Focardi, G. Giacomelli, L. Monari, J.A. Beany, R.A. Donald, P. Mason, L.W. Jones and D.O. Caldwell, to be published in Nuovo Cimento.

14) L. Van Hove, Revs.Modern Phys. 36, 655 (1964).

15) G. Cocconi, V.T. Cocconi, A.D. Krisch, J. Orear, R. Rubinstein, D.B. Scarl, B.J. Ulrich, W.F. Baker, E.W. Jenkins and A.L. Read, to be published in Phys.Rev.

16) G. Cocconi, Nuovo Cimento 33, 643 (1964).

17) A. Krisch, Phys.Rev.Letters 11, 217 (1963).

18) J. Orear, Physics Letters 13, 190 (1964).

19) R. Serber, Revs.Modern Phys. 36, 649 (1964).

20) G. Fast and R. Hagedorn, Nuovo Cimento 27, 208 (1963).
G. Fast, R. Hagedorn and L.W. Jones, Nuovo Cimento 27, 856 (1963).
L.W. Jones, Physics Letters 8, 287 (1964).
R. Hagedorn, Nuovo Cimento 35, 216 (1965).
A. Bialas and V. Weisskopf, to be published in Nuovo Cimento, see also reference 16 in this context.

21) T.T. Wu and L.N. Yang, Phys.Rev. 137, B708 (1965).

22) D. Fischer and G. Goldhaber, Phys.Rev. 95, 1350 (1954).

23) L. Kirillova, L. Khristov, V. Nikitin, M. Shafranova, L. Strunov, V. Sviridov, Z. Korbel, L. Rob, P. Markov, Kh. Tchernev, T. Todorov and A. Zlateva, Physics Letters 13, 93 (1964), and Dubna Report E-1820 (1964).

24) H. Lohrmann, H. Meyer and H. Winzeler, Physics Letters 13, 78 (1964).

25) G. Bellettini, G. Cocconi, A.N. Diddens, E. Lillethun, J. Pahl, J.P. Scanlon, J. Walters, A.M. Wetherell and P. Zanella, Physics Letters 14, 164 (1965).

26) K.J. Foley, R.S. Gilmore, R.S. Jones, S.J. Lindenbaum, W.A. Love, S. Ozaki, E.H. Willen, R. Yamada and L.C.L. Yuan, reported at the Int.Conf. on High-Energy Physics (1964) Dubna, and Phys.Rev.Letters 14, 74 (1965).

27) A.E. Taylor, A. Ashmore, W.S. Chapman, D.F. Falla, W.H. Range, D.B. Scott, A. Astbury, F. Capocci and T.G. Walker, Physics Letters 14, 54 (1965).

28) H.A. Bethe, Ann.Phys. 3, 190 (1958).

29) N.N. Achasov and V.P. Pleshakov, Report T.F.-11 (1964), U.S.S.R. Academy of Science, Novosibirsk.

30) P. Söding, Physics Letters 8, 285 (1964).

31) M.L. Goldberger, Y. Nambu and R. Oehme, Ann.Phys. 2, 226 (1957).

32) R.H. Dalitz, Proc.Phys.Soc. A65, 175 (1952).

33) L. Wolfenstein and J. Ashkin, Phys.Rev. 85, 947 (1952).

34) P. Bareyre, J.F. Detoeuf, L.W. Smith, R.D. Tripp and L. van Rossum, Nuovo Cimento 20, 1049 (1961).
V.P. Kanavets, I.I. Levintov, B.V. Morozov, M.D. Shafranov, Zh. Eksperim.i.Teor.Fiz. 45, 1272 (1963).

35) F.W. Betz, J.F. Arens, H.E. Dost, M.J. Hansroul, L.E. Holloway, C.H. Schultz, G. Shapiro, W.K. Troka, H.M. Steiner, D.Chamberlain, B.D. Dieterle, P.D. Grannis, L. van Rossum and D.M. Weldon, UCRL 11440 (1964).

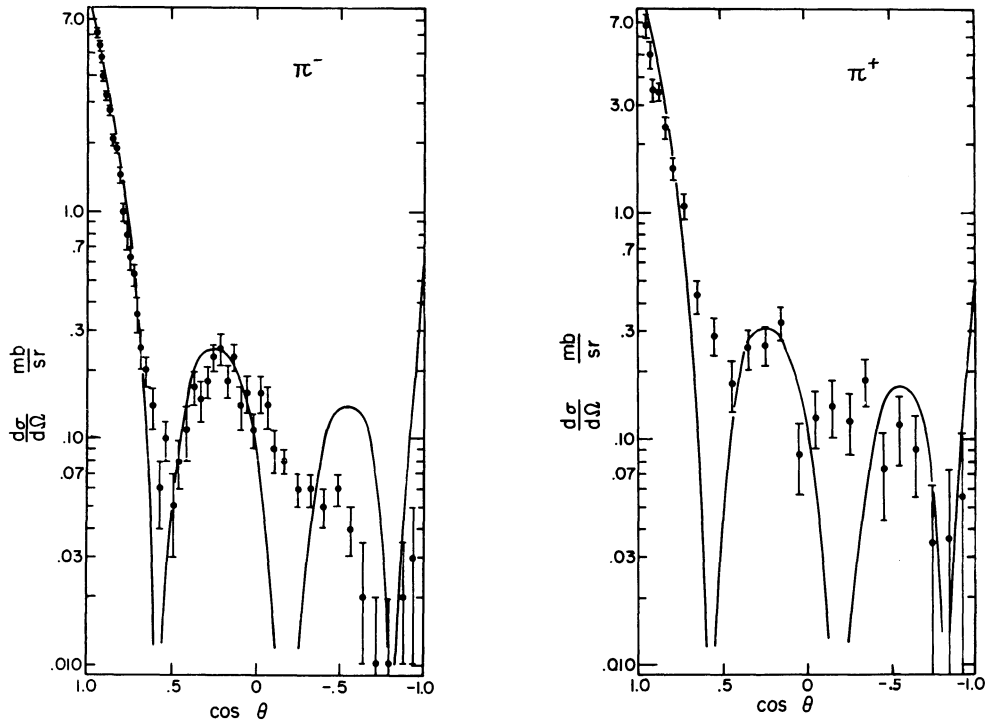

Fig. 1 π^--p and π^+-p angular distributions measured at 2 GeV/c by Damouth et al.[6]. The superimposed curves are an optical model fit of Simmons[8].

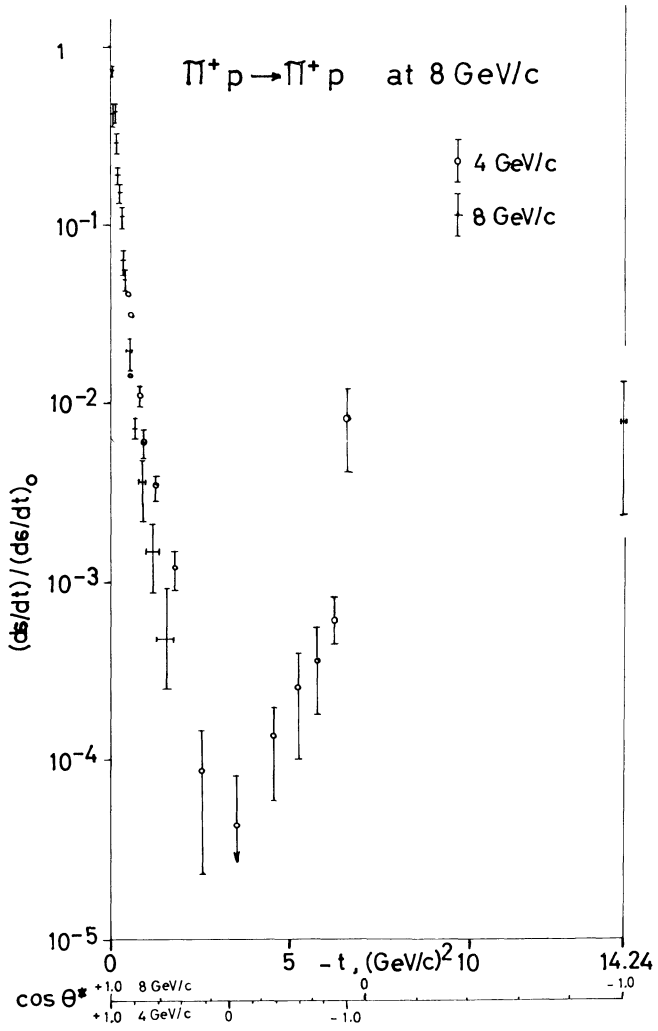

Fig. 2 π^+-p differential cross-sections at 4 GeV/c [10] and at 8 GeV/c [11].

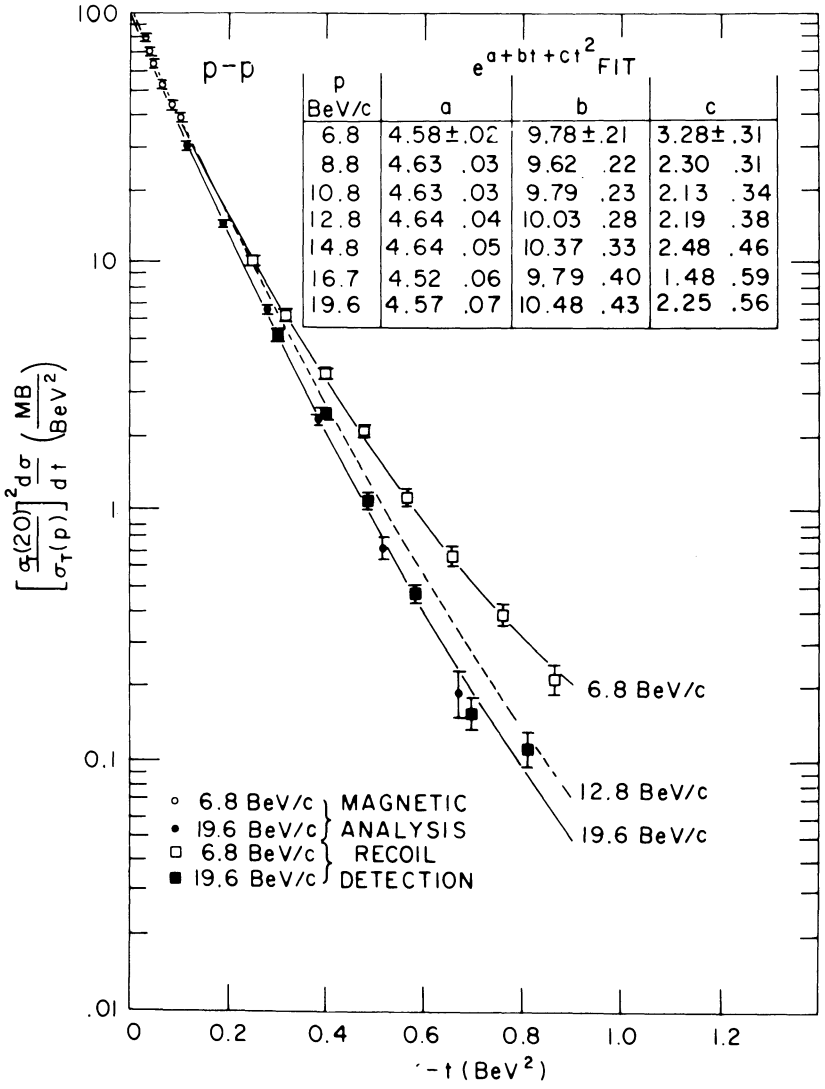

Fig. 3 Differential cross-sections for elastic p-p scattering measured by Foley et al.[12]. The inset gives a certain fit to the experimental points.

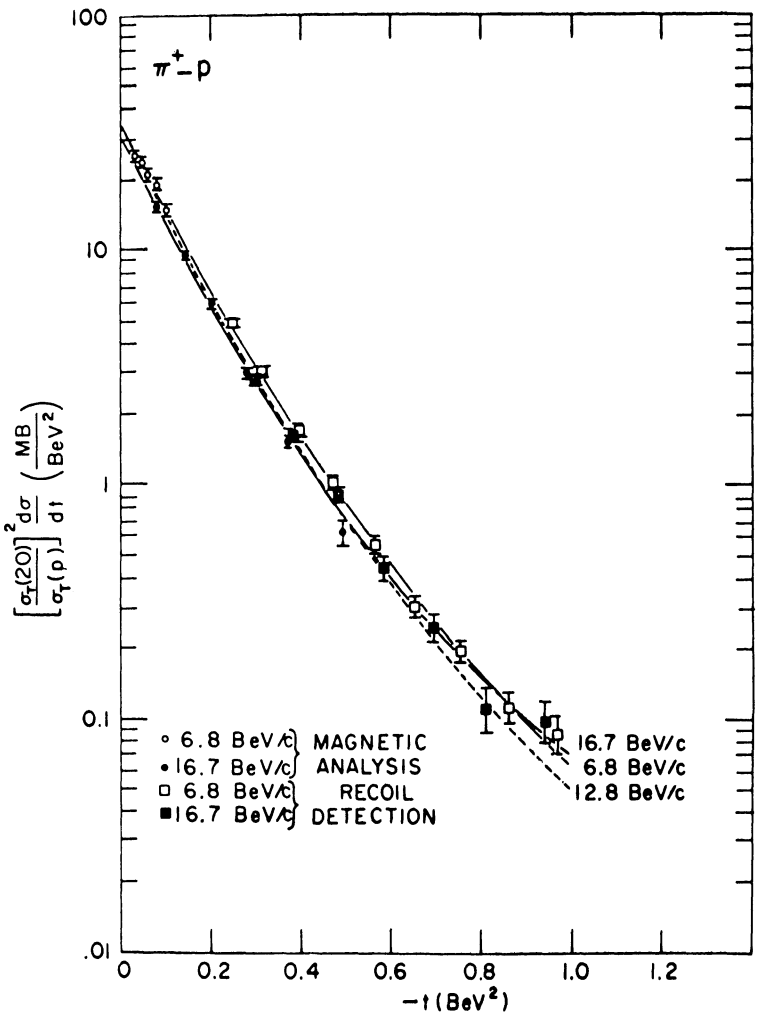

Fig. 4 π^+-p differential cross-sections measured by Foley et al.[12].

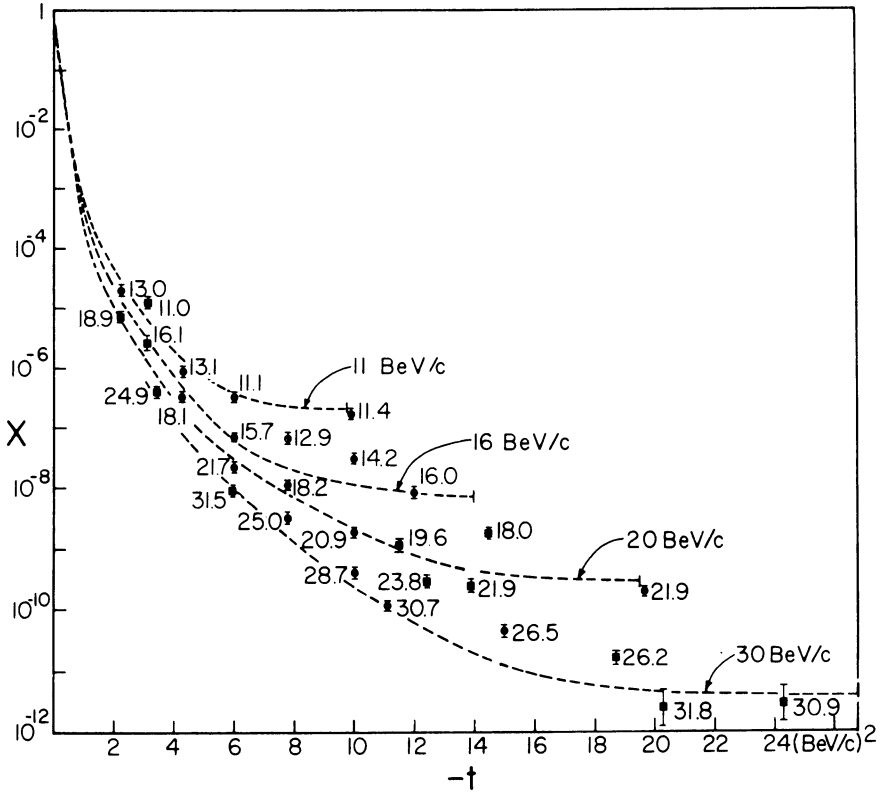

Fig. 5 Large momentum transfer p-p cross-sections measured by Cocconi et al.[15]. $X = (d\sigma/dt)/(d\sigma/dt)_0$.

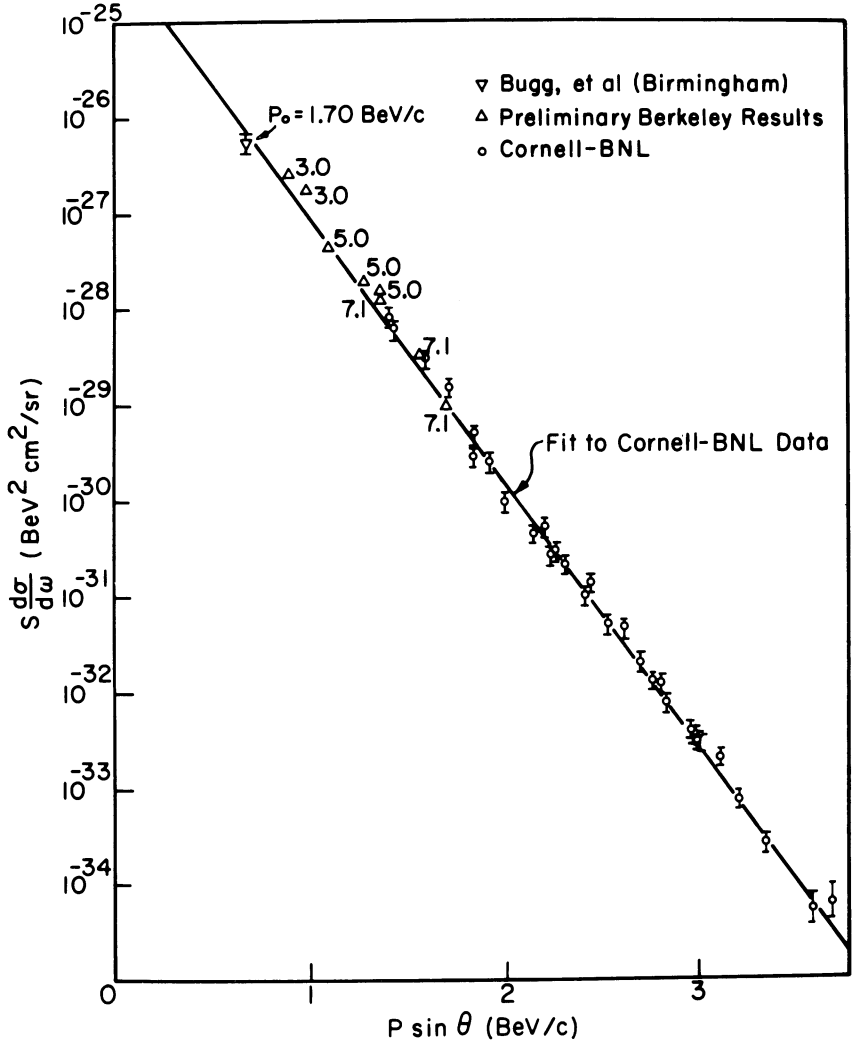

Fig. 6 Fit to p-p elastic cross-sections by Orear[18]. $(d\sigma/d\Omega)$ is given in the c.m.s.

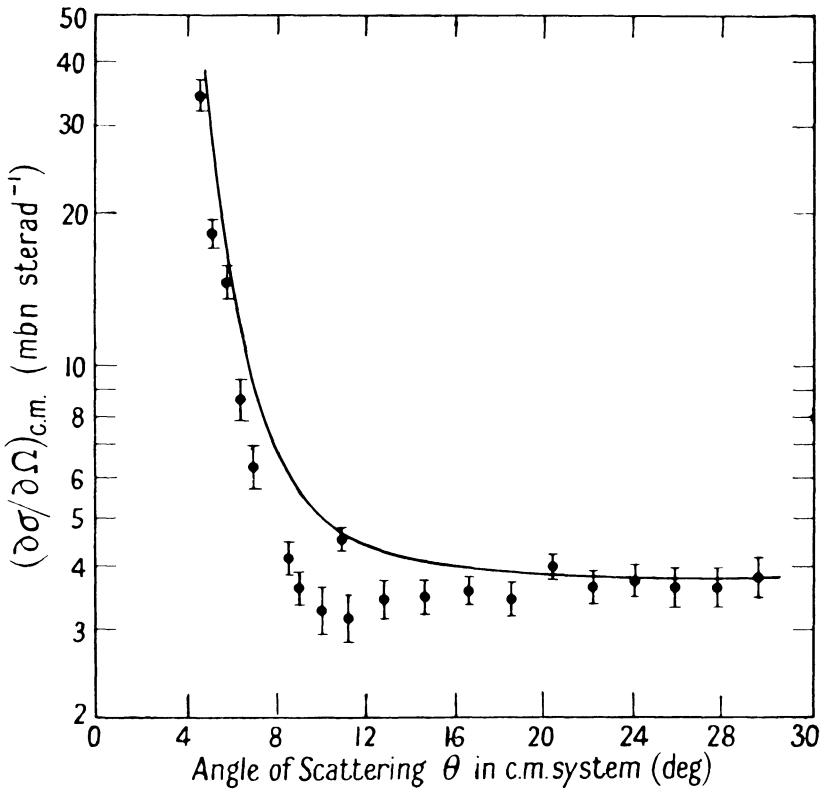

Fig. 7 Forward p-p angular distribution measured at 0.8 GeV/c by Fischer and Goldhaber[22].

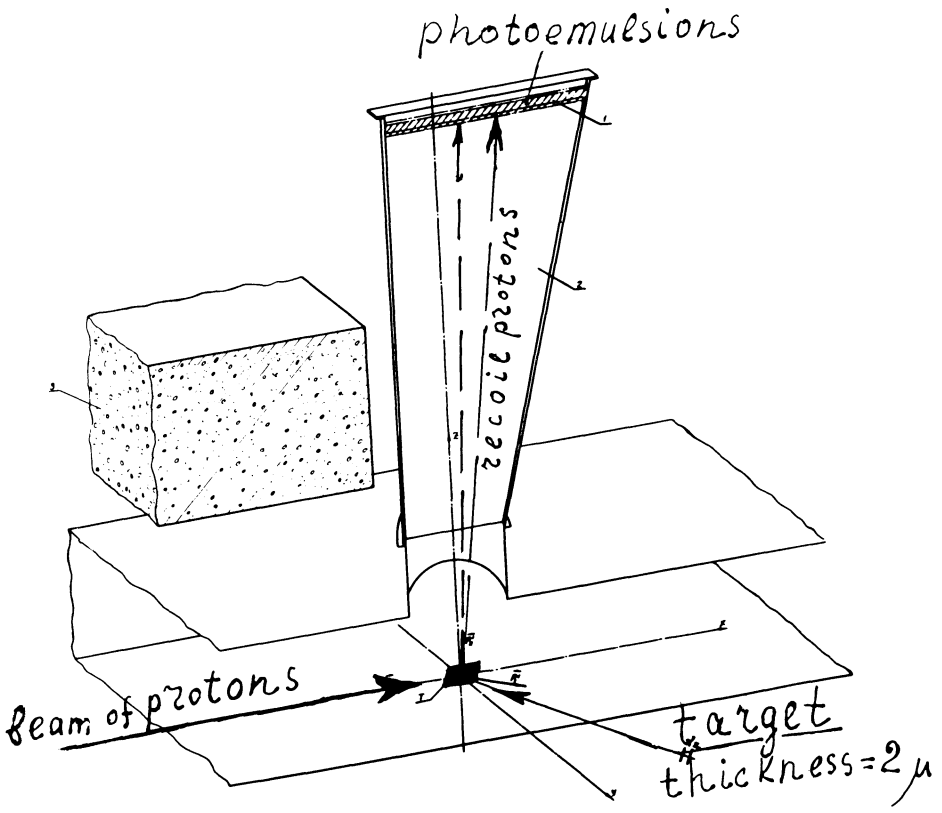

Fig. 8 Recoil proton technique used by the Dubna group[23] to measure small-angle p-p scattering.

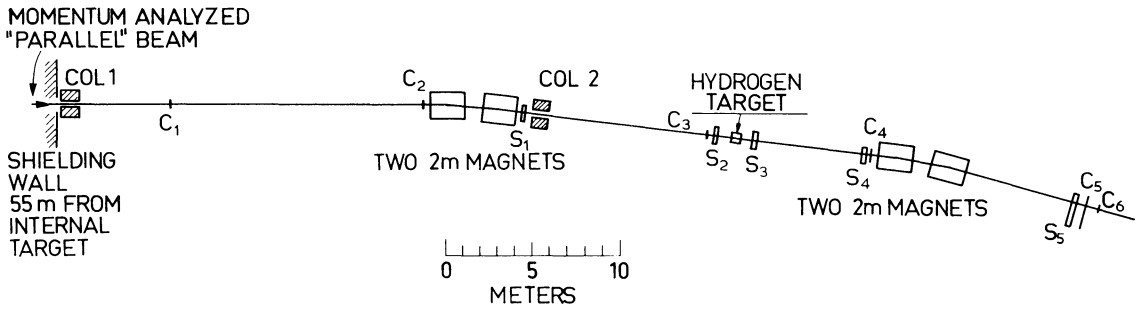

Fig. 9 Layout of CERN sonic spark chamber experiment[25] to measure small-angle p-p scattering. $C_1 - C_6$ are scintillation counters and $S_1 - S_5$ are sonic spark chambers.

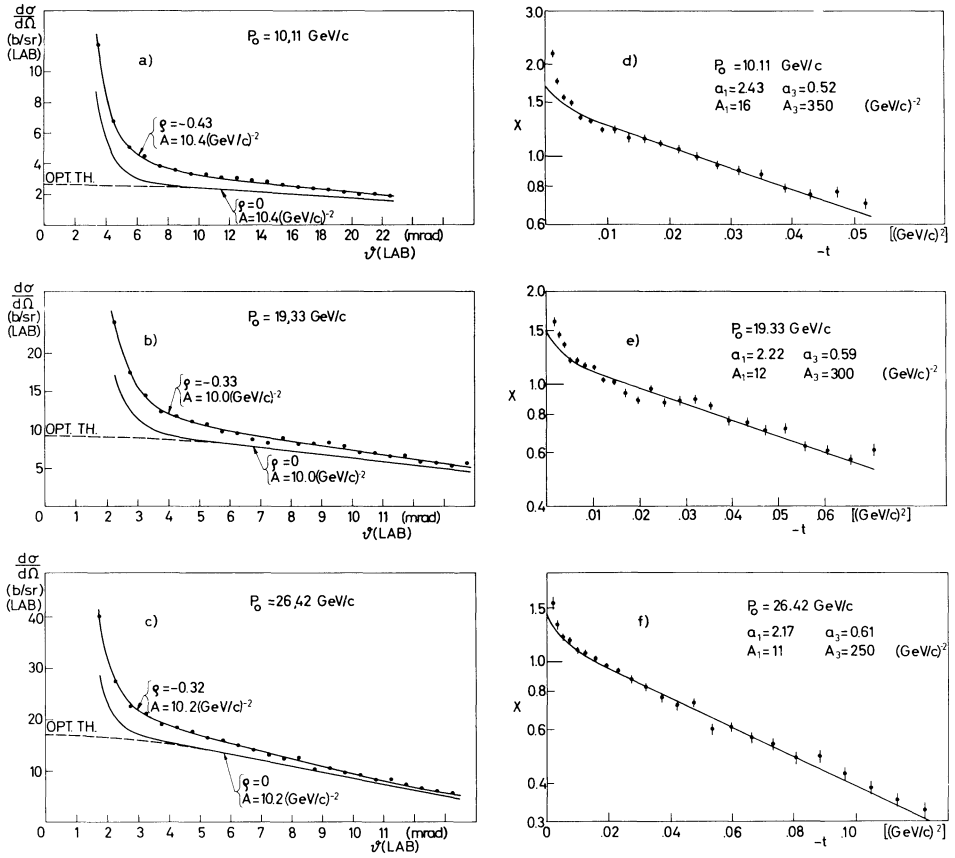

Fig. 10 Angular distributions obtained in CERN small-angle p-p scattering experiment[25]. The three graphs to the left with Θ as abscissa show good complex spin independent fits, those on the right rather poor purely imaginary singlet-triplet amplitude fits. X is the difference between the measured and the Coulomb cross-sections, normalized to the optical theorem value.

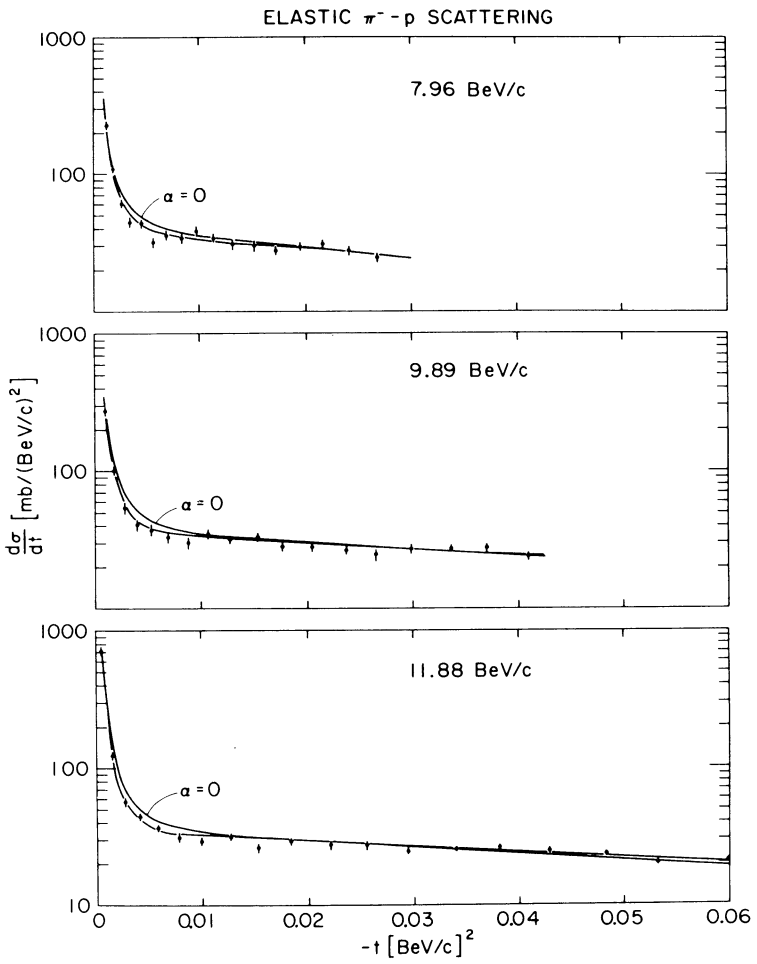

Fig. 11 Small-angle π^--p elastic angular distributions measured by Foley et al.[26]. The curves labelled $\alpha = 0$ are calculated for a pure imaginary amplitude.

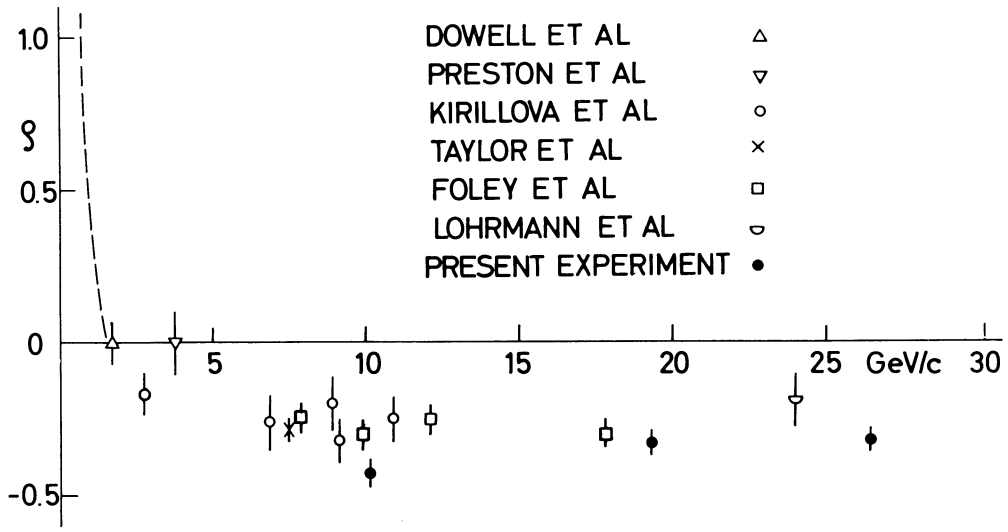

Fig. 12 The ratio of the real to imaginary p-p forward amplitude ρ obtained from various small-angle scattering experiments.

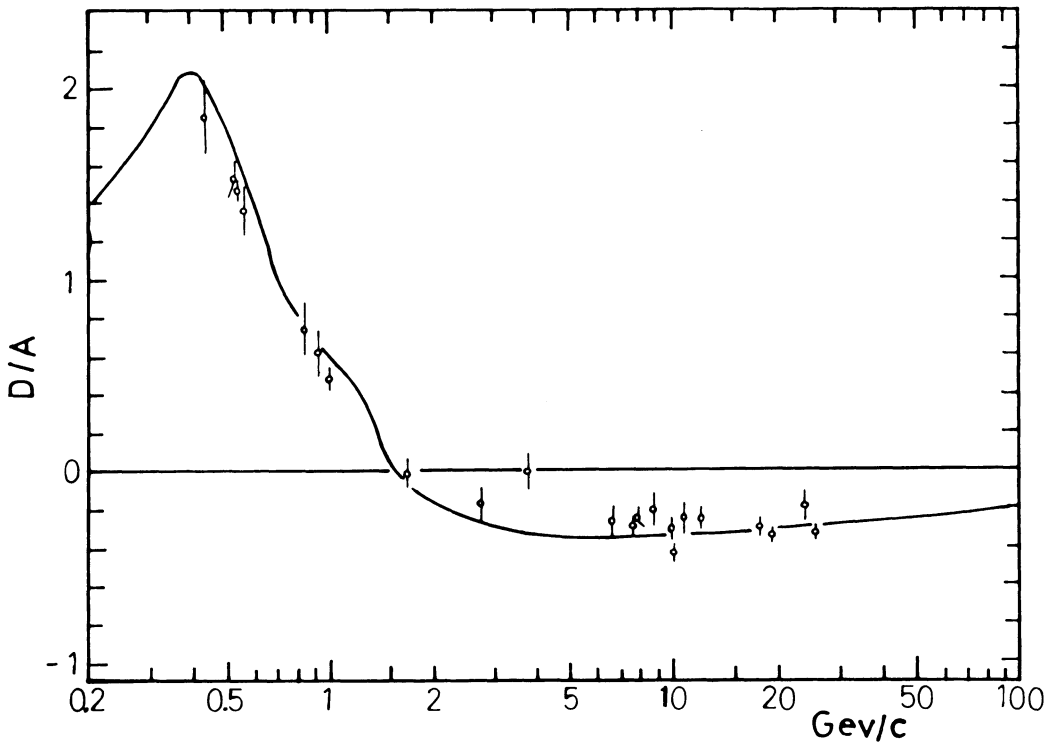

Fig. 13 The result of Söding's evaluation[30] of the nucleon dispersion relations to find the ratio of real to imaginary p-p forward amplitudes (here called D/A). The reproduction of the trend of the experimental points is very good.

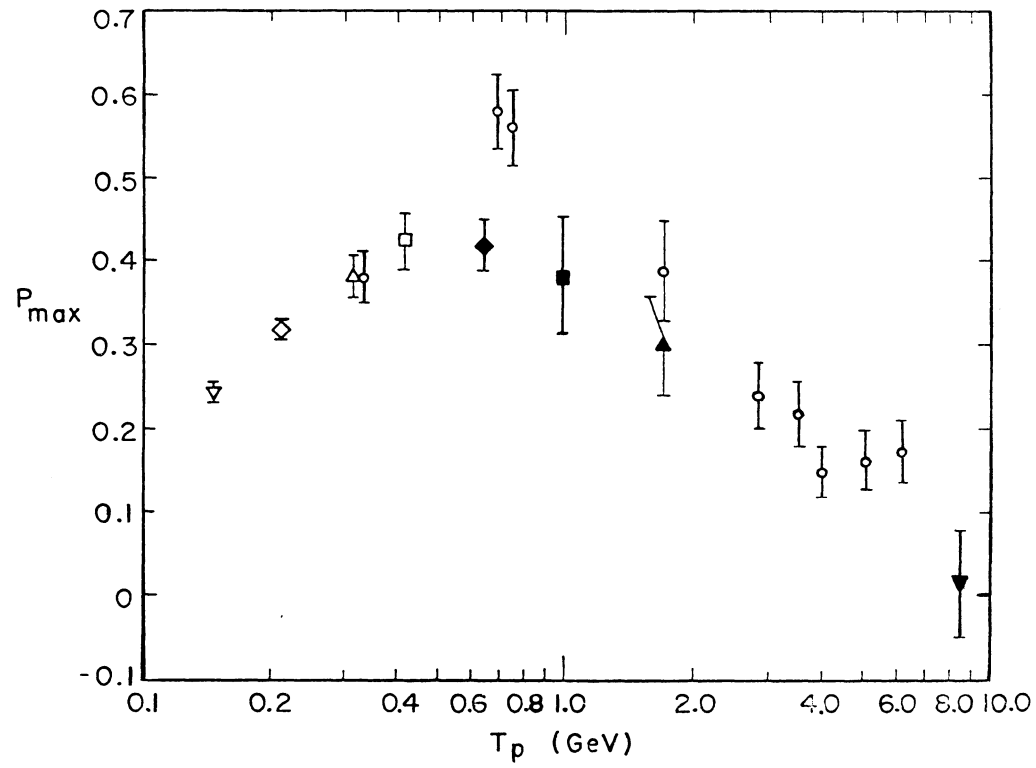

Fig. 14 The maximum value of the polarization found in elastic p-p scattering as a function of energy. This collection of data is given by Betz et al.[35].

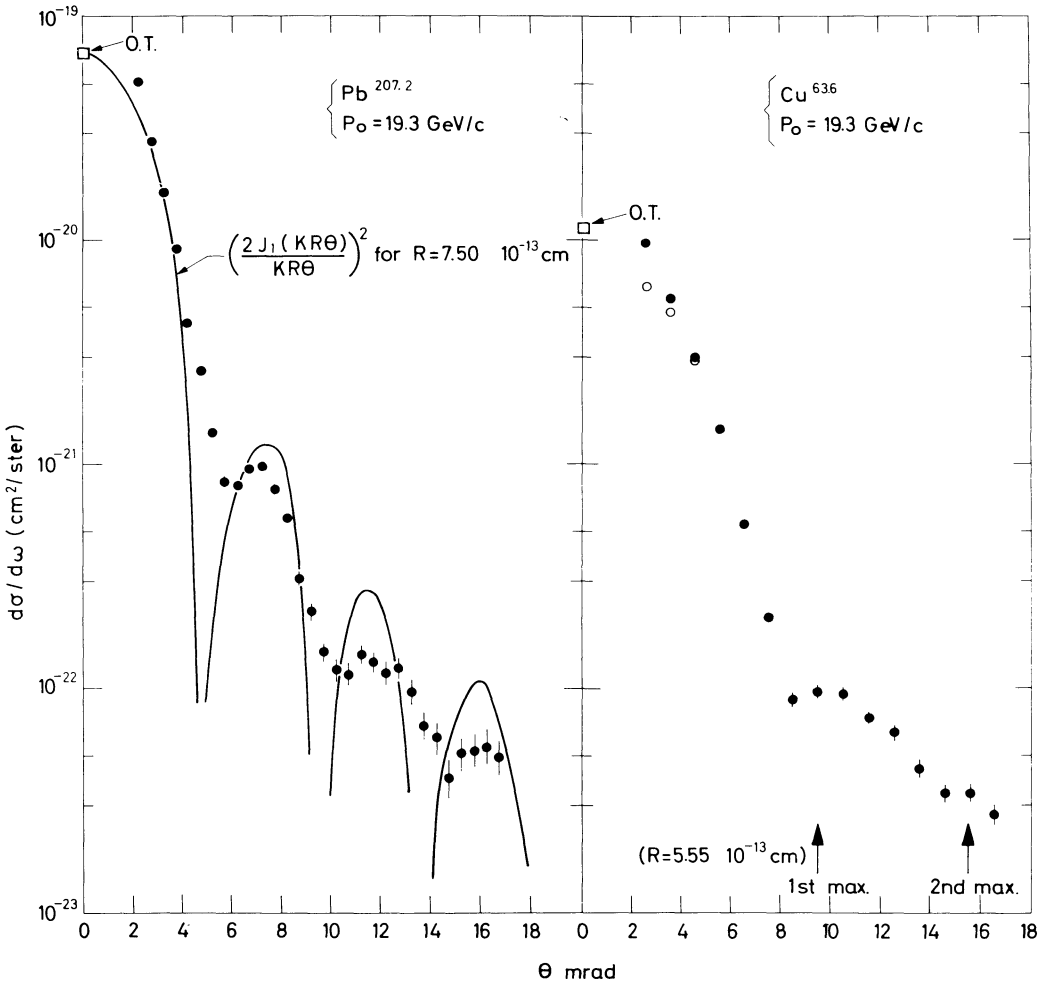

Fig. 15 Preliminary angular distributions for the scattering of 19.3 GeV/c protons by Pb and by Cu measured by Bellettini et al. using the system described in reference 25). The presence of masked subsidiary diffraction maxima is clearly seen. A Bessel function angular distribution is shown with the Pb data, a nuclear radius of 7.5 f was used to compute the distribution. The Cu graph shows the position of the secondary and tertiary maxima obtained from the Bessel function behaviour using R = 5.55 f.

LIST OF PARTICIPANTS

1965 CERN EASTER SCHOOL BAD KREUZNACH

Lecturers

BECKMANN, P., Institut für Theoretische Physik der Universität, Mainz

DALITZ, R.H., Rutherford High Energy Laboratory, Chilton, Didcot, Berks.

GREGORY, B.P., CERN

HEISENBERG, W., Max-Planck Institut für Physik und Astrophysik, Munich

HOHLER, G., Institut für Theoretische Kernphysik, Technische Hochschule, Karlsruhe

MEYER-BERKHOUT, U., DESY, Hamburg

O'CEALLAIGH, C., Cosmic Ray Section, School of Cosmic Physics, Dublin Institute for Advanced Studies, Dublin

PERKINS, D.H., H.H. Wills Physics Laboratory, Bristol

PILKUHN, H., CERN

ROLLNIK, H., Physikalisches Institut der Universität, Bonn

RUBBIA, C., CERN

SCHMITZ, N., Max-Planck Institut für Physik und Astrophysik, Munich

TRIPP, R.D., CERN

VAN HOVE, L., CERN

VELTMAN, M., CERN

WETHERELL, A.M., CERN

WINTER, K., CERN

ZICHICHI, A., CERN

* * *

ADERHOLT, M., Institute of Physics, Aachen
ALLARD, J.F., Faculté des Sciences, Orsay
BARDADIN, M.M., Institute of Experimental Physics, Warsaw
BEISEL, H., High Energy Physics Institute, Heidelberg
BELLOTTI, E., Institute of Physics, Milan
BETTINI, A., Institute of Physics, Padua
BORECKA, I., DESY, Hamburg
BORREANI, G., Institute of Physics, Turin
BUSCHHORN, G., Institute of Experimental Physics, Hamburg
CHARRIERE, G., Nuclear Research Laboratory, Lausanne
COX, C.R., Rutherford High Energy Laboratory, Chilton
CRABB, D.G., University of Southampton, Southampton
DAMERELL, C.J.S., Department of Nuclear Physics, Oxford
DAMGAARD, G., Institute for Theoretical Physics, Copenhagen
DEFOIX, C.G., Collège de France, Paris
DORNAN, P.J., Cavendish Laboratory, Cambridge
DREVERMANN, H., Physikalisches Institut der Universität, Bonn
EIDE, A.J., Institute of Physics, Oslo
ERSKINE, R., University of Glasgow, Glasgow
FAIN, J., Laboratoire de Physique Nucléaire, Clermont-Ferrand
FISCHER, M., Institut de Physique Nucléaire, Villeurbanne
FOGLI, G., Institute of Physics, Bari
GIL PEREZ, D., Institute of Physics, Valencia
GOLDBERG, M., Institut de Radium, Paris

GRANET, P.Y.L., Laboratoire de Physique Corpusculaire à Haute Energie, Saclay
GREEN, K., H.H. Wills Physics Laboratory, Bristol
GROSSO, C., Institute of Physics, Turin
GUISAN, O., Laboratoire de Physique Corpusculaire à Haute Energie, Saclay
HARCKHAM, A.E., University of Manchester, Manchester
HEARD, K.S., Rutherford High Energy Laboratory, Chilton
HENZI, R., Institut de Physique, Neuchatel
HOLMGREN, S.O., Institute of Physics, Stockholm
HOOGLAND, W., Zeeman Laboratorium, Amsterdam
JONES, T.W., University of Birmingham, Birmingham
JULLIAN, S., Faculté des Sciences, Orsay
KAMAL, A.A., Osmania University, Hyderabad
KISSLER, K.H., Physikalisches Institut der Universität, Bonn
KNIES, G., DESY, Hamburg
KOSE, R., Physikalisches Institut der Universität, Bonn
KREHBIEL, H.F., DESY, Hamburg
KURTZ, N., Centre de Recherches Nucléaires, Strasbourg
LAKSHMI, N.T.V., H.H. Wills Physics Laboratory, Bristol
LITT, J., Queen Mary College, London
LLORET, A., Ecole Polytechnique, Paris
LOCKE, D.H., Department of Nuclear Physics, Oxford
LORENZ, E., Max-Planck Institut für Physik und Astrophysik, Munich
LOWYS, J.P., Collège de France, Paris
LUETCHFORD, B.S., University College, London
MACDONALD, F., University of Birmingham, Birmingham
MERKEL, B., Faculté des Sciences, Orsay
MORRISON, R.J., DESY, Hamburg
NAGY, E., Joint Institute for Nuclear Research, Dubna
NIGRO, M., Institute of Physics, Padua
NOVAK, M., Institute of Physics, Prague
OLHEDE, T.E., Institute of Physics, Stockholm
O'SULLIVAN, D.F., Institute for Advanced Studies, Dublin
PASCUAL, R., Institute of Physics, Valencia
PAUL, E., Physikalisches Institut der Universität, Bonn
PIEKARZ, J., Institute of Experimental Physics, Warsaw
POLS, C.L.A., University of Nijmegen, Nijmegen
POSE, D., High Energy Physics Research Centre, Zeuthen-Berlin
POTTER, K.M., University College, London
RAHMAN, I.ur., Imperial College of Science and Technology, London
RAUBOLD, E., Institute of Experimental Physics, Hamburg
SCHARENGUIVEL, J.H., Cavendish Laboratory, Cambridge
SCHMIDT, D., DESY, Hamburg
SCHORSCH, W., Max-Planck Institut für Physik und Astrophysik, Munich
SCHUEBLIN, P., Institute of Exact Sciences, Berne
SCONZA, A., Institute of Physics, Padua
STANLEY, R.D., University College, Dublin
STEFFEN, P., High Energy Physics Institute, Heidelberg
TORNQVIST, N.A., University of Helsinki, Helsinki
TULI, S.K., University of Birmingham, Birmingham
VANDERHAGHEN, R., Ecole Polytechnique, Paris
VILAIN, P., Laboratoire de Physique des Hautes Energies, Bruxelles
WALKER, R.N.F., Westfield College, London
WEBER, H., Institute of Physics, Aachen
WEIGL, J., Max-Planck Institut für Physik und Astrophysik, Munich
WEILNBOCK, W., Max-Planck Institut für Physik und Astrophysik, Munich
WEIZEL, R., Physikalisches Institut der Universität, Bonn
WEYER-MENKHOFF, F.O., Max-Planck Institut für Physik und Astrophysik, Munich
WIECZOREK, E., High Energy Physics Research Centre, Zeuthen-Berlin
WINDMOLDERS, R., Laboratoire des Hautes Energies, Bruxelles
YOUNG, E.C.M., H.H. Wills Physics Laboratory, Bristol